Chapter 5
Mineralogy of Suizhou Shock Veins

5.1 General Remarks

The shock metamorphic effects observed in meteorites can be described in terms of either deformation or transformation or some combination of the two. As mentioned in Chap. 3, the deformation effects include fracturing, plastic deformation, twinning, and mosaicism within constituent minerals. Planar deformation features (PDFs) have been attributed to deformational processes, but they have also been shown to contain transformed material, either diaplectic glass or high-pressure phases (Xie and Chao 1987; Goltrant et al. 1991; Bowden 2002).

Transformational effects observed in shocked meteorites include shock melting, which commonly result in localized melt veins and pockets, transformation of minerals to high-pressure polymorphs, formation of diaplectic glass, and crystallization of highly deformed material. The high-pressure minerals that occur in shocked meteorites formed by either crystallization of silicate liquids in shock melt veins and pockets (Chen et al. 1996a; Xie and Chen 2009) or solid-state transformation of the constituent minerals in meteorites (Chen et al. 1996a). Solid-state phase transformation can provide important constraints on shock conditions of a meteorite, but transformation pressures are difficult to calibrate accurately because of kinetic effects and the heterogeneous nature of the initial transient shock pressure (Sharp and DeCarli 2006). Crystallization of chondritic melt provides an alternative means of constraining the crystallization pressure, which can be related to the shock pressure of the sample.

High-pressure minerals are common in and around shock melt veins in highly shocked meteorites (Chen et al. 1996a; Xie et al. 2001a). Ringwoodite, the spinel-structured polymorph of olivine, was firstly discovered in the Tenham L6 chondrite (Binns et al. 1969). However, this new high-pressure mineral had already been observed in the Coorara chondrite one year before by Mason et al. (1968), but

X. Xie and M. Chen, *Suizhou Meteorite: Mineralogy and Shock Metamorphism*, Springer Geochemistry/Mineralogy, DOI 10.1007/978-3-662-48479-1_5

it was misidentified as garnet based on X-ray diffraction data from the majorite garnet in the sample. Smith and Mason (1970) clarified the mistake when they published the discovery of majorite garnet in Coorara. The majorite that they describe occurred in a fine-grained mixture of garnet, Fe oxide, and iron, which must have been crystallized from chondritic melt such as that described by Chen et al. (1996a). The fact that these garnets had higher concentrations of Na, Al, and Cr than the orthopyroxenes in the sample confirms that they crystallized from the melt. In the same paper, Smith and Mason described an isotropic phase with an orthopyroxene composition that they speculated was also majorite. It was clear from this early work that ringwoodite and majorite were observed in close association with melt veins in shocked chondrites.

Putnis and Price (1975) used transmission electron microscopy to characterize the microstructures of ringwoodite in Tenham and subsequently discovered the β-spinel polymorph of olivine, which they later named wadsleyite. In 1996, that is 25 years later since the time of ringwoodite and majorite discoveries, Chen et al. (1996a) found two distinguished high-pressure assemblages in shock melt veins in the Sixiangkou L6 chondrite: (i) majorite–pyrope solid solution plus magnesiowüstite that crystallized at high pressures and temperatures from a shock-induced silicate melt of bulk Sixiangkou composition and (ii) ringwoodite plus low-calcium majorite that were produced by solid-state transformation of olivine and low-calcium pyroxene. After that, numerous other high-pressure minerals, such as hollandite-structured plagioclase, $MgSiO_3$ perovskite glass, akimotoite (an ilmenite-structured polymorph of $MgSiO_3$), tuite (a high-pressure polymorph of whitlockite), and two post-spinel polymorphs of chromite, have been discovered in shocked chondrites. It should be pointed out that in nearly all cases, the high-pressure polymorphs only occur within shock melt veins or adjacent to them.

The Suizhou chondrite contains a few thin melt veins of 0.02–0.20 mm in width (Fig. 5.1). According to previous investigators, FeNi metal and troilite in shock veins occur in the form of eutectic blebs (Shen and Zhuang 1990), and the silicate minerals in the veins were only brecciated by shock, and no high-pressure minerals were found in the veins (Wang 1993). On the other hand, most high-pressure-phase-bearing L6 chondrites studied so far contain thick shock veins up to one or several millimeters in width, such as those in Sixiangkou, Peace River (Chen et al. 1996b, 1998), and Tenham meteorites (Sharp et al. 1997a). Two assemblages of high-pressure phases, coarse-grained ringwoodite (or wadsleyite) + majorite + lingunite (hollandite-structured plagioclase), and fine-grained majorite–$pyrope_{ss}$ + magnesiowüstite were found in these thick shock melt veins. However, high-pressure phases are not reported from those L6 chondrites that shock veins are very thin and very poorly developed. So it is reasonable to assume that the very thin shock-vein-bearing Suizhou L6 chondrite would not have contained high-pressure phases.

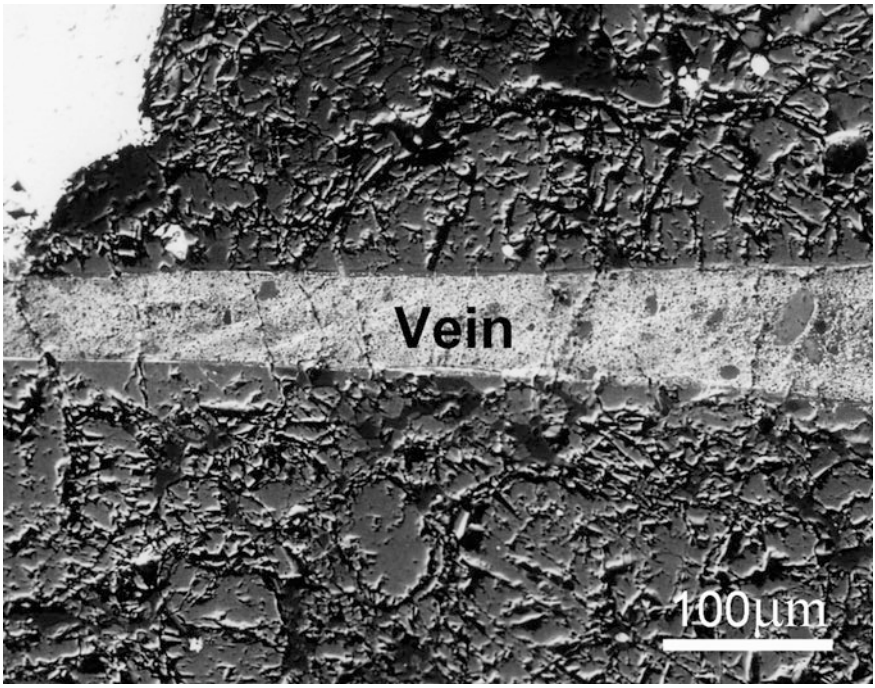

Fig. 5.1 BSE image showing a solid shock melt vein of 70–90 μm in width in the Suizhou meteorite. Note the sharpness of the vein boundaries with its surrounding unmelted chondritic rock and the presence of some coarse-grained high-pressure minerals distributed in the fine-grained vein matrix

However, as we have described in Chap. 4, our recent micro-mineralogical studies did reveal that the shock melt veins of the Suizhou chondrite are really full of high-pressure phases. Furthermore, similar to the thick shock melt veins in many other L6 chondrites (Chen et al. 1996a; Sharp et al. 1997a), two types of high-pressure mineral assemblages were also developed in the very thin Suizhou veins (Figs. 5.1 and 5.2), namely the coarse-grained assemblage of ringwoodite + majorite + akimotoite + perovskite + lingunite ($NaAlSi_3O_8$ hollandite) + tuite (the high-pressure polymorph of whitlockite) + xieite and the CF phase (two high-pressure polymorphs of chromite), and the fine-grained assemblage of matrix minerals majorite–pyrope solid solution + magnesiowüstite + microcrystalline ringwoodite (Xie et al. 2001a, 2002, 2003, 2011a, b; Chen et al. 2003a, b). These two types of high-pressure mineral constitute up to 90 % of materials in veins by volume. The other 10 % constituents of veins are fine-grained metal–troilite eutectic intergrowths and blebs which fill the interstices of majorite–$pyrope_{ss}$ or in the form of metal–sulfide veinlets (Xie et al. 2001a). This means that almost all minerals in the Suizhou shock veins have transformed to their high-pressure polymorphs. This is really a very rare and unique case that up to 10 minerals in the Suizhou shock

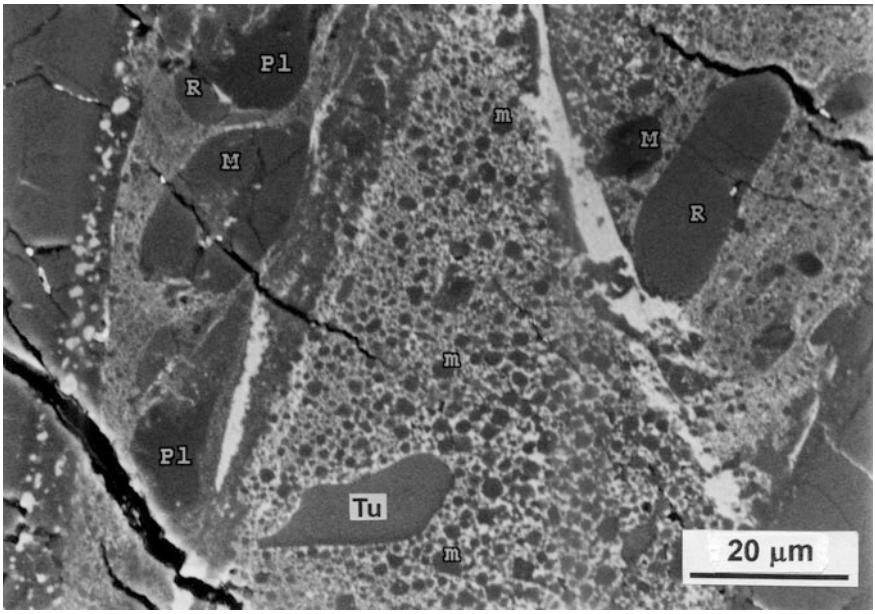

Fig. 5.2 BSE image of a shock melt vein showing the coarse-grained high-pressure assemblage consisting of ringwoodite (*R*), majorite (*M*), $NaAlSi_3O_8$ hollandite (*Pl*), and tuite (*Tu*) and the fine-grained matrix consisting of majorite–pyrope garnet (*m*) and FeNi metal + FeS in intergrowth (*white colored*)

melt veins have transformed to their high-pressure polymorphs. The only one mineral that we could not find its high-pressure polymorph is ilmenite. In this chapter, we describe the characteristics of the high-pressure mineral phases in Suizhou melt veins.

5.2 Coarse-Grained High-Pressure Mineral Phases

5.2.1 Ringwoodite, the Spinel-Structured $(Mg,Fe)_2SiO_4$

The γ-phase of olivine was firstly obtained at high-pressure and high-temperature experiments by Ringwood and Major (1966). Prewitt (1998) pointed out that "the only known natural occurrence of a $(Mg,Fe)_2SiO_4$ spinel is in the shocked meteorites". The high-pressure spinel polymorph of $(Mg,Fe)_2SiO_4$ olivine was first reported by Binns et al. (1969) and Binns (1970) in black shock veins in the Tenham L6 ordinary chondrite and was named as "ringwoodite" after the name of the famous Australian petrologist, Professor Ringwood. Ringwoodite has now been widely recognized in shock melt veins of many other highly shocked ordinary chondrites of shock stage 6, such as Catherwood (Coleman 1977), Sixiangkou

(Chen et al. 1996a), Peace River (Chen et al. 1996b), Mbale (Chen et al. 1998), Suizhou (Xie et al. 2001a), and some other meteorites, as well as in the shock melt veins of a few H-group chondrites, such as Yanzhuang (Chen and Xie 1993) and an Antarctic meteorite Y-75100 (Kimura et al. 2000).

The formula for the spinel-type structure is B_2AO_4. The crystal structure of ringwoodite can be viewed as the diagonal crisscrossing chains of MgO octahedra linked together by isolated SiO_4 tetrahedra. The oxygen anions are in a cubic closely packed arrangement with the B cation in octahedral sites and the A cation in tetrahedral. The octahedra form edge-sharing chains that are linked together by the isolated tetrahedra. All atoms are in special positions, and the only variable for the structure is the cubic cell edge and the x position of the oxygen atom (Prewitt and Downs 1998). As far as the Earth's interior is concerned, $(Mg,Fe)_2SiO_4$ ringwoodite is the most important mineral phase in the mantle's transition zone. Under the condition of lower mantle, ringwoodite transforms to (Mg,Fe)O magnesiowüstite + $(Mg,Fe)SiO_3$ perovskite.

During our recent micro-mineralogical studies on the shock melt veins of the Suizhou L6 chondrite, we also found quite a lot of ringwoodite grains in the shock melt veins of this meteorite (Xie et al. 2001a). The physical and chemical properties of the Suizhou ringwoodite are described in the following sections.

Occurrence

The Suizhou polycrystalline grains of ringwoodite of 10–50 μm in length are smooth, rounded, and unfractured. SEM and LRM investigations showed that these grains are single-phase ringwoodite (Figs. 5.2, 5.3 and 5.4). In comparison with the heavily deformed and fractured grains of host olivine in the Suizhou unmelted chondritic rock, the smooth and unfractured features of the large ringwoodite grains in Suizhou shock veins imply that these grains experienced strong shock compression, and the rounded outline of the ringwoodite fragments is indicative of partial resorption into the fine-grained molten matrix during the shock event.

Sometimes, we observe a few fractures or cracks penetrating the ringwoodite grains in the Suizhou shock veins (Figs. 5.2, 5.3, and 5.4), but they are not produced by shock compression but by cooling shrinkage after thermal expansion of the melt veins.

Chemical Composition

Electron microprobe analyses revealed that the Suizhou ringwoodite grains have the same chemical composition as the olivine outside the melt veins (Table 5.1). It is clear that these ringwoodite grains must have formed directly from olivine through isochemical solid-state phase transformation under high pressures and no additional elements were incorporated with these grains from the surrounding matrix melt.

Raman Spectroscopy

A micro-Raman spectrum obtained from a 30-μm-long grain of the Suizhou ringwoodite displays two strong Raman peaks at 796 and 841 cm^{-1} (Fig. 5.5a). This spectrum is comparable with that of γ-Mg_2SiO_4 (spinel) (McMillan and Akaogi 1987) and is different with that of olivine outside the veins, whose spectrum shows

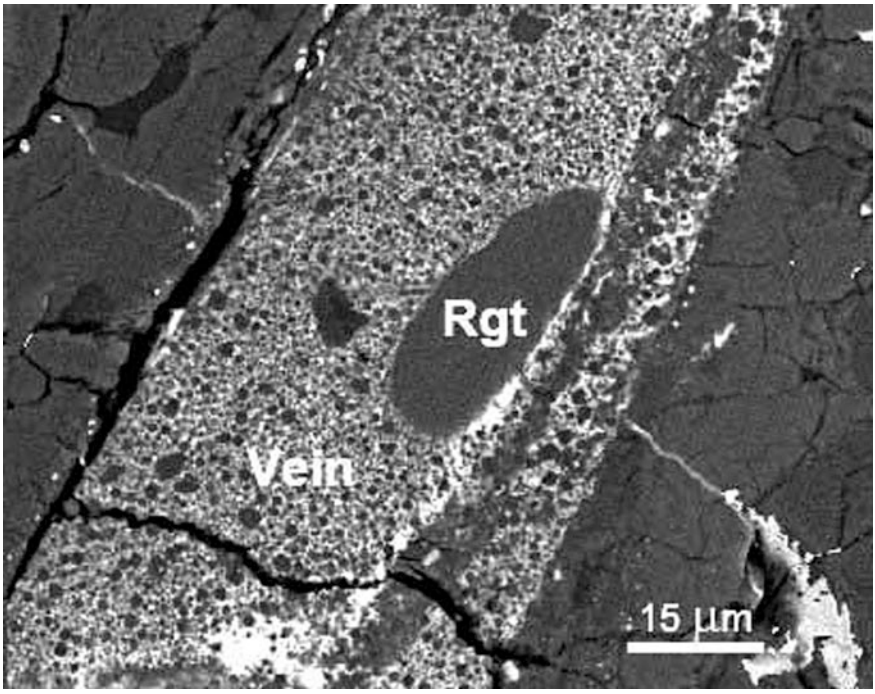

Fig. 5.3 BSE image showing an elongated ringwoodite grain (*Rgt*) in a shock vein of the Suizhou meteorite. Note the fine-grained majorite–pyrope garnet (*dark gray*) and the metal–sulfide intergrowth (*white*) in the vein

two main peaks at 821 and 851 cm^{-1}. Although the two respective Raman peaks for both olivine and ringwoodite are assigned to the symmetric and asymmetric stretching vibrations of SiO_4 tetrahedra, ringwoodite, having higher symmetry and less distortion of SiO_4 tetrahedra than olivine, shows the decreasing of Raman peak height and shifting of Raman peaks to the direction of smaller wave numbers.

X-ray Diffraction

The X-ray diffraction pattern of the Suizhou ringwoodite was obtained by using the in situ micro-diffraction analysis. Since the ringwoodite grain is surrounded by other fine-grained minerals of the vein matrix, the result shows the diffraction lines of ringwoodite together with lines of majorite–pyrope garnet, kamacite, and troilite. Among them, the following lines belong to ringwoodite (in Å): 2.446 (100), 1.431 (50), 2.026 (35), 2.878 (20), 1.561 (20), 1.059 (20), and 1.056 (10). These data are consistent with those of standard ringwoodite of JCPDS No. 21-1258.

Olivine–Ringwoodite Transformation Mechanism

It was revealed that the ringwoodite in very highly shocked chondrites occurs as polycrystalline aggregates that have the same chemical composition as the olivine in the same samples (Chen et al. 1996a; Langenhorst et al. 1995; Xie et al. 2001a). This implies that ringwoodite formed from olivine via a solid-state transformation

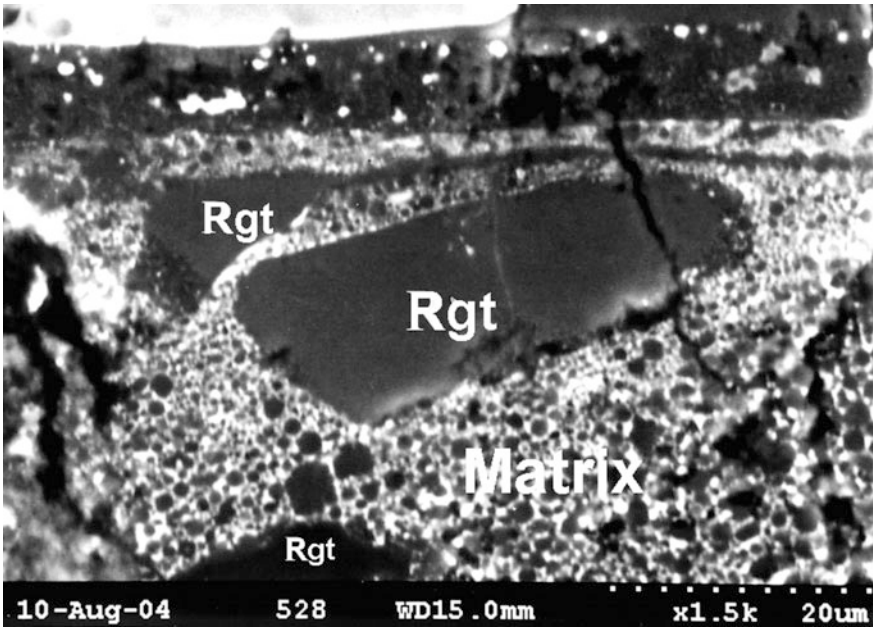

Fig. 5.4 BSE image showing some large polycrystalline ringwoodite grains (*Rgt*) surrounded by fine-grained matrix (*Matrix*) in a shock vein of the Suizhou meteorite

Table 5.1 Chemical composition of ringwoodite in the Suizhou shock veins (wt%)

	SZ-Rwt-1	SZ-Rwt-2	SZ-Rwt-3	SZ-Rwt	Ringwoodite average	Olivine average
SiO_2	38.202	38.439	38.211	38.706	38.389	38.249
TiO_2	0.003	0.000	0.056	0.000	0.015	0.015
Al_2O_3	0.007	0.000	0.008	0.002	0.004	0.000
Cr_2O_3	0.045	0.021	0.082	0.027	0.044	0.013
MgO	38.542	38.771	38.471	38.964	38.687	39.174
CaO	0.028	0.052	0.046	0.053	0.045	0.006
MnO	0.488	0.542	0.494	0.397	0.480	0.481
FeO	23.356	23.532	22.973	23.171	23.258	22.343
NiO	0.000	0.063	0.038	0.060	0.040	0.039
Na_2O	0.000	0.000	0.000	0.000	0.000	0.014
K_2O	0.015	0.000	0.014	0.016	0.011	0.011
Total	100.686	101.420	100.393	101.396	100.973	100.345
Fa	25.25	25.27	24.98	24.93	25.11	24.12
Fo	74.26	74.20	74.54	74.71	74.43	75.3
Mo	0.04	0.06	0.06	0.07	0.06	0.01
Li	0.00	0.07	0.04	0.06	0.04	0.04
Te	0.53	0.59	0.54	0.43	0.52	0.52

All values were determined by EPMA in wt%
Fa—fayalite, Fo—forsterite, Mo—monticellite, Li—liebenbergite, Te—tephroite

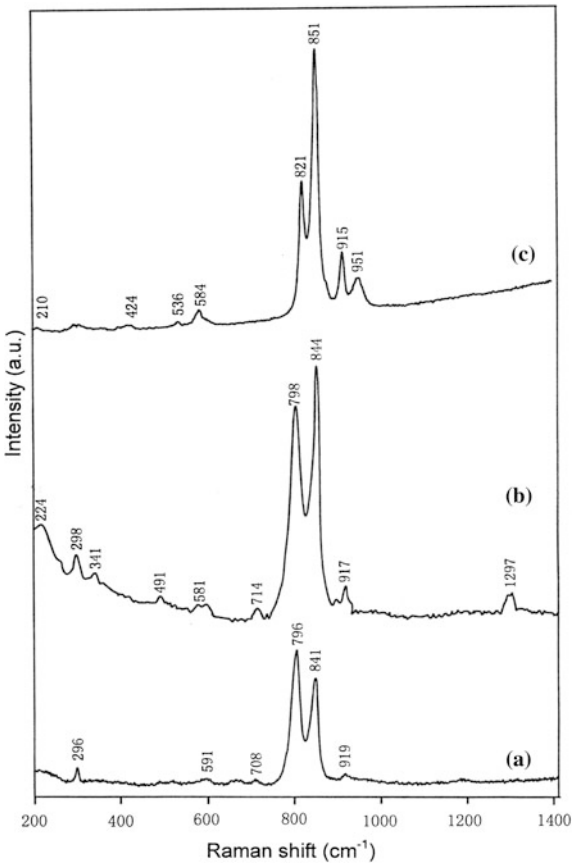

Fig. 5.5 Raman spectra of ringwoodite in Suizhou shock melt veins (*a*), γ-Mg_2SiO_4 (spinel) (*b*), and olivine outside the Suizhou veins (*c*)

mechanism during shock compression (Chen et al. 1996a). TEM examination of the polycrystalline ringwoodite in chondrites generally shows randomly oriented ringwoodite crystallites that range from about one hundred nanometers (Price et al. 1979) to several micrometers (Chen et al. 1996a). The random orientation and homogeneous distribution of ringwoodite crystallites indicate homogeneous intracrystalline nucleation throughout the olivine rather than heterogeneous nucleation on grain boundaries, which is dominate mechanism at pressures closer to the equilibrium phase boundary (Kerschofer et al. 2000; Mosenfelder et al. 2001). The presence of small amounts of glassy material in ringwoodites from Tenham meteorite (Price et al. 1979) has been interpreted as remnants of a prograde high-density olivine glass that was an intermediate phase in the transformation of olivine to ringwoodite. However, such glassy phases have not been reported in more recent studies, and static high-pressure experiments never demonstrated that the olivine–ringwoodite phase transition path goes via an intermediate glass phase (Agee et al. 1995; Zhang and Herzberg 1994). In most samples of highly shocked chondrites, the ringwoodite composition is constant, implying that there was no

Fe–Mg exchange during the transformation, and therefore, the ringwoodite crystallites grew by interface growth rather than diffusion-controlled growth (Sharp and DeCarli 2006).

Chen et al. (2004b) reported the first natural occurrence of ringwoodite lamellae in the olivine grains inside and in the areas to the shock veins of the Sixiangkou meteorite. They found that inside the veins where pressure and temperature were higher than elsewhere, ringwoodite lamellae formed parallel to the {101} planes of olivine, whereas outside they lie parallel to the (100) plane of olivine. The lamellae replaced the host olivine from a few percent to complete. They assumed that formation of these lamellae is related to a diffusion-controlled growth of ringwoodite along shear-induced planar defects in olivine. Hence, these ringwoodite lamellae show distinct growth mechanism.

It has been revealed that the ringwoodite grains in the shock melt veins of the Suizhou chondrite have the same chemical composition as the olivine in the unmelted chondritic rock (Table 5.1). We consider that these ringwoodite grains must have formed directly from olivine through solid-state phase transformation under high pressures. The polycrystalline nature of the Suizhou ringwoodite grains and the constant composition for different ringwoodite grains indicate the homogeneous features in chemical composition of ringwoodite crystallites within grains. Therefore, it is reasonable to assume that olivine–ringwoodite transformation mechanism in the Suizhou meteorite can be interpreted to be the homogeneous intracrystalline nucleation of ringwoodite crystallites throughout the host olivine grain and followed by the interface-controlled growth of crystallites in the grain.

***P-T* Conditions**

Ringwoodite is the most abundant mineral in the Earth's transition zone between the 520 and 660 discontinuities (Anderson and Bass 1986). Static high-pressure kinetic experiments have shown that dry hot-pressed San Carlos olivine transforms to ringwoodite, on an observable timescale, only above 900 °C at 18–20 GPa (Kerschofer et al. 1996, 1998, 2000). According to the conditions of formation of other high-pressure minerals of the veins, such as majorite, hollandite, and magnesiowüstite, it was assumed that ringwoodite in the Suizhou veins formed at 18–23 GPa and 1800–1900 °C. This pressure regime corresponds to the pressure range of the mantle transition zone, e.g., 400–660 km deep in the Earth's mantle.

5.2.2 Majorite, the Garnet-Structured (Mg,Fe)SiO_3

Majorite is the high-pressure polymorph of pyroxene with garnet structure. This polymorph ($MgSiO_3$ garnet) is a stable phase in the pressure range 19–24 GPa at the temperature between 1700 and 2600 °C (Kato and Kumazawa 1985). Smith and Mason (1970) reported the first natural occurrence of majorite in a veinlet in the Coorara meteorite, produced by high-pressure transformation of low-Ca pyroxene

to the higher density garnet structure and was named after the Professor A. Major. The majorite is extremely fine-grained and difficult to analyze, but has an Mg/(Mg + Fe) ratio of ~0.25. Coleman (1997) also described the occurrence of majorite in Catherwood (L6) chondrite and reported compositional data. Price et al. (1979) examined the microstructures of majorite in shock veins in the Tenham L6 chondrite. Since then, the low-Ca majorite has been discovered in the shock melt veins of a series of L-group chondrites, such as Sixiangkou (Chen et al. 1996a), Peace River (Chen et al. 1996b), Mbale (Chen et al. 1998b), Suizhou (Xie et al. 2001a), and some other L6 chondrites, as well as in the shock melt veins of a few H-group chondrites, such as Yanzhuang (Chen and Xie 1993a) and an Antarctic meteorite Y-75100 (Kimura et al. 2000). Low-Ca majorite in shock veins of the Sixiangkou L6 chondrite occurs as rounded polycrystalline grains, 15–300 μm in size, associated with ringwoodite and lingunite (the hollandite-structured plagioclase). This majorite contains a subgrain dislocation microstructure consistent with dislocation climb. The majorite has a composition essentially identical to unshocked low-Ca pyroxene in the Sixiangkou unmelted chondritic rock and probably formed by solid-state transformation of low-Ca pyroxene.

The majorite has space group *Ia3d* and occurs as equant grains. The equant grains are 50–500 nm in size and have 120° grain junctions. The crystal structure of majorite can be viewed as a rather rigid framework of corner-sharing octahedra (B-site) and tetrahedra, with the A-site atom located in interstices that have a dodecahedral shape.

During our recent micro-mineralogical studies on the shock melt veins of the Suizhou L6 chondrite, we also found quite a lot of majorite grains in the shock melt veins of this meteorite (Xie et al. 2001a). The brief introductions of the Suizhou majorite are described in the following sections.

Occurrence

Polycrystalline grains of low-Ca majorite occur in the shock melt veins of the Suizhou meteorite with the grain sizes ranging from 8 to 50 μm in diameter (Figs. 5.2 and 5.6). These grains are also smooth and unfractured and have dark gray color under the SEM. Figure 4.6 is a BSE image of the Suizhou meteorite showing that the shock vein contains coarse-grained polycrystalline majorite, ringwoodite, and hollandite-structured polymorph of plagioclase, as well as the polycrystalline fine-grained matrix. It is understandable that this majorite is a pseudomorph after pyroxene and shows a fine-grained polygranular texture.

Chemical Composition

Electron microprobe analyses show that Suizhou low-Ca majorite has the same chemical composition as the low-Ca pyroxene outside the veins (Table 5.2). Hence, the coarse-grained low-Ca majorite is formed from low-Ca pyroxene through solid-state phase transition under high pressures. However, the electron microprobe analyses revealed that the idiomorphic fine-grained majorite garnets in Suizhou veins are richer in Al_2O_3, CaO, Na_2O, and Cr_2O_3 in comparison with that of low-Ca pyroxene outside the veins (Table 5.2). It is evident that these two kinds of majorite have different origins of their formation.

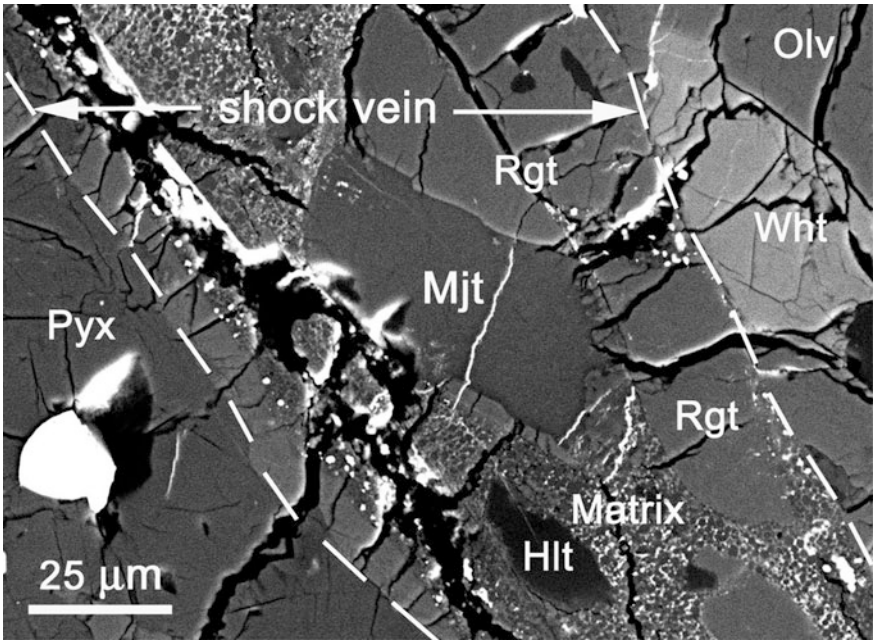

Fig. 5.6 A BSE image of the Suizhou meteorite showing that the shock melt vein contains coarse-grained, polycrystalline majorite (*Mjt*), ringwoodite (*Rgt*), and hollandite-structured polymorph of plagioclase (*Hlt*), as well as the polycrystalline fine-grained matrix (*Matrix*). Olv = olivine, Pyx = pyroxene, Wht = whitlockite (Chen et al. 2004c)

Table 5.2 Chemical composition of majorite in the Suizhou shock veins (wt%)

	SZ-Mjt-1	SZ-Mjt-2	SZ-Mjt-3	SZ-Mjt-4	Majorite average	Pyroxene average
SiO_2	55.965	56.458	55.068	55.695	55.797	55.775
TiO_2	0.158	0.192	0.164	0.252	0.191	0.162
Al_2O_3	0.153	0.187	0.156	0.148	0.123	0.158
Cr_2O_3	0.124	0.106	0.169	0.085	0.121	0.110
MgO	29.182	28.130	29.033	29.218	28.891	29.239
CaO	0.736	0.772	0.678	0.652	0.710	0.715
MnO	0.503	0.519	0.518	0.458	0.499	0.496
FeO	14.477	13.828	14.881	14.272	14.365	13.952
NiO	0.124	0.048	0.092	0.041	0.076	0.007
Na_2O	0.024	0.426	0.000	0.025	0.119	0.043
K_2O	0.007	0.063	0.018	0.003	0.023	0.009
Total	101.451	100.729	100.768	100.848	100.915	100.666
Fs	20.74	21.91	20.11	20.63	20.85	20.12
En	77.85	76.58	78.57	78.12	77.78	78.41
Wo	1.41	1.51	1.32	1.25	1.37	1.38

All values were determined by EPMA in wt%
Fs—ferrosite, En—enstatite, Wo—wollastonite

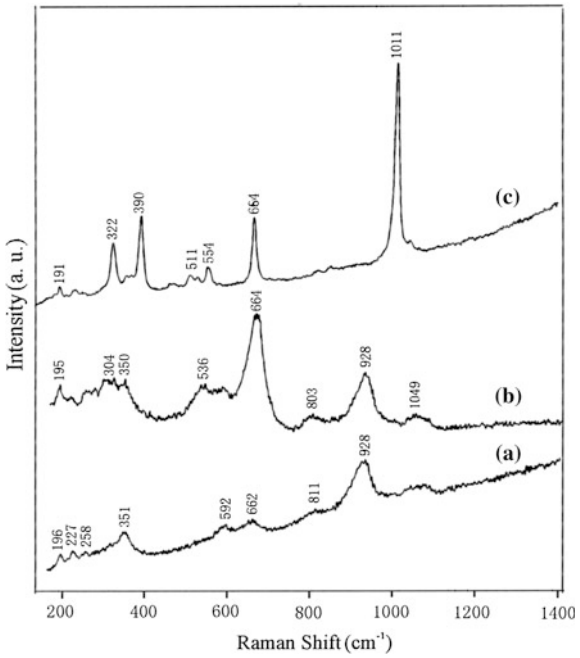

Fig. 5.7 Raman spectra of majorite (*a*), majorite–pyrope$_{ss}$ (*b*) in Suizhou melt veins, and pyroxene outside the Suizhou veins (*c*)

Raman Spectroscopy

The Raman spectrum of a Suizhou coarse-grained low-Ca majorite grain displays Raman peaks at 928, 662, 592, and 351 cm^{-1} (Fig. 5.7a). The Raman spectrum of another polycrystalline majorite grain in the Suizhou chondritic rock displays sharp strong bands at 926 and 590 cm^{-1} and weak bands at 315, 373, 654, 804, and 1056 cm^{-1}. The strong peak at 926–928 cm^{-1} corresponds to the stretching vibrations of the SiO_4 tetrahedra. Since the Raman spectra of majorite are significantly different for those of low-Ca pyroxene, we can easily identify the majorite phase from its precursor pyroxene by Raman spectroscopy.

X-ray Diffraction

The in situ micro-diffraction analysis on the Suizhou meteorite is shown in Fig. 5.8, in which tiny grains of majorite in a shock vein matrix are exposed to X-ray of 0.03-mm collimator with $\omega = 22°$ for 2 h. The result shows the diffraction lines of majorite with minor kamacite and troilite. The following lines belong to majorite (in Å): 2.574 (100), 2.878 (80), 1.541 (50), 2.455 (45), 1.598 (40), 2.261 (30), 2.350 (30), 2.037 (20), 1.868 (20), and 1.664 (15). These data are consistent with those of standard majorite of JCPDS No. 25-0483.

Low-Ca Pyroxene–Majorite Transformation Mechanism

It has been found that majorite in most shocked chondrites occurs as polycrystalline aggregates that have the same chemical composition as the low-Ca pyroxene in the unmelted chondritic rock (Chen et al. 1996a, Xie et al. 2001a). This implies that majorite formed from low-Ca pyroxene also via a solid-state transformation

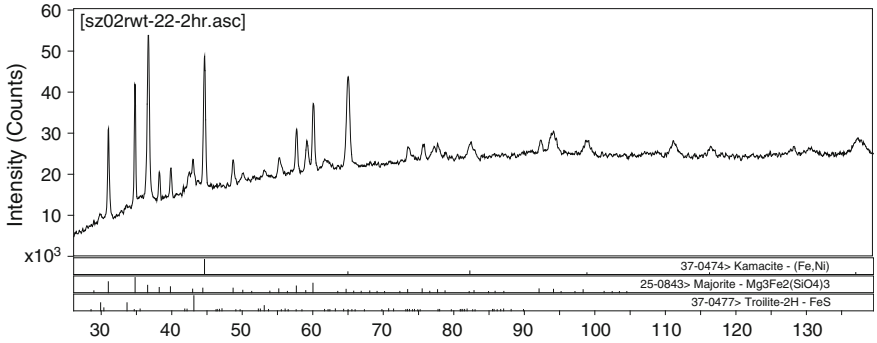

Fig. 5.8 X-ray micro-diffraction pattern of majorite in a shock vein matrix in the Suizhou meteorite (2θ-I profile showing the diffraction lines of majorite with minor kamacite and troilite)

mechanism during shock compression (Chen et al. 1996a). The mechanism of transformation of pyroxene to majorite appears to be the same as that of ringwoodite: homogeneous intracrystalline nucleation of majorite crystallites followed by interface-controlled growth (Sharp and DeCarli 2006). Price et al. (1979) suggested that shocked pyroxene first did not transform to majorite directly but transforms into a prograde glass from which majorite subsequently crystallized. However, such intermediate glassy phases have not been reported in more recently studies, and the static high-pressure experiments never demonstrated that the orthopyroxene–majorite phase transition path goes via an intermediate glass phase (Agee et al. 1995; Wang and Takahashi 2000; Chen et al. 2004a). Therefore, we firmly stand for a mechanism of homogeneous nucleation and interface-controlled growth in the solid state for the coarse-grained majorite in the shock melt veins of the Suizhou meteorite.

***P-T* Condition**

High-pressure experiments indicated that $MgSiO_3$ majorite has a *P-T* stability field between 16 and 22.5 GPa and 1600–2500 °C (Gasparik 1992; Presnall and Gasparik 1990; Chen et al. 2004a), and the presence of majorite garnet plus ringwoodite constrains the *P-T* condition of 18–23 GPa and 1800–1900 °C (Agee et al. 1995). On the basis of coarse-grained high-pressure assemblage in the Suizhou shock melt veins, we believe that the Suizhou majorite formed at high pressure up to 23–24 GPa and temperature up to 1900–2000 °C. This pressure regime corresponds to the pressure range from the lower part of mantle transition zone to the upper part of the lower mantle, e.g., 600–700 km deep in the Earth's mantle.

5.2.3 Akimotoite, the Ilmenite-Structured (Mg,Fe)SiO_3

At high pressure and temperature, pyroxene transforms to high-pressure polymorphs including majorite (the garnet-structured (Mg,Fe)SiO_3), akimotoite (the

ilmenite-structured (Mg,Fe)SiO_3), and perovskite (the perovskite-structured (Mg, Fe)SiO_3. The ilmenite-structured (Mg,Fe)SiO_3, which was synthesized by Kawai et al. (1974) and identified as having an ilmenite structure by Liu (1976), is a potentially important mantle mineral that has not been previously found in terrestrial rocks. This high-pressure dense polymorph has only been found in the shock melt veins of chondrites, but not widely identified in these meteorites. Up to now, only a few meteorites were reported to contain very small amount of akimotoite.

Sharp et al. (1997a, b) examined shock melt veins in the Acfer 040 (L5-6, S6) chondrite using TEM technique and observed prismatic or plate-like grains with the composition $MgSiO_3$, with minor concentrations of FeO, Al_2O_3, Na_2O, and Cr_2O_3. Based on electron diffraction studies, the phase was unambiguously identified as ilmenite-structured $MgSiO_3$ with space group R-3, the first occurrence of this phase in nature. The $MgSiO_3$ ilmenite occurs with ringwoodite and an amorphous phase which may have been $MgSiO_3$ perovskite, but became amorphous during depressurization. Because $MgSiO_3$ ilmenite is not predicted as a stable phase at high pressure, Sharp et al. (1997a, b) argued that it crystallized metastably during post-shock decompression and heating.

Tomioka and Fujino (1997) also identified the mineral $MgSiO_3$ ilmenite in the shock-induced veins in the Tenham L6 chondrite using ATEM technique. This mineral is adjacent to clinopyroxene in fragments and formed aggregates with each grain <1.4 μm in length. The examined hexagonal structure, *d*-spacings, angles, space group (R-3), and systematic extinctions of electron diffraction patterns of this mineral are all consistent with those of ilmenite. Chemical analyses of $MgSiO_3$ ilmenite grains were carried out with an energy-dispersive analytical system attached to the ATEM and found that these grains have similar compositions to the adjacent clinopyroxene grains. $MgSiO_3$ ilmenite grains in the Tenham meteorite have two morphologies. One is granular-shaped (<0.4 μm in length), and the other is columnar (<1.4 μm in length). Both types of grains do not show any microstructures except a low density of dislocations. Tomioka and Fujino (1997) argued that the columnar-type ilmenite has the shear transformation mechanism for the clinopyroxene–ilmenite transition, because the topotaxial relation indicates that this process may have proceeded by the displacement of the closely packed layers of oxygen on (100) plane for clinopyroxene, whereas the granular ilmenite, which has no topotaxial relationship with clinopyroxene, would have formed by the nucleation and growth mechanism, probably under the slower cooling rates. This $MgSiO_3$-ilmenite was than approved as a new mineral with the mineral name akimotoite (Tomioka and Fujino 1999).

Ferroir et al. (2008) reported observations of four textural relationships between pyroxene and akimotoite in former pyroxene grains entrained in the shear melt vein and in pyroxene grains attached to the wall of the melt vein in the Tenham L6 chondrite. They suggested that akimotoite is mainly formed by solid-state transformation of former pyroxenes with subsequent diffusion of calcium, aluminum, and sodium from the chondritic melt of the shear melt vein.

The other occurrences of akimotoite in chondrites were reported in succession by Xie et al. (2005b) in the Suizhou chondrite and then by Zhang et al. (2006) and

Miyagima et al. (2007) in the Sixiangkou chondrite. Akimotoite was identified by its characteristic plate-like morphology in the TEM images, selected area electron diffraction patterns, and quantitative energy-dispersive X-ray spectra. The akimotoite-bearing fine-grained matrix of the melt vein is classified as a metal–troilite-poor lithology by Chen et al. (1996a). Akimotoite crystals range in size from 0.3 to 3 μm and the plate-like idiomorphic crystals are elongated parallel to the $(110)_{hex}$ direction. The coexisting phases are a majorite–pyrope solid solution, ringwoodite, FeNi metal, troilite (FeS), and a silicate glass. Akimotoite, which is considered to be a subsolidus phase in the Mg_2SiO_4–$MgSiO_3$ system (Gasparik 1992), crystallized with ringwoodite and majorite from the immiscible silicate and metal–sulfide liquids in the melt vein at very high temperatures and high pressures on the order of 2000 °C at 23 GPa. These values are estimated from the occurrence of the liquidus pair, majorite garnet and magnesiowüstite, at the central core of the Sixiangkou melt vein (Chen et al. 1996a). On the other hand, melting experiments in the CV3 chondrite Allende did not reveal akimotoite as a liquidus phase during cooling under equilibrium conditions (Agee et al. 1995). However, akimotoite is considered to have crystallized metastably at the margin of the melt vein where the cooling rate from high temperature was highest due to rapid heat transport to the matrix so that supercooling was large (Sharp et al. 1997a, b; Xie et al. 2006). The crystallization of akimotoite in the Sixiangkou chondrite is also inferred to have occurred as a result of supercooling of the melt at the margin of the melt vein, at a low oxygen fugacity (fO_2) as documented by the coexistence with FeNi metal.

During our recent micro-mineralogical studies on the shock melt veins of the Suizhou L6 chondrite, akimotoite was also identified in the shock-produced melt veins or in the area directly adjacent to the shock melt veins of this meteorite (Chen and Xie 2015). The physical and chemical properties of the Suizhou akimotoite are described in the following sections.

Occurrence

A most important occurrence of akimotoite in the Suizhou meteorite is to occur along the fractures inside pyroxene fragments enclosed in melt as irregular zones of akimotoite (Fig. 5.9). The width of akimotoite zones is about 2–4 μm. On the BSE image, akimotoite shows dark gray color which is little bit lighter than the very dark pyroxene. Another occurrence is to appear in the edge of pyroxene or fractures in these pyroxene grains in contact with the melt vein. This second occurrence of akimotoite in the Suizhou meteorite is in a granular texture where the crystal grains have a topotaxial relationship with the host pyroxene and form a rather narrow zone of randomly oriented akimotoite grains in between intact pyroxene and shock-produced $(Mg,Fe)SiO_3$ glass which is in direct contact with a shock melt vein (Fig. 5.10). The grain size of akimotoite is in the range of 2–4 μm. On the BSE image, it shows gray color which is also lighter than the pyroxene and the $(Mg,Fe)SiO_3$ glass.

Chemical Composition

Energy-dispersive spectroscopic analyses show that akimotoite in the Suizhou melt veins or in the area directly adjacent to Suizhou shock veins has an identical composition as its host low-Ca pyroxene (Table 5.3). The contents of the main

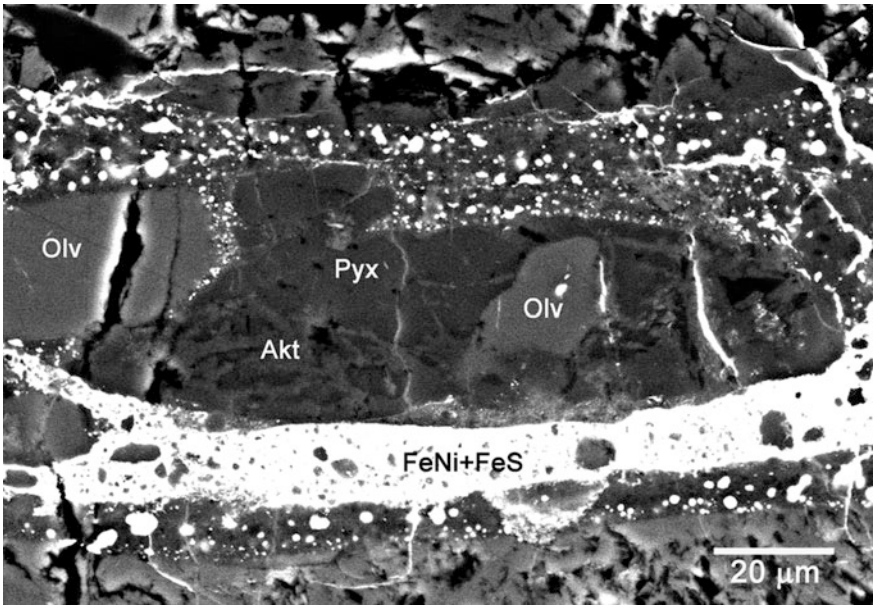

Fig. 5.9 BSE image of an area directly adjacent to a shock vein in Suizhou meteorite showing the occurrence of akimotoite (*Akt*) occurring along the fractures inside pyroxene (*Pyx*) fragments enclosed in melt. Olv = olivine, FeNi + FeS = metal + troilite intergrowth (Chen and Xie 2015)

constituents MgO, FeO, and SiO_2, as well as the minor constituents, such as MnO, CaO, Al_2O_3, Cr_2O_3, TiO_2, and K_2O, are almost identical for both akimotoite and the host pyroxene. It is clear that akimotoite in the Suizhou meteorite must have formed directly from pyroxene through isochemical solid-state phase transformation under high pressures.

Raman Spectroscopy

The Raman spectrum of the Suizhou akimotoite displays Raman bands at 798, 676, 614, 478, 406, and 344 cm^{-1} (Fig. 5.11a). The strong peak at 798 cm^{-1} corresponds to the stretching vibrations of the SiO_4 tetrahedra. Raman spectrum of akimotoite is distinct from its host orthopyroxene, which show clear Raman bands at 1014, 927, 793, 677, 658, 520, 407, 385, 335, and 233 cm^{-1} (Fig. 5.10b). Since the Raman spectrum of akimotoite is significantly different for that of low-Ca pyroxene, we can easily identify the akimotoite phase from its precursor pyroxene by Raman spectroscopy.

Low-Ca Pyroxene-Akimotoite Transformation Mechanism

In the transformation of pyroxene to akimotoite in the shock veins of the Tenham meteorite, akimotoite occurs in a granular texture as well as in columnar texture where the crystals have a topotaxial relationship with the pyroxene (Tomioka and Fujino 1997). The granular texture consists of randomly oriented crystallites from 100 to 200 nm, which is consistent with homogeneous intracrystalline nucleation

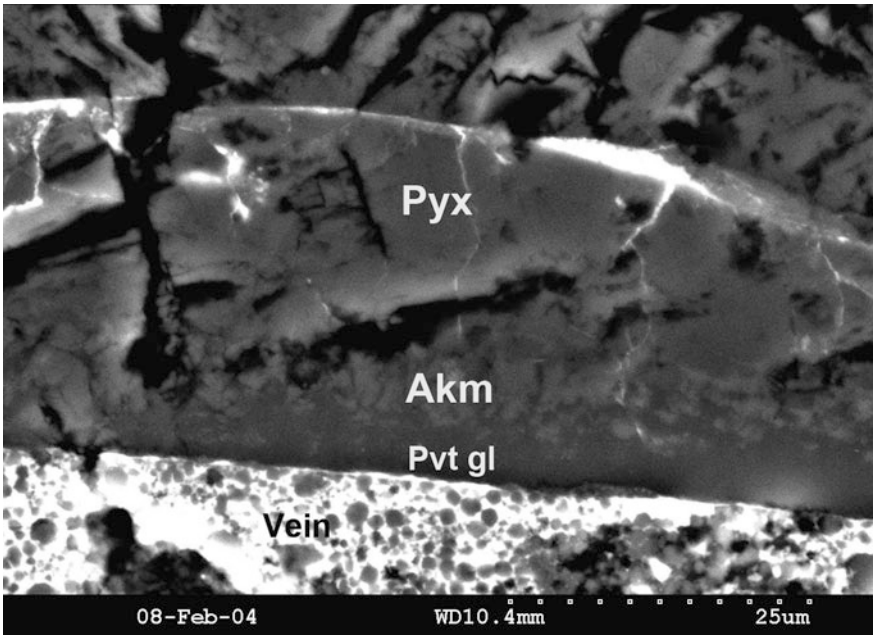

Fig. 5.10 BSE image showing the occurrence of granular akimotoite (*Akt*) in between the low-Ca pyroxene (*Pyx*) and (Mg,Fe)SiO_3 glass (*Pvt gl*) in a shock melt vein (*Vein*) in the Suizhou meteorite (Chen and Xie 2015)

Table 5.3 Chemical compositions of akimotoite and its host pyroxene in the Suizhou meteorite

Oxides	Akimotoite	Host pyroxene
FeO	13.71	13.76
MgO	27.79	27.86
MnO	0.45	0.47
CaO	0.89	0.86
K_2O	0.05	0.03
Na_2O	n.d.	n.d.
Al_2O_3	0.24	0.21
Cr_2O_3	0.16	0.18
TiO_2	0.16	0.19
SiO_2	56.55	56.44
Total	100	100

All data are measured by EDS in wt%
n.d. not detected

and interface-controlled growth similar to that of coarse-grained polycrystalline ringwoodite and majorite. Tomioka and Fujino (1997) interpreted the columnar texture as resulting from a martensitic-like mechanism. However, the TEM data presented by Tomioka and Fujino (1997) are also consistent with a coherent nucleation mechanism without martensitic-like shear (Sharp and DeCarli 2006).

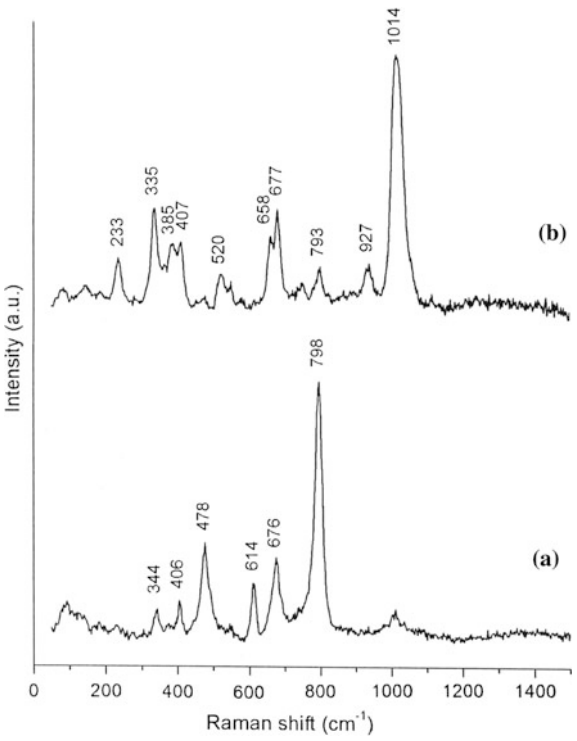

Fig. 5.11 Raman spectra of akimotoite (*a*) and host pyroxene (*b*) in the Suizhou meteorite (Chen and Xie 2015)

Miyagima et al. (2007) reported another mechanism of akimotoite formation in the shock melt veins of the Sixiangkou meteorite, namely the crystallization of akimotoite from shock-induced silicate melt. Akimotoite was identified in this meteorite by its characteristic plate-like morphology. The early crystallization of akimotoite from shock-induced silicate melt can be documented by its idiomorphic crystal morphology, absence of intergrowth textures with clinopyroxene, the coexistence with irregular crystals of majorite in the surrounding area, and higher contents of Al_2O_3 and Cr_2O_3 in akimotoite than clinopyroxene.

In the case of the Suizhou meteorite, akimotoite has two transformation mechanisms. Akimotoite that occurs along the fractures inside pyroxene fragments in the shock-produced melt veins and has the identical composition as low-Ca pyroxene forms from the solid-state transition of orthopyroxene. Akimotoite occurs in a granular texture where the crystal grains have a topotaxial relationship with the host pyroxene and forms a thin belt of randomly oriented akimotoite grains in between pyroxene and $(Mg,Fe)SiO_3$ glass belt which is in direct contact with a shock melt vein and is considered to be formed through homogeneous intracrystalline nucleation and interface-controlled growth similar to that of coarse-grained polycrystalline ringwoodite and majorite.

***P-T* Conditions**

The occurrence of akimotoite in the Suizhou chondrite demonstrates that the akimotoite forms at the region with high pressure and low temperature. It is well known from experiments that at high pressure and high temperature, pyroxene transforms to majorite. The transformation of enstatite to akimotoite requires temperatures in excess of 1550 °C at 22 GPa (Hogrefe et al. 1994). At much higher temperature, pyroxene becomes molten, and subsequently, majorite–pyrope garnet is crystallized from melt at high pressure and temperature. It is common to see the coexistence of coarse-grained polycrystalline ringwoodite aggregates and polycrystalline majorite aggregates, and the high-pressure polymorphs of olivine and pyroxene formed from solid-state transitions, respectively, in the shock vein of meteorites including the Suizhou chondrite. However, akimotoite never occurs in contacting with ringwoodite. Obviously, the solid-state transitions both olivine to ringwoodite and pyroxene to majorite need both high pressure and high temperature.

5.2.4 *Vitrified (Mg,Fe)SiO_3 Perovskite*

Perovskite is a mineral with the composition $CaTiO_3$ and originally was thought to be cubic with Ca coordinated by 12 oxygens in a cubo-octahedral geometry and Ti in an octahedron. Further work showed that it is actually orthorhombic and that Ca is coordinated by eight oxygens. (Mg,Fe)SiO_3 perovskite, being one of the high-pressure polymorphs of pyroxene, is inferred to be the most abundant mineral phase in the Earth's lower mantle.

It is difficult to know who was the first scientist to realize the $MgSiO_3$ enstatite or Mg_2SiO_4 olivine which might transform to the perovskite structure at high pressure, but it was mentioned as a possibility by Ringwood (1962), and Ringwood and Major (1966) synthesized germanates with the orthorhombic perovskite structure, which was possible with an existing high-pressure apparatus. In the first successful experiment on a silicate, Liu (1974) obtained silicate perovskite by starting with pyrope ($Mg_3Al_2Si_3O_{12}$) and laser heating it in a diamond anvil cell at 27–32 GPa to produce $MgSiO_3$ perovskite plus corundum. Today, silicate perovskite is synthesized easily in diamond cells and in large-volume, multianvil apparatus at pressures of 22 GPa and above. Single crystal structure and elastic properties are determined by several investigators. There have, however, been arguments about the range of stability of perovskite at high temperatures and whether it might break down into MgO and SiO_2 under conditions existing in the lower mantle (Saxena et al. 1996). This was disputed by Mao et al. (1997) and Serghiou et al. (1998), and the exact conditions required for perovskite stability are still an open question (Prewitt and Downs 1998). Fei et al. (1996) presented a diagram showing that there is maximum amount of Fe^{2+} that (Mg,Fe)SiO_3 perovskite can accommodate at any given

pressure and temperature. Mao et al. (1997) and McCammon (1998) found that $(Mg,Fe)SiO_3$ perovskite synthesized in both diamond cells and multianvil presses contain a significant amount of Fe^{3+} that can stabilize the structure. This also implies that Al^{3+} can have the same effect and the amount of Fe^{3+} and Al^{3+} in the lower mantle will have a strong influence on the range of stability of perovskite.

$(Mg,Fe)SiO_3$ perovskite has not been found in terrestrial rocks and thus has no mineral name. However, natural $(Mg,Fe)SiO_3$ perovskite was identified in shocked meteorites. Up to now, only two meteorites were reported to contain very small amount of perovskite. Tomioka and Fujino (1997) found that crystalline perovskite transformed from orthopyroxene in the Tenham meteorite. Sharp et al. (1997b) found vitrified perovskite in the shock melt veins of the Acfer 040 meteorite, which was interpreted as an amorphized perovskite during pressure release. The natural occurrence of perovskite is not only important for clarifying the phase transformations of pyroxene and the history of pressure and temperature in shocked meteorites, but also for understanding the phase transformation processes in the Earth's mantle.

In addition to high-pressure polymorphs, pyroxene may also be transformed to amorphous phase or glass at shock-produced high pressure and temperature. Pyroxene glass has been reported mainly on the TEM observations in some shocked meteorites, such as the retrograde glass inverted from majorite in the shock melt veins of Tenham meteorite (Price et al. 1979), the nanometer-sized pyroxene glass as a result of incipient shock melting in the ALH 84001 meteorite (Bell et al. 1999), and the Si–Al-rich glass and augite glass in shocked martian meteorites (Malavergne et al. 2001), and the $CaSiO_3$-rich glass is transformed from diopside in an H chondrite (Tomioka and Kimura 2003).

In comparison with previously found perovskite, vitrified perovskite, and pyroxene glass, in this section we describe a unique occurrence of fine-grained multigranular $(Mg,Fe)SiO_3$ glass that intimately coexisted with majorite (Fig. 5.12) or akimotoite (Fig. 5.10) inside or contacting the Suizhou shock veins. We found large ovoid and zonal $(Mg,Fe)SiO_3$ glass grains that appear to represent the most extensive pyroxene–perovskite transformation observed in meteorites (Chen et al. 2004b).

Occurrence

Chen et al. (2004b) reported that within the shock melt veins in the Suizhou chondrite, some ovoid $(Mg,Fe)SiO_3$ glass grains with crust–core structure in which the grains are up to 120 μm in size. These $(Mg,Fe)SiO_3$ glass grains usually consist of a polycrystalline majorite rim surrounding an ovoid polygranular glassy silicate interior and are surrounded by the fine-grained matrix of garnet, ringwoodite, magnesiowüstite, FeNi metal, and troilite (Figs. 5.12 and 5.13). The majorite rim and the glassy interior have a very similar fine-grained structure. The glassy interior is made of subround or ovoid pockets ranging 60–90 μm in length and 30–70 μm in width. Abundant radiating fractures and cracks were observed in the majorite rim, whereby the cracks terminate at the surface of the glassy interior and the surrounding fine-grained matrix. High-magnification images revealed a granular texture of 1–3 μm in size in both the majorite rim and in the glassy phase. There is a

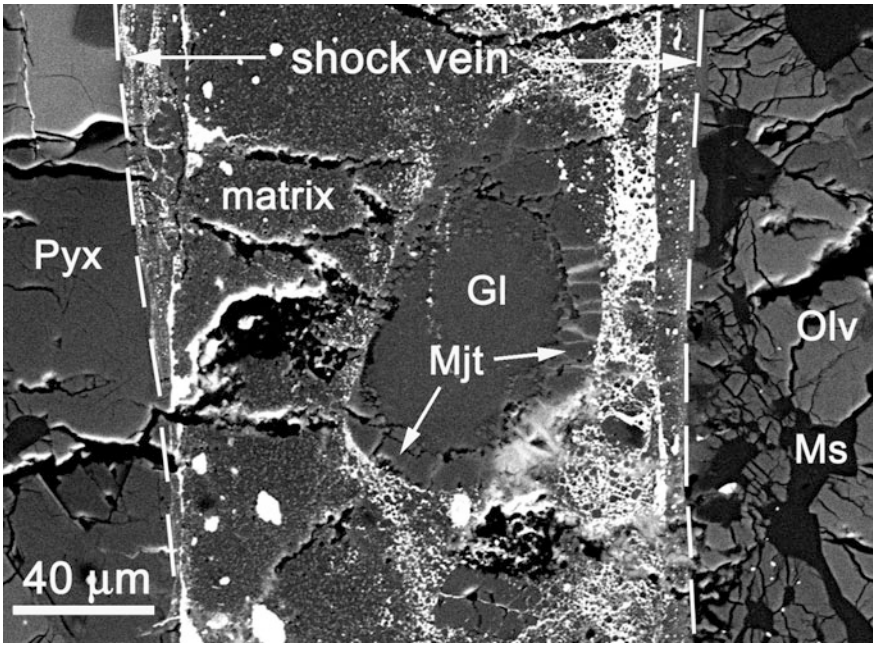

Fig. 5.12 BSE image depicting an ovoid grain consisting of a majorite rim (*Mjt*) and a (Mg,Fe)SiO_3 perovskite glassy interior (*Gl*) in the shock vein. The brighter material inside the shock vein is metal–troilite; Olv = olivine; Pyx = pyroxene; Ms = maskelynite (Chen et al. 2004b)

rough and uneven boundary between the majorite rim and the glassy interior. Small amounts of majorite inclusions of less than several micrometers in size occur in a narrow zone of 5–10 μm in width in the glassy interior adjacent to the inner wall of the majorite rim. Some majorite extends as branches from the inner wall of the majorite rim into the glassy interior (Figs. 5.12 and 5.13). It appears that there is a zone consisting of a mixture of two materials, i.e., majorite plus glass.

Our study strongly suggests that some precursor pyroxene grains inside the Suizhou shock melt veins were transformed to perovskite within the pyroxene grains due to a relatively low temperature, while at the rim region, pyroxene grains are transformed to majorite due to a higher temperature. After pressure release, perovskite is vitrified at post-shock temperature (Chen et al. 2004b).

Chemical Composition

Microprobe analyses show that the low-Ca pyroxene in the chondritic host, the perovskite glassy phase, and the majorite in the ovoid grains are identical in composition, especially the contents of Al_2O_3, CaO, Cr_2O_3, and Na_2O in these three phases are very low and very similar (Table 5.4). This means that the majorite rim in the ovoid grains and their glassy interior have the same composition as their precursor low-Ca pyroxene of the Suizhou meteorite, implying that there were no change in composition during the phase transition processes of pyroxene and no

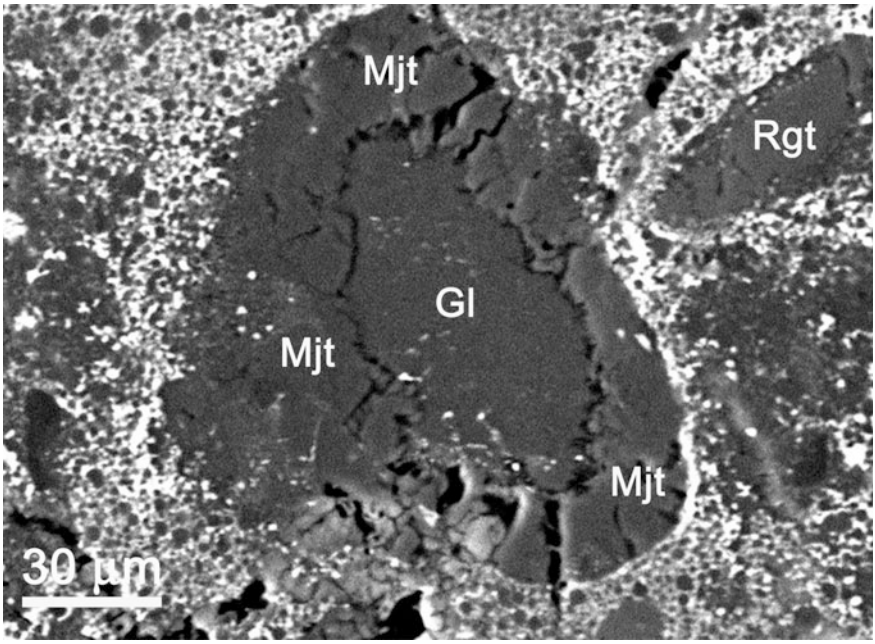

Fig. 5.13 BSE image showing another ovoid grain consisting of a majorite rim (*Mjt*) and a (Mg, Fe)SiO_3 perovskite glassy interior (*Gl*) in the Suizhou shock vein. The *brighter spots* in the glassy interior and the majorite rim are metal and troilite that could have been brought into pyroxene along fractures before the phase transition took place (Chen et al. 2004b)

Table 5.4 Electron microprobe analyses of (Mg,Fe)SiO_3 mineral phases (wt%)

Oxides	Low-Ca pyroxene (10)	Majorite (7)	Silicate glass (7)	Majorite–pyrope (8)
SiO_2	55.82	55.71	55.86	50.42
TiO_2	0.20	0.15	0.17	0.12
Al_2O_3	0.16	0.26	0.35	3.71
FeO	13.64	13.48	12.95	13.83
MnO	0.43	0.46	0.50	0.47
MgO	28.28	28.50	28.37	28.05
CaO	0.73	0.80	0.74	1.92
Na_2O	0.03	0.10	0.08	0.91
K_2O	0.01	0.01	0.03	0.05
Cr_2O_3	0.13	0.15	0.18	0.41
Total	99.43	99.62	99.23	99.79

The numbers in parenthesis are analysis number

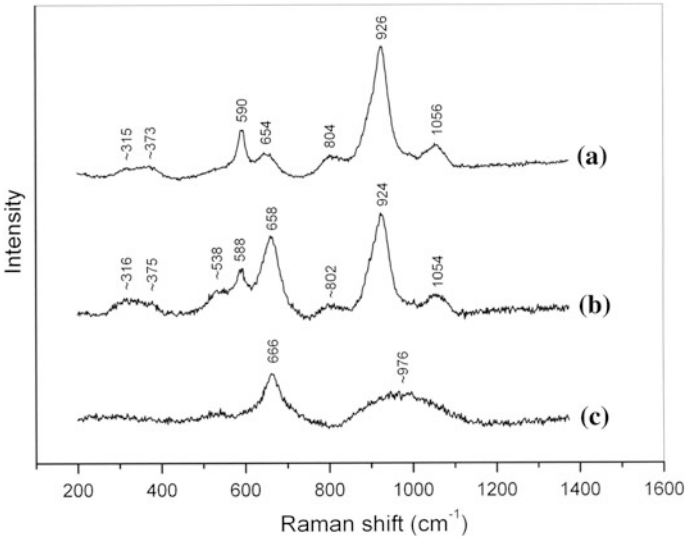

Fig. 5.14 Raman spectra of majorite that contains no glass core (*a*); majorite from the rim of an ovoid grain in Fig. 5.11 (*b*), and (Mg,Fe)SiO_3 perovskite glass from the interior of an ovoid grain in Fig. 5.11 (*c*) (Chen et al. 2004b)

exchanges in chemical elements with surrounding shock-induced silicate melt (Chen et al. 2004b).

Raman Spectroscopy

The Raman spectra of majorite and two (Mg,Fe)SiO_3 phases in an ovoid grain in Suizhou shock vein are shown in Fig. 5.14. The Raman spectrum of majorite that contains no glass core displays sharp bands at 926 and 690 cm^{-1} and weak bands at 315, 373, 654, 804, and 1056 cm^{-1} (Fig. 5.14a). The Raman spectrum of majorite in the rim of the ovoid grain displays sharp bands at 924 and 658 cm^{-1} and weak bands at 316, 375, 538, 588, 802, and 1054 cm^{-1} (Fig. 5.14b), whereas the Raman spectrum of the ovoid grain's glassy interior contains only two broad bands at 976 and 666 cm^{-1} which is typical for MgO–SiO_2 glasses (Fig. 5.14c), which could be attributed to Si–O stretching vibration of SiO_4 tetrahedra and to the inter-tetrahedra Si–O–Si vibration, respectively (McMillan 1984a, b).

Low-Ca Pyroxene–Perovskite Transformation Mechanism

So far, no crystalline (Mg,Fe)SiO_3 perovskite has been confirmed in natural assemblages. The best candidates for finding (Mg,Fe)SiO_3 perovskite are shock-metamorphosed meteorites. Sharp et al. (1997a, b) reported an amorphous (Mg,Fe)SiO_3 phase in association with akimotoite in the shock vein matrix of the Acfer 040 meteorite. These equant amorphous grains are rich in Al_2O_3, CaO, and Na_2O and are believed to have formed as crystalline phase originally from shock-induced dense melt. The formation of a amorphous (Mg,Fe)SiO_3 was interpreted to have amorphized from perovskite after pressure release. However,

Tomioka and Fujino (1997) reported the presence of $(Mg,Fe)SiO_3$ perovskite in the shock veins of the Tenham meteorite. The perovskite is found adjacent to some strongly deformed pyroxene fragments within the shock veins, showing that pyroxene was partially replaced by perovskite without melting. The TEM data presented by Tomioka and Fujino (1997) are consistent with a coherent nucleation mechanism without martensitic-like shear, and the pyroxene in Tenham meteorite is also partially transformed to a granular intergrowth of 200-nm $(Mg,Fe)SiO_3$ perovskite crystallites with the same chemical composition as the precursor pyroxene. This occurrence is consistent with homogeneous nucleation and interface growth.

The granular or equant texture of both the perovskite glass interior and the majorite rim of ovoid grains in Suizhou shock veins shows the material in the interior, and likewise, the majorite rim was a polycrystalline phase before the amorphization of the former. The similarity in the texture of the majorite rim and the amorphous interior strongly suggests a common origin during dynamic process. Furthermore, the $(Mg,Fe)SiO_3$ perovskite glass of the interior and the majorite in the rim have the same chemical composition as the precursor pyroxene. All these occurrences are indicative for a homogeneous nucleation and interface growth.

***P-T* Conditions**

High-pressure experiments indicated that $MgSiO_3$ crystallizes in perovskite structures above 23 GPa and at $\sim$2000 °C (Liu 1974, 1976; Gasparik 1992; Chen et al. 2004a). The finding of a large amount of $(Mg,Fe)SiO_3$ glassy phase, a vitrified perovskite, together with majorite has an important implication for phase transformation processes and the P-T history of shock veins.

5.2.5 *Lingunite, the Hollandite-Structured Plagioclase*

Hollandite is a structure type named after the mineral $BaMn_8O_{16}$. $NaAlSi_3O_8$ hollandite is the high-pressure polymorph of plagioclase which has the crystal structure of hollandite. The structure of hollandite is constructed of edge-sharing octahedra that form a four-sided eight-membered channel that is capable of containing a low-valence large-radius cation (Prewitt and Downs 1998). Together, the O atoms and the large cation form a hexagonal closely packed structure, a sort of analogue to the cubic closely packed perovskite. Ringwood et al. (1967) transformed sanidine into the hollandite structure with Al and Si randomly occupying the octahedral sites at 12 GPa and 900 °C. This was the first oxide structure identified with both Al and Si displaying sixfold coordination and only the second, after stishovite, with ^{6}Si. They postulated that feldspars are the most abundant minerals in the Earth' crust, and it is possible that the hollandite structure with ^{6}Al and ^{6}Si may be a common phase within the transition zone of the mantle. Liu (1978) reported the synthesis of $NaAlSi_3O_8$ hollandite at 21–24 GPa from jadeite plus stishovite. Above 24 GPa, the $NaAlSi_3O_8$ hollandite transforms to the calcium

ferrite structure. Yamada et al. (1984) determined the crystal structure of the $KAlSi_3O_8$ phase by powder diffraction methods, and Zhang et al. (1993) reported the structure as a function of pressure.

First natural occurrence of $NaAlSi_3O_8$ hollandite was reported by Gillet et al. (2000). This high-pressure polymorph of plagioclase was found in the shock melt veins of a Chinese meteorite—Sixiangkou L6 chondrite—and occurs as intergrowths of $NaAlSi_3O_8$ hollandite + albitic glass. Most of the observed glass + hollandite intergrowths are surrounded by ringwoodite grains or the liquidus majorite–$pyrope_{SS}$ + magnesiowüstite, and in some rare cases, jadeitic pyroxene has also been found. The density of this new mineral is 3.80 gm/cm^{-1}, which is about 40 to 50 % higher than that of plagioclase (Gillet et al. 2000). The hollandite-structured plagioclase occurs in and adjacent to shock melt veins in meteorites. It consists of randomly oriented nanocrystals that range in size from 10 to about 100 nm. Optically, the hollandite-structured plagioclase is isotropic and looks like maskelynite (quenched dense plagioclase glass) or melted plagioclase (normal glass).

Another occurrence of $NaAlSi_3O_8$ hollandite in the shock veins of the Tenham chondrite was reported by Tomioka et al. (2000). It occurs as aggregates of extremely fine grains of several tens of nanometers. The hollandite phase seems to have formed from host feldspar in a solid-state reaction during the shock event.

During our recent micro-mineralogical studies on the shock melt veins of the Suizhou L6 chondrite, we also found quite a lot of $NaAlSi_3O_8$ hollandite grains in the shock melt veins of this meteorite (Xie et al. 2001b).

In 2004, the mineral hollandite-structured plagioclase was approved as a new mineral by the Committee of New Minerals, Nomenclatures and Classifications (CNMNC), and this new mineral was named as lingunite after the well-known experimental petrologist Liu, who first synthesized the $NaAlSi_3O_8$ hollandite in laboratory and conducted further characterization of this mineral (Liu 1978; Liu and El Goresy 2007).

The physical and chemical properties, as well as transformation mechanism of lingunite observed in shock melt veins of the Suizhou meteorite, are described in the following sections.

Occurrence

Lingunite, the $NaAlSi_3O_8$ hollandite, occurs as one of the major constituents of coarse-grained high-pressure mineral assemblage in the veins of Suizhou chondrite. The dark colored (under SEM) irregular or rounded grains of lingunite are smooth and unfractured with grain sizes ranging from 8 to 25 μm in diameter. No fractures among the other high-pressure polymorphs in the coarse-grained assemblage of the veins are ringwoodite, majorite, and tuite (Figs. 5.2 and 5.15). These high-pressure minerals are surrounded by the fine-grained majorite–$pyrope_{SS}$ + magnesiuwüstite and metal–troilite eutectic intergrowths.

Chemical Composition

The composition of hollandite-structured feldspars in shocked meteorites ranges from $KAlSi_3O_8$-rich (Langenhorst and Poirier 2000) to $NaAlSi_3O_8$-rich (Gillet et al.

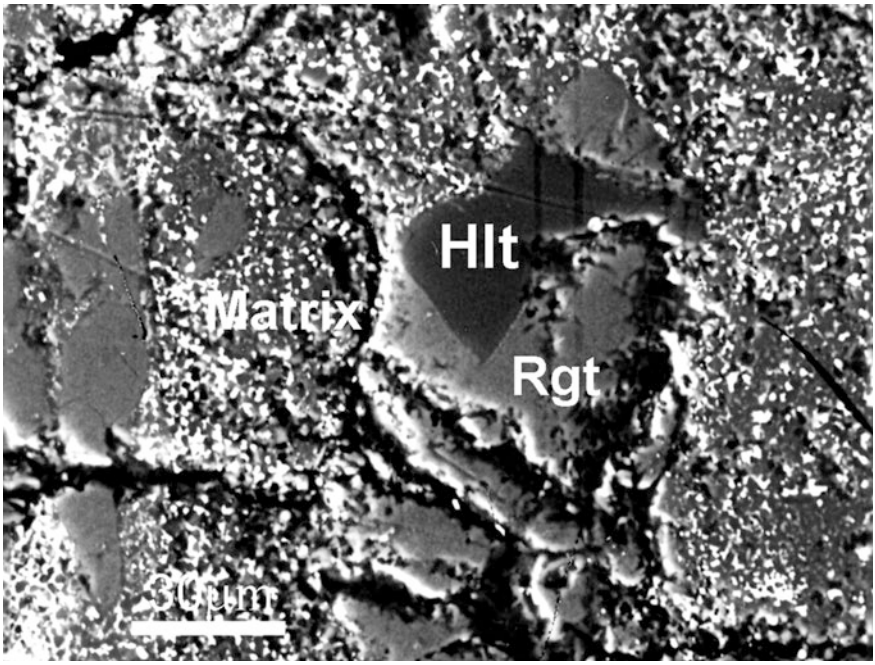

Fig. 5.15 BSE image showing a lingunite, the hollandite-structured $NaAlSi_3O_8$, grain (*Hlt*) in a Suizhou shock vein. Note the smooth and unfractured surface of the grain. Rgt = ringwoodite, Matrix = fine-grained vein matrix

2000) and intermediate plagioclase compositions (Langenhorst and Poirier 2000; Xie and Sharp 2004).

The chemical composition of lingunite in shock melt veins of Suizhou was determined by EPMA. Table 5.5 shows the chemical composition of lingunite and that of plagioclase outside the vein. From this table, we can see that lingunite in shock melt veins has almost the same chemical composition as that of plagioclase (oligoclase) outside the veins. This implies that the Suizhou lingunite was directly formed from plagioclase by phase transformation. The slightly higher FeO, MgO, and Na_2O contents and lower K_2O content in lingunite may be related to the influence of the shock-induced hot silicate melt in its surroundings.

Raman Spectroscopy

The Raman spectroscopic study of the lingunite in Suizhou melt veins and that of plagioclase outside the veins revealed that the Raman spectra of these two minerals are quite different (Fig. 5.16_1). The main peaks for plagioclase outside the veins are at 508 and 1110 cm^{-1} (Fig. 5.16_3). They correspond to Raman modes of Si–O–Si bending vibration and Si–O stretching of the SiO_4 tetrahedra, respectively, whereas the intense peak for lingunite is at 765 cm^{-1}, which is assigned to the Si–O stretching vibrations in the SiO_6 octahedra. The Raman spectrum of Suizhou

Table 5.5 Chemical composition of linguine in the Suizhou shock veins (wt%)

Oxides	SZ-Lglt-1	SZ-Lgt-2	SZ-Lgt-3	SZ-Lgt-4	Lingunite average	Plagioclase average
SiO_2	65.015	65.131	66.161	65.778	65.521	65.764
TiO_2	0.035	0.066	0.000	0.065	0.042	0.043
Al_2O_3	22.270	21.576	20.720	21.401	21.492	21.767
Cr_2O_3	0.000	0.011	0.000	0.022	0.008	0.027
MgO	0.145	0.886	0.506	0.965	0.625	0.004
CaO	2.139	2.454	2.211	2.059	2.216	2.209
MnO	0.000	0.047	0.047	0.000	0.025	0.017
FeO	1.091	1.176	0.925	1.127	1.080	0.414
BaO	0.000	0.000	0.000	0.000	0.000	0.018
Na_2O	9.300	8.401	9.302	9.533	9.134	8.867
K_2O	0.979	1.311	0.969	0.886	1.036	1.313
Total	100.974	101.059	100.841	101.836	101.179	100.443
An	83.59	81.82	83.34	84.71	83.37	80.94
Or	5.79	4.97	5.71	5.18	5.42	8.89
An	10.62	13.21	10.95	10.11	11.22	11.14
Cs	0.00	0.00	0.00	0.00	0.000	0.03

All values were determined by EPMA in wt%
Ab—Albite, Or—Orthoclase, An—Anorthite, Cs—Cesium

hollandite-structured $NaAlSi_3O_8$ can be compared with that of lingunite experimentally transformed from $KAlSi_3O_8$ feldspar (in the M'bale L6 meteorite) at 22 GPa and 1500 K (Fig. 5.16_2) and that of lingunite in Sixiangkou melt veins (Gillet et al. 2000). The lingunite in the Sixiangkou is interwoven with plagioclase glass. The lack of the broad band from 490 to 500 cm^{-1} and the less intense band near 1100 cm^{-1} in the grain of Suizhou lingunite indicates that no silicate glassy phase, such as albitic glass, occurs in the grain (Fig. 5.16_1). It is evident that this would be the first case of finding single-phase crystalline lingunite in natural materials.

Plagioclase–Lingunite Transformation Mechanism

In many heavily shocked chondrites, the transformation of plagioclase to the hollandite structure, like the olivine and pyroxene transformations mentioned in the last paragraphs, occurs in and adjacent to shock melt veins (Chen et al. 1996a, b; Gillet et al. 2000; Xie et al. 2001b). The origin of various hollandite-structured polymorphs of feldspars has been interpreted to be solid-state transformation (Tomioka et al. 2000; Langenhorst and Poirier 2000; Xie and Sharp 2004) and crystallization from melt (Gillet et al. 2000). The nanocrystalline granular texture is consistent with both origins if the melt was pure feldspar composition liquid (Sharp and DeCarli 2006). If formed by a solid-state mechanism, the microstructure suggests homogeneous nucleation and interface-controlled growth, as in the formation of ringwoodite. If the polycrystalline lingunites in melt veins are crystallized from feldspar composition liquids during shock compression, the feldspar composition

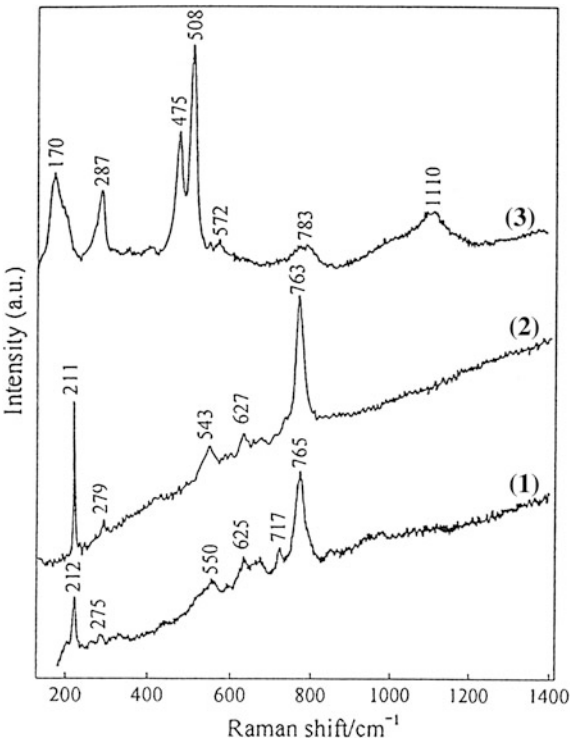

Fig. 5.16 Raman spectra of lingunite ($NaAlSi_3O_8$ hollandite) in the Suizhou melt veins (*1*), experimentally produced $KAlSi_3O_8$-hollandite (*2*) and plagioclase outside the Suizhou veins (*3*)

liquid did not mix with the surrounding chondritic liquid, as one would expect if the liquids are miscible. This suggests that most of the transformation is via a solid-state mechanism. However, veins of lingunite extending away from polycrystalline aggregates in Sixiangkou L6 chondrite indicate that at least some of the plagioclase was molten during shock. The distinction between solid-state transformation and liquid crystallization is an important consideration when using the presence of lingunite to constrain shock pressures (Sharp and DeCarli 2006).

P-T Conditions

On the basis of high-pressure experiments, the presence of lingunite in Suizhou melt veins indicates that the pressure in the veins would not be higher than 23 GPa (Liu 1978). The occurrence of other coarse-grained and fine-grained high-pressure phases constraints the pressure in Suizhou melt veins to be in the range of 18–24 GPa and the temperatures between 1700 and 2300 °C (Xie et al. 2001a; Chen et al. 2003a). It is evident that the hollandite-structured plagioclase would be stable at high pressure up to 23–24 GPa and high temperature up to 1900–2000 °C. Such pressure and temperature regime corresponds to the pressure range from the lower part of mantle transition zone to the upper part of the lower mantle, e.g., 600–700 km deep in the Earth's mantle.

Geochemical Significance

Plagioclase is one of the most common rock-forming minerals in the Earth's crust. The discoveries of lingunite in natural materials, such as in Sixiangkou and Suizhou meteorites, are of important significance in understanding the Earth's mantle geochemistry, because this high-pressure phase is likely to form and survive in the transition zone and the upper part of the lower mantle (Liu 1978; Agee et al. 1995). In spite of its dense structure (40–50 % denser than plagioclase), the large four-sided tunnels along *c*-axis in the structure of this high-pressure phase might accommodate important large mono- and divalent cations, including Na, K, Rb, Sr, and Ba, and carry them from the Earth's surface down into the deep mantle during the subduction processes (Akaogi 2000). Some high-pressure partitioning experiments suggest that, when partial melting occurs in subducted crustal materials, hollandite-type plagioclase can preferentially incorporate several incompatible elements (K, Pb, Sr, light rare earth elements, and so forth) but is not likely to be a host for uranium and heavy rare earth elements (REE), relatively to the coexisting melt (Akaogi 2000). Therefore, the stability of lingunite will strongly influence trace element geochemistry of magma produced in the deep mantle as well as alkali transport processes in the transition zone and the lower mantle.

5.2.6 Tuite, the Dense Polymorph of Whitlockite

It is well known that whitlockite ($Ca_3(PO_4)_2$), together with apatite ($Ca_5(PO_4)_3$(F, OH, Cl)), is among the most important phosphate minerals found in lunar rocks, meteorites, and terrestrial rocks. The compound $Ca_3(PO_4)_2$ has four polymorphs including ά-, α-, β-, and γ-phases, in which the β-phase (whitlockite) is stable at ambient conditions, the γ-phase is stable at high pressure, and the ά- and α-phases are stable at high temperatures (Sugiyama and Tokonami 1987). The trigonal γ-$Ca_3(PO_4)_2$ is a dense phase isostructural with $Ba_3(PO_4)_2$ (Roux et al. 1978), which is 113 % denser than β-$Ca_3(PO_4)_2$. Thermodynamic computations indicate that whitlockite has a relatively low density making it unstable at higher pressures and that it transforms to γ-$Ca_3(PO_4)_2$ at pressures above 2.5 GPa at 1000 °C (Murayama et al. 1986). Multianvil high-pressure experiments using hydroxylapatite and fluorapatite as starting materials revealed that apatite decomposes to γ-$Ca_3(PO_4)_2$ at pressures above 12 GPa and temperatures from 1100 to 2300 °C (Murayama et al. 1986; Roux et al. 1978). Chen et al. (1995a, b) reported that chlorapatite in the shock veins of Sixiangkou meteorite was transformed to the phase A, an unknown high-pressure polymorph of phosphate mineral, at pressures about 23 GPa and temperatures about 2000 °C. However, no high-pressure polymorph of whitlockite was positively identified in any terrestrial and extraterrestrial rocks in the years of last century. Fortunately, the author of this book found the first natural occurrence of the high-pressure polymorph of whitlockite in a shock melt vein of the Suizhou

meteorite. This new mineral and the mineral name "tuite" were approved by the Commission on New Minerals, Nomenclature and Classification (CNMNC) of the International Mineralogical Association (IMA) in 2002 (Xie et al. 2002, 2003). The occurrence, physical and chemical properties, and the formation mechanism of this new mineral are described in the following sections.

Occurrence

Tuite, the new high-pressure anhydrous phosphate phase, occurs in the Suizhou melt veins in the form of tabular polycrystalline grains with rounded outline in both tops. There are only four tuite grains that have been found in the Suizhou veins. The larger three grains are 20 μm × 10 μm, 18 μm × 15 μm, and 18 μm × 6 μm in sizes (Figs. 5.17, 5.18, and 5.19) and the smallest one is only 5 μm × 2.5 μm in size. The surface of tuite grains in the Suizhou vein is very smooth, and neither type showed any fractures, cleavages, or particular microstructure.

In Suizhou shock veins, tuite coexists with other high-pressure phases such as ringwoodite, majorite, and lingunite (Fig. 4.2). The grains of tuite are surrounded by fine-grained vein matrix consisted of majorite–pyrope garnet, FeNi metal, and troilite. Under reflected light and SEM in back-scattered electron mode, tuite grains show gray color that is close to that of ringwoodite and majorite, but lighter than lingunite. However, our synthetic tuite crystals are colorless and transparent with high refractive index and low birefringence. The luster of tuite is vitreous to resinous, and its steak is white.

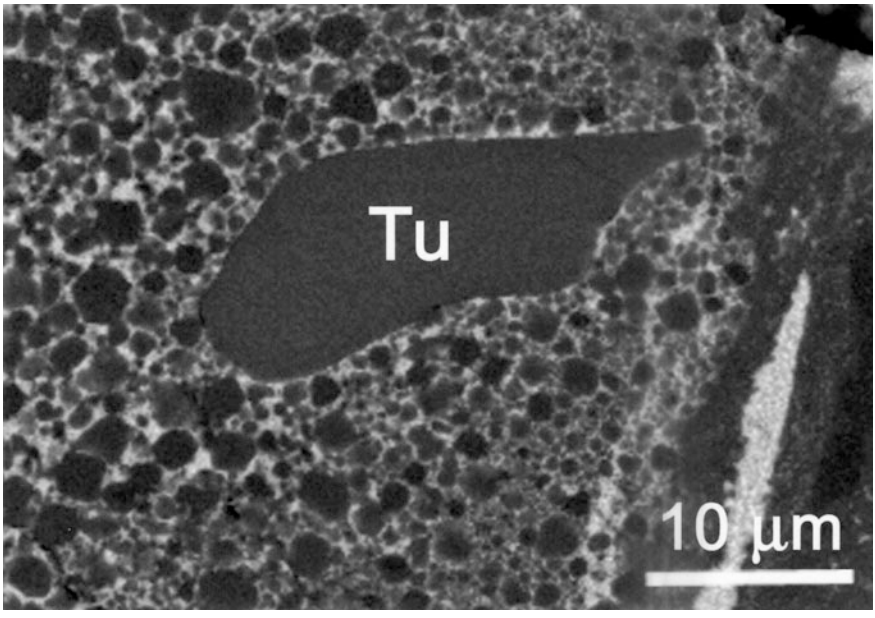

Fig. 5.17 BSE image of a tuite (*Tu*) grain in a shock vein of the Suizhou meteorite

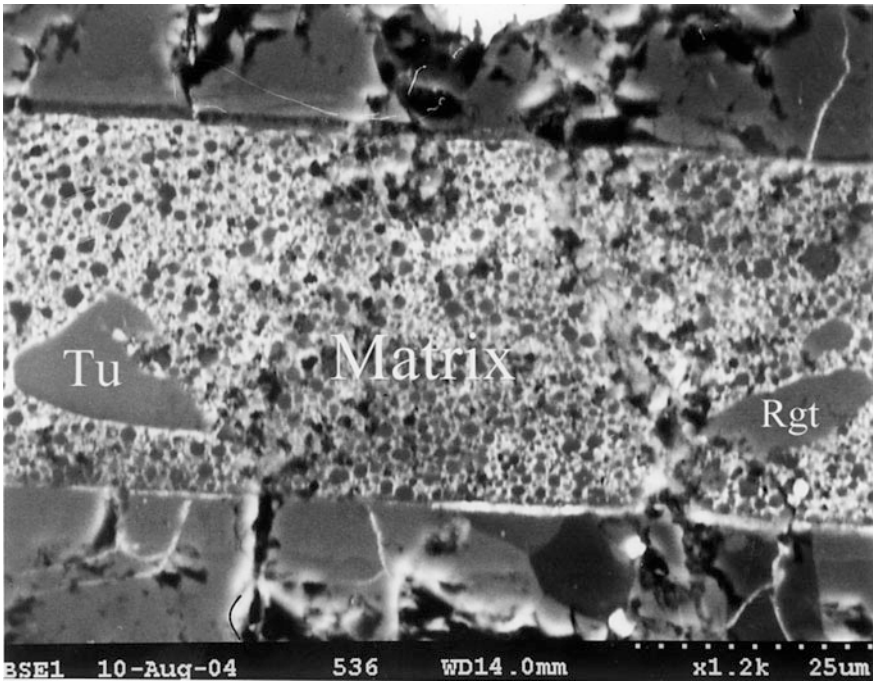

Fig. 5.18 BSE image of another tuite (*Tu*) grain in a shock vein of the Suizhou meteorite. Rgt = ringwoodite, Matrix = fine-grained vein matrix

Optical Properties

Tuite cannot be identified through an optical microscope in transmitted light due to its very small size and thickness and very low abundance. Furthermore, the presence of matrix minerals (FeNi metal, Fe-sulfide, and garnet) underneath the tuite grains in a 30-μm-thick polished thin section makes these tuite grains (about 5 μm in thickness) almost "opaque." Therefore, the optical properties of tuite were determined on the colorless and transparent synthetic tuite crystals of 60–130 μm in size.

The results of our measurements for synthetic tuite crystals are as follows: uniaxial (+), ε = 1.706 (3) and ω = 1.701 (4). Our results show that the optical properties of tuite are in good consistence with the description of Murayama et al. (1986) for their synthetic high-pressure $Ca_3(PO_4)_2$ phase that shows high refractive indices and low birefringence and are markedly different from those of natural whitlockite from Palermo, New Hampshire, USA, which has chemical composition (CaO-46.90, MgO-2.53, P_2O_5-45.68 wt%) similar to that of our tuite in Suizhou but shows uniaxial (−) optical sign with refractive indices of ω = 1.629 and ε = 1.626 (Frondel 1941).

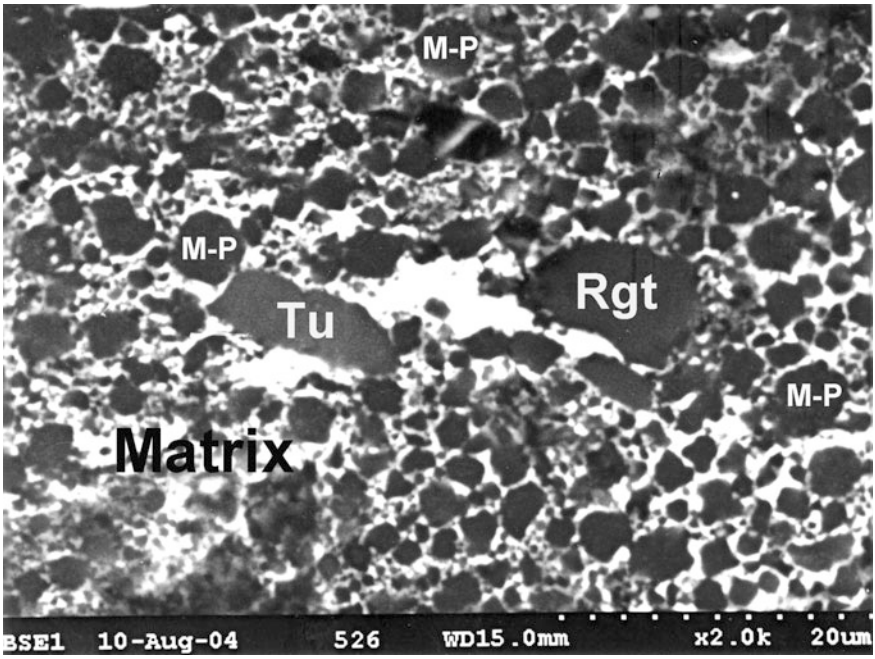

Fig. 5.19 BSE image of the third tuite (*Tu*) grain observed in a shock vein of the Suizhou meteorite. Rgt = ringwoodite, M-P = majorite–pyrope garnet in solid solution, Matrix = fine-grained vein matrix

Chemical Composition

Chemical composition of tuite in the Suizhou meteorite was obtained with a Cameca SX-51 electron probe micro-analyzer. The tabular tuite grain of 10 × 20 μm in size on a polished thin section was probed in three areas (Table 5.6). Results show that this mineral appears homogeneous with empirical formula $Ca_{17.55}(Mg_{1.89}, Fe_{0.11})_{2.00}(Na_{1.93},K_{0.02})_{1.96}(P_{1.01}O_4)_{14}$, or $(Ca_{2.52}Mg_{0.26})_{2.78}Na_{0.25}(P_{1.02}O_4)_2$ which is very similar to that of whitlockite outside the vein, and there are no additional elements incorporated with this high-pressure phosphate phase from the surrounding matrix melt, and no chlorine was detected. Hence, tuite is thought to have been transformed directly from original whitlockite during a shock event and not produced from decomposition of chlorapatite. The simplified formula for tuite may be given as $(Ca,Mg,Na)_3(PO_4)_2$ or $Ca_3(PO_4)_2$.

Raman Spectroscopy

The Raman spectra for the 10 μm × 20 μm grain of tuite in a Suizhou shock vein are shown in Fig. 5.20. They were conducted on the same 3 points of this tuite grain where EPMA data were measured. Interestingly, all three obtained spectra are almost identical and show only one intense peak at 974–975 cm^{-1} with a shoulder at 997 cm^{-1}, two less intense peaks at 411 and 577–578 cm^{-1}, and three weak peaks at 191–192 cm^{-1}, 640–641 cm^{-1}, and 1095 cm^{-1}. The intense Raman peak at

Table 5.6 Electron microprobe analyses of tuite and whitlockite (wt%)

	Tuite				Whitlockite
	1	2	3	Average	
TiO_2	0.06	0.03	0.04	0.04	0.06
FeO	0.33	0.44	0.37	0.38	0.28
MgO	3.60	3.55	3.59	3.58	3.27
CaO	45.91	46.41	46.10	46.14	46.62
NiO	0.03	0.09	0.03	0.05	0.08
Na_2O	2.78	2.82	2.81	2.80	2.57
K_2O	0.05	0.09	0.07	0.07	0.03
Cr_2O_3	0.00	0.01	0.00	0.00	0.03
P_2O_5	47.14	47.19	47.15	47.16	47.67
Total	99.90	100.63	100.16	100.22	100.61

Formula of tuite is given as follows: $Ca_{17.55}(Mg_{1.89},Fe_{0.11})_{2.00}(Na_{1.93},K_{0.03})_{1.96}(P_{1.01}O_4)_{14}$, or $(Ca_{2.51},Mg_{0.29})_{2.80}Na_{0.28}(P_{1.01}O_4)_2$

Formula of whitlockite is given as follows: $Ca_{17.63}(Mg_{1.72},Fe_{0.08})_{1.80}(Na_{1.76},K_{0.02})_{1.78}(P_{1.02}O_4)_{14}$, or $(Ca_{2.52}Mg_{0.26})_{2.78}Na_{0.25}(P_{1.02}O_4)_2$

The calculation bases for both formulae are $O = 56$ and $O = 8$, respectively

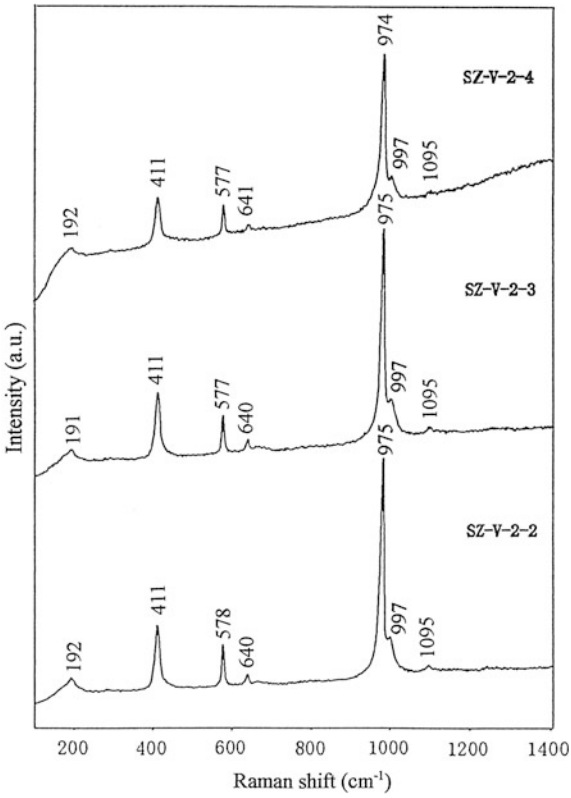

Fig. 5.20 Raman spectra of the Suizhou tuite measured in three spots (SZ-V-2-2 to SZ-V-2-4) (Xie et al. 2003)

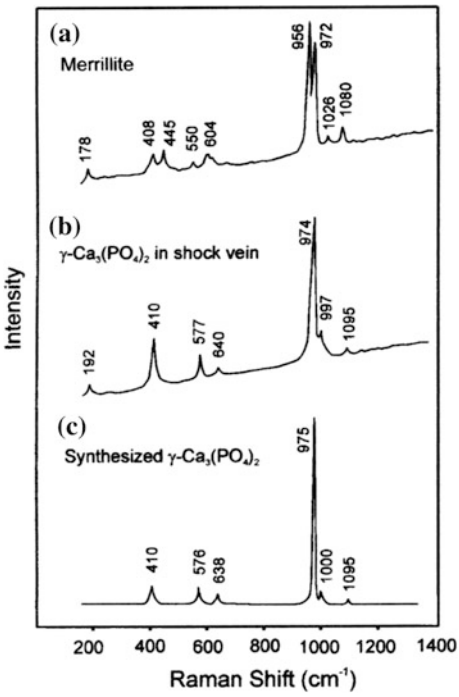

Fig. 5.21 Comparison of Raman spectra of Suizhou whitlockite (merrillite) (*a*), γ-$Ca_3(PO_4)_3$ (tuite) in Suizhou veins (*b*), and synthesized γ-$Ca_3(PO_4)_3$ (*c*) (Xie et al. 2002)

974–975 cm^{-1} can be assigned to the $v1$ symmetric stretching vibration of PO_4 group, and the peak at 1095 cm^{-1} corresponds to $v3$ asymmetric stretching vibration of PO_4, whereas those at 577–578 cm^{-1} and 640–641 cm^{-1} are associated with $v4$ bending mode and those less than 411 cm^{-1} with the lattice modes.

For comparison, the Raman spectra of Suizhou whitlockite, natural γ-$Ca_3(PO_4)_3$ (tuite) in Suizhou veins, and synthesized γ-$Ca_3(PO_4)_3$ are shown in Fig. 5.21. Here, we can see that the Raman spectra of natural and synthetic γ-$Ca_3(PO_4)_3$ are identical, different from that of whitlockite.

It should be pointed out that the Raman spectra of tuite display only one strong peak at 974–975 cm^{-1} that is quite different from the strong doublet of REE-poor whitlockite from 950 to 976 cm^{-1} (Chen et al. 1995a; Jolliff et al. 1996). The well-resolved strong peak of tuite at 974 to −975 cm^{-1} is also distinct from the asymmetric single peak or the very poorly resolved doublet from REE-rich whitlockite (Jolliff et al. 1996). Since both tuite in Suizhou veins and whitlockite outside the Suizhou veins have the same REE-poor composition, and the shock vein is full of high-pressure minerals, the compositional and structural data suggest that a phase transformation from whitlockite to its high-pressure polymorph did take place in the Suizhou shock veins.

X-ray Diffraction Data of Synthetic Tuite

Natural tuite grains we found in the Suizhou shock veins are extremely small. The larger one is 20 μm × 10 μm, and the smaller one is only 5 μm × 2.5 μm in sizes.

These grains are surrounded all round and underneath by the vein matrix minerals, namely majorite garnet, FeNi metal, and troilite (Fig. 5.17). It is impossible to obtain X-ray diffraction pattern from such complicated mineral samples. So, it is important to find X-ray diffraction data of synthetic tuite first. However, Murayama et al. (1986) stated that they examined the synthetic γ-$Ca_3(PO_4)_2$ phase by X-ray powder diffraction analysis, but no diffraction data of this phase have been published in the literature. Therefore, we had to synthesize the γ-$Ca_3(PO_4)_2$ phase in the laboratory at 14 GPa and 1400 °C using $Ca_3(PO_4)_2$ powder as starting material and a multianvil apparatus at the Geophysical Laboratory of the Carnegie Institution of Washington. Then, we collected powder X-ray diffraction data for our synthetic tuite with a Rigaku PSPC-MDG2000 X-ray micro-diffractometer equipped with an imaging plate detector system. All collected diffraction peaks of synthetic tuite are sharp.

The recorded powder X-ray diffraction lines are shown in Fig. 5.22, and the data are listed in Table 5.7. The X-ray diffraction data reveal that the synthetic tuite has a trigonal unit cell with cell parameters of a = 5.2576 and c = 18.7049, and density (calc.) = 3.452 (g/cm^3) (Table 5.8). Our synthetic tuite phase is identical to the high-pressure γ-$Ca_3(PO_4)_2$ phase found by Maruyama et al. (1986) as the decomposition product of apatite at high pressures and temperatures. The structure refinements are also based on crystal structural model for the γ-$Ca_3(PO_4)_2$ phase proposed by Sugiyama and Tokonami (1987). The calculated d-values agree very well with the observed X-ray diffraction data (Xie et al. 2002).

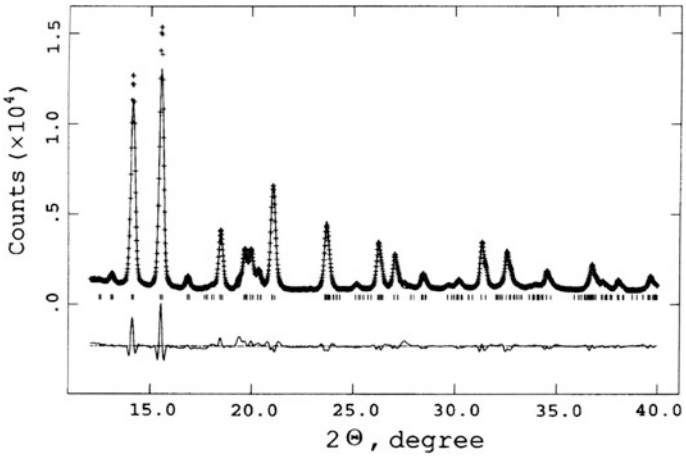

Fig. 5.22 Observed (*crosses*) and calculated (*solid line*) X-ray diffraction pattern for the synthesized γ-$Ca_3(PO_4)_3$ high-pressure phase. The observed data were collected with a wavelength of 0.70927 Å (Mo). *Tick marks* for peak positions of the high-pressure phase are shown below the pattern. The *difference curve* is shown at the *bottom*. The refinement is based on the space group R-3 m with trigonal cell parameters, a = 5.2576 (2) Å and c = 18.7049 (13) Å (Xie et al. 2002)

Table 5.7 X-ray powder diffraction data of synthetic γ-$Ca_3(PO_4)_2$ and tuite

h k l	Synthetic γ-$Ca_3(PO_4)_2$		Tuite	
	$d_{meas.}$	I/I_0	$d_{meas.}$	I/I_0
1 0 1	4.4240	1.6	4.428	6.5
0 0 6	3.1175	4.0	3.118	5.7
1 0 5	2.8905	83	2.891	80.3
1 1 0	2.6288	100	2.628	100
1 1 3	2.4223	4.7	2.423	4.6
2 0 2	2.2120	24.3	2.214	20.3
1 0 8	2.0799	6.2	2.080	5.0
0 0 9	2.0783	10.5	2.078	12.2
2 0 4	2.0469	16.1	2.047	15.7
1 1 6	2.0097	8.2	2.009	8.0
2 0 5	1.9448	50.0	1.945	47.3
2 0 7	1.7324	3.0	1.734	4.3
0 1 10	1.7302	30.8	1.730	24.5
1 1 9	1.6303	3.1	1.627	5.9
1 2 5	1.5634	23.2	1.567	22.2
3 0 0	1.5177	18.2	1.518	18.6
2 0 10	1.4452	8.8	1.445	10.7
1 2 8	1.3860	1.7		
3 0 6	1.3646	1.6		
0 2 11	1.3624	4.4		
2 2 0	1.3144	27.0		
1 2 10	1.2665	23.9		
0 0 15	1.2470	1.2		
1 3 5	1.1965	11.9		
4 0 2	1.1300	1.4		
1 1 15	1.1267	17		
2 2 9	1.1109	4.9		
4 0 4	1.1060	1.2		
4 0 5	1.0890	6.7		
1 3 10	1.0466	10.6		
2 3 5	1.0061	7.4		
1 4 0	0.9936	8.5		
0 4 10	0.9724	2.4		
0 3 15	0.9635	9.5		
1 0 19	0.9622	1.2		
1 0 20	0.9161	2.0		
2 3 10	0.9120	5.7		
2 2 15	0.9046	2.6		
5 0 5	0.8848	1.5		

Table 5.8 Cell parameters of synthesized and natural polymorphs of $Ca_3(PO_4)_2$

Parameters	Synthesized γ-$Ca_3(PO_4)_2$	Synthesized γ-$Ca_3(PO_4)_2$	Natural γ-$Ca_3(PO_4)_2$	Natural β-$Ca_3(PO_4)_2$
a (Å)	5.2487 (6)	5.2576 (2)	5.258 (1)	10.37
c (Å)	18.6735 (36)	18.7049 (13)	18.727 (3)	37.19
Volume (Å^3)	445.5 (1)	447.7 (6)	448.3 (6)	
Composition	$Ca_3(PO_4)_2$	$Ca_3(PO_4)_2$	$Ca_3(PO_4)_2$	$Ca_3(PO_4)_2$
Z	3	3	3	21
Density (calc.) (g/cm^3)	3.469	3.452	3.447	3.12
Density (meas.) (g/cm^3)	3.462	–	–	3.12
Source	Sugiyama and Tokonami (1987)	Xie et al. (2002)	Xie et al. (2002)	Gopal (1974)

Synchrotron Radiation X-ray Diffraction Data of Natural Tuite

The EPMA and Raman spectroscopic investigations revealed that natural tuite has identical chemical composition of whitlockite, but its crystal structure is different with that of whitlockite. Therefore, it is important to obtain its X-ray diffraction data for comparing with those obtained from the synthetic tuite and for characterization of this mineral. For this reason, the larger tuite grain in a thin section was chosen for synchrotron radiation X-ray diffraction in situ analysis.

The X-ray beam of 15 μm × 15 μm in size was focused on the tuite grain of 10 μm × 20 μm in size (Fig. 5.17). The X-ray patterns in fixed orientation of sample indicate polycrystalline nature of the grain, and the collected diffraction lines came not only from the tuite grain but also from all three fine-grained matrix minerals surrounding and underneath the tuite grain. Since the X-ray diffraction patterns of these three matrix minerals are well known, we were able to find a set of lines that do not belong to these minerals but to tuite. Finally, 17 diffraction lines were collected from this natural tuite grain (Xie et al. 2003).

The synchrotron radiation X-ray diffraction lines of natural tuite were compared with the observed X-ray diffraction lines of synthetic tuite. It was found that all reflections ($h\ k\ l$ = 105, 110, 113, 113, 202, 204, 116, 205, 10 10, 125, 300, etc.) and some of their overtones (101, 220, 20 10, etc.) on the diagram of synthetic tuite can be compared with the diffraction lines we collected from natural tuite (Fig. 5.23). Therefore, the powder diffraction pattern of 17 lines with d-values, intensities (I), relative intensities (I/I_o), and Miller indices ($h\ k\ l$) for natural tuite was successfully obtained (Table 5.7).

The trigonal unit cell parameters for natural tuite in the Suizhou meteorite were then calculated as follows: a = 5.258 (1) Å and c = 18.727 (3) Å; space group R-3 m; and density (calc.) = 3.447 (g/cm^3), where the numbers in parentheses are standard deviations in the last significant digits. The structure refinements are also based on crystal structural model for the γ-$Ca_3(PO_4)_2$ phase proposed by Sugiyama and Tokonami (1987).

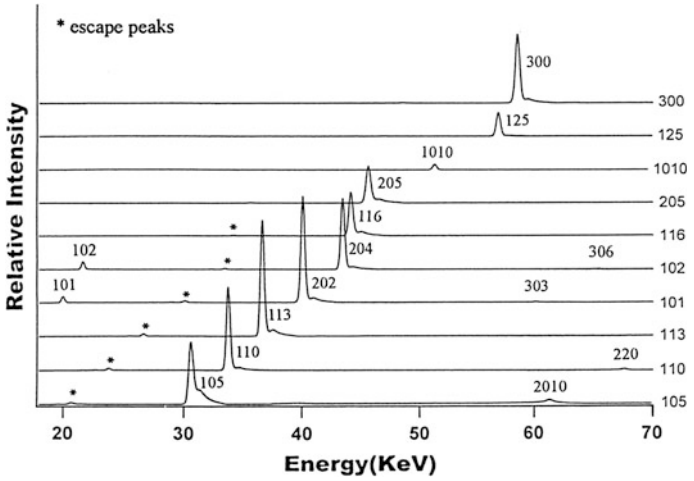

Fig. 5.23 SRXRD patterns of synthetic tuite with randomly picked 10 reflections (Xie et al. 2002)

Whitlockite–Tuite Transformation Mechanism

It was revealed that the tuite grains in the shock veins of the Suizhou chondrite occur as polycrystalline aggregates that have the same chemical composition as the whitlockite in the unmelted chondritic rock of the same chondrite (Xie et al. 2002, 2003). This implies that tuite formed not through decomposition of apatite as it was revealed by experiments of Murayama et al. (1986), but from its host mineral whitlockite via an isochemical solid-state transformation mechanism during shock compression (Xie et al. 2003, 2005a, b).

The polycrystalline nature of the Suizhou tuite grains and the constant composition for three different tuite grains indicate the homogeneous features in chemical composition of tuite crystallites within grains. Therefore, it is reasonable to assume that whitlockite–tuite transformation mechanism in the Suizhou meteorite can be interpreted to be the homogeneous intracrystalline nucleation of tuite crystallites throughout the host whitlockite grain and followed by the interface-controlled growth of crystallites in the grain.

P-T Conditions

It is revealed that shock-produced *P-T* conditions in Suizhou veins were adequate to result in the formation of a series of high-pressure phases. Phase transition from plagioclase to lingunite constrains the pressure and temperature in the shock vein to about 23 GPa and 2000 °C (Liu 1978; Yagi et al. 1994; Gillett et al. 2000; Xie et al. 2001b). Such *P-T* conditions developed in the veins are also available for the solid-state phase transformations from olivine to ringwoodite and from pyroxene to

majorite (Chen et al. 1996a; Xie et al. 2001b). Even though the phase diagrams in Murayama et al. (1986) indicate that the γ-$Ca_3(PO_4)_2$ might form at as low as 12 GPa, it would still be present at 20 GPa or higher. The *P-T* condition suggested by tuite is consistent with the *P-T* conditions (up to 20–23 GPa and 1900–2000 °C) indicated by the other high-pressure phases in Suizhou veins.

Like the Suizhou meteorite, the shock veins of Sixiangkou meteorite contain abundant high-pressure minerals including ringwoodite, majorite, lingunite, fine-grained majorite–pyrope garnet, and magnesiowüstite, which set an upper bound for *P-T* regime of shock vein to be 20–24 GPa and ∼2000 °C (Chen et al. 1996a; Gillet et al. 2000). One may expect that the whitlockite in the shock veins of Sixiangkou should have been also transformed into its high-pressure polymorphs. However, no phase transitions from whitlockite to γ-$Ca_3(PO_4)_2$ phase are observed from its shock veins (Chen et al. 1995a, b). Experiments indicate that the transformation from whitlockite to γ-$Ca_3(PO_4)_2$ takes place at a pressure lower than 20 GPa (Murayama et al. 1986; Sugiyama and Tokonami 1987). It, therefore, shows that the shock-induced pressures in the shock veins of both Suizhou and Sixiangkou are sufficient for the phase transition from whitlockite to γ-$Ca_3(PO_4)_2$. Considering that the Sixiangkou was much more severely shock-metamorphosed than the Suizhou and that there is a great difference in the abundance and thickness of shock veins between the Suizhou and the Sixiangkou, we explain that their cooling history could play a key role in the quenching of this high-pressure polymorph of whitlockite. Evidently, the extremely thin shock veins in the Suizhou meteorite reserve nearly all shock-induced high-pressure phases, whereas an back transformation from the γ-$Ca_3(PO_4)_2$ to whitlockite should have taken place in the shock veins of the Sixiangkou meteorite. In fact, Chen et al. (1995a, b) have observed a difference in Raman spectra between the intact whitlockite in the chondritic region and the whitlockite in the shock veins of Sixiangkou, which could be a hint for the back transformation from the γ-$Ca_3(PO_4)_2$ phase to whitlockite.

Geochemical Significance

Tuite, as the dense phase of whitlockite, has a larger density in comparison with the common minerals in the Earth's mantle, such as majorite garnet and the spinel phase of ferromagnesian orthosilicates, and may stably exist at the Earth's deep horizon. The γ-$Ca_3(PO_4)_2$-structured phases, including tuite, have 12-coordinated Ca(1) site and 10-coordinated Ca(2) site with mean *M-O* distances of 2.74 and 2.59 Å, respectively (Sugiyama and Tokonami 1987). These bonds are much longer than those of 8-coordinated Ca site in garnet and diopside (*M-O* ≈ 2.40 Å). Consequently, the γ-$Ca_3(PO_4)_2$-structured phases have the potential to accommodate very large lithophile elements (VLLE), such as Sr and Ba, and REE, more easily than common mantle minerals and persist as stable crystalline phases in the whole upper mantle (Beswick and Carmichael 1978; Murayama et al. 1986). Therefore, we have identified at least one important natural crystalline phase that is expected to function as a reservoir of VLLE and REE in the deep upper mantle.

5.2.7 High-Pressure Phase of Chlorapatite Decomposition

Apatite [$Ca_5(PO_4)_3(OH,F,Cl)$] and whitlockite [$Ca_3(PO_4)_2$] are among the most important phosphate minerals found in terrestrial rocks, lunar samples, and meteorites (Griffin et al. 1972; Prewitt 1975; Dowty 1977; Buchwald 1984; Nash 1984; Rubin 1997; Engvik et al. 2009). It is known that apatite occurring in meteorites is mainly chlorapatite [$Ca_5(PO_4)_3Cl$]. Chen et al. (1995a, b) reported that chlorapatite in shock veins of the Sixiangkou meteorite was transformed to an unknown high-pressure polymorph called phase A. Subsequently, Xie et al. (2002, 2003) found the high-pressure polymorph of whitlockite with the structure of γ-$Ca_3(PO_4)_2$ in shock veins of the Suizhou meteorite and named it tuite. This section reports our discovery of tuite from a shock vein of the same Suizhou meteorite, which is believed to have formed through the decomposition of chlorapatite, rather than phase transformation from whitlockite (Xie et al. 2013).

Such a decomposition process has also been verified by our high-pressure experiment using synthetic chlorapatite as starting material at 15 GPa and 1573 K (Xie et al. 2013). By comparing the EPMA data and Raman spectra from our natural and synthetic tuites with those for phase A found in shock veins of the Sixiangkou meteorite by Chen et al. (1995a, b), we conclude that phase A is actually a product of incomplete decomposition of chlorapatite. It is revealed that phase A is different in some extend from our tuite phase formed from chlorapatite decomposition both in chemical composition and in crystal structure. Hence, we assume that these two tuite grains in the Suizhou vein can be considered as the high-pressure phase of chlorapatite decomposition.

Occurrence

In a shock vein of the Suizhou meteorite, we detected three Ca-phosphate grains from the EDS measurements (Fig. 5.24). The first smaller one (labeled T1 in Fig. 5.25) is ~10 μm × 20 μm, the second larger one (labeled T2 in Fig. 5.25) ~20 μm × 35 μm, and the third larger one (labeled T3 in Fig. 5.26) ~12 μm × 20 μm. These three grains exhibit no cracks or fractures and are gray in color under reflected light, looking like other high-pressure silicate minerals, such as ringwoodite and majorite in the vein. However, our EDS study revealed that they are not silicate but phosphate of calcium, and their Raman spectra (Fig. 5.27a, b) are almost identical to that of tuite (γ-$Ca_3(PO_4)_2$), the high-pressure polymorph of whitlockite (Fig. 5.20).

Chemical Composition

The EPMA results reveal that, in addition to the major components CaO and P_2O_5, the T1 and T2 grains contain minor amounts of Na_2O and MgO (Table 5.9). Most remarkably, these two grains also contain small amounts of Cl (0.15 wt% in T1 and 1.65 wt% in T2). The marked difference in the Cl content between T1 and T2 leads us to conclude that grain T1 represents a complete transformation product of chlorapatite to tuite, whereas grain T2, though mostly tuite, is likely to contain some relics of the precursor chlorapatite.

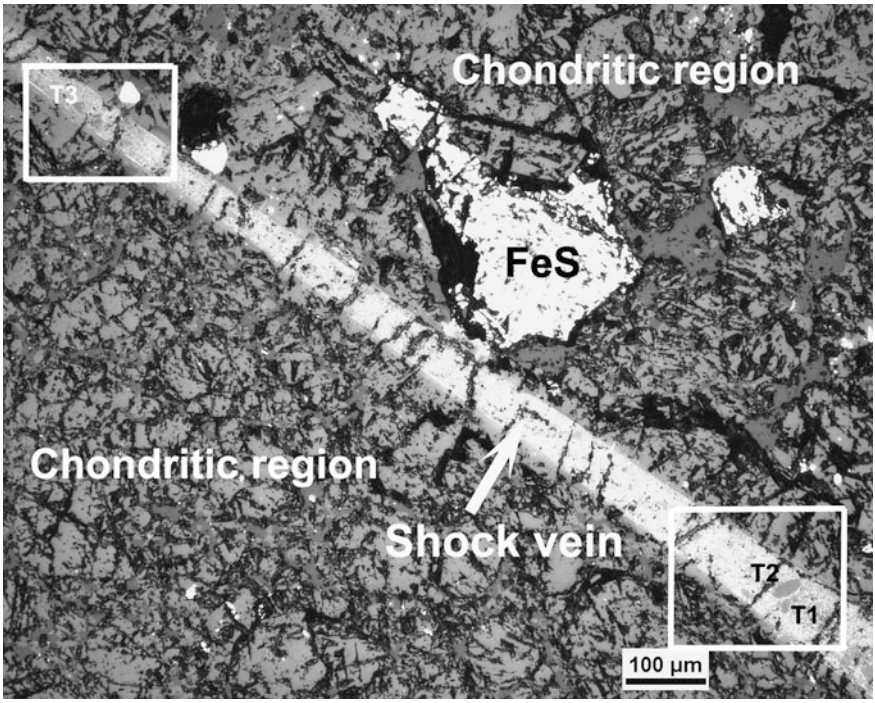

Fig. 5.24 Reflected light microphotograph showing a Suizhou shock vein containing two tuite grains *T1* and *T2* inside the *lower right rectangle* and another tuite grain *T3* inside the *upper left rectangle area* (Xie et al. 2013)

It is interesting to mention that the observed third phosphate grain (T3) occurs in the same shock vein where tuite grains T1 and T2 occurred (Fig. 5.24). On the basis of electron microprobe analysis (Table 5.9, last column) and Raman spectroscopy, the T3 grain is identified as tuite as well, but its precursor mineral is whitlockite, rather than chlorapatite, because it contains 2.88 wt% of Na_2O and 3.43 wt% of MgO, and no detectable Cl.

Raman Spectroscopy

The Raman spectra of the T1 and T2 grains (Fig. 5.27a, b) are directly comparable to the spectrum of tuite transformed from whitlockite at high pressure (Fig. 5.20). Specifically, both Raman spectra of the T1 and T2 grains display an intense peak at 977 cm^{-1}; three less intense peaks at 1096, 412, and 577 cm^{-1}; and two weak peaks at 1001–1002 and 640 cm^{-1}, which are characteristic for Raman spectrum of tuite.

On the basis of Raman spectroscopy and EPMA data, we conclude that the grain T1 has completely transformed to tuite, whereas grain T2, though mostly tuite, is likely to contain some relics of the precursor chlorapatite. In fact, the very weak peak at 957 cm^{-1} on the Raman spectrum for the T2 grain (Fig. 5.27b) may lend further support to our conclusion, because this peak does not belong to tuite, but is characteristic of chlorapatite.

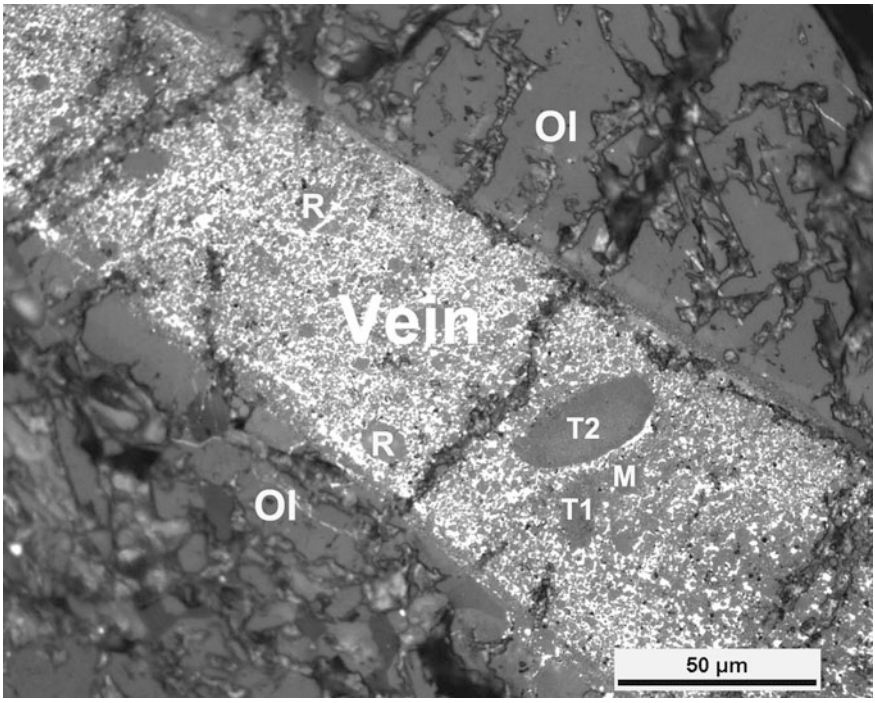

Fig. 5.25 Enlarged reflected light microphotograph of the *lower right rectangle area* in Fig. 5.4, showing the two tuite grains *T1* and *T2*. R = ringwoodite, M = majorite, Ol = olivine (Xie et al. 2013)

Synthesized High-Pressure Phase Tuite from Chlorapatite

The phase transition of chlorapatite to tuite was conducted using synthetic chlorapatite as starting material at high-pressure and high-temperature condition. First, reagent-grade $CaCO_3$, NH_4Cl, and $NH_4H_2PO_4$ powders were mixed in a proportion corresponding to the $Ca_5(PO_4)_3Cl$ stoichiometry. The mixture was ground for 2 h in an agate mortar and pressed into pellets with a diameter of 5 mm under uniaxial pressure of 30 MPa. Second, the pellets were sintered in a conventional muffle furnace at 1273 K for 36 h to form a single phase of $Ca_5(PO_4)_3Cl$, which was confirmed by powder X-ray diffractometer. Third, the $Ca_5(PO_4)_3Cl$ was used as the starting material and put into a Pt capsule to synthesis tuite at 15 GPa and 1573 K for 24 h using a multianvil apparatus. The high-pressure and high-temperature experimental details were described in Xue et al. (2009). Our high-pressure synthesized semi-euhedral tuite crystals up to 50 μm in size are shown in Fig. 5.28.

The electron microprobe analyses on ten synthesized tuite crystals produced an average composition (wt%): CaO—54.24, P_2O_5—46.23, total—100.48, yielding a chemical formula of $Ca_3(PO_4)_2$ when normalized on the basis of 8 O atoms. The Raman spectrum of synthetic tuite is given in Fig. 5.27c, which consists of one intense peak at 977 cm^{-1}; two less intense peaks at 412 and 1095 cm^{-1}; and three

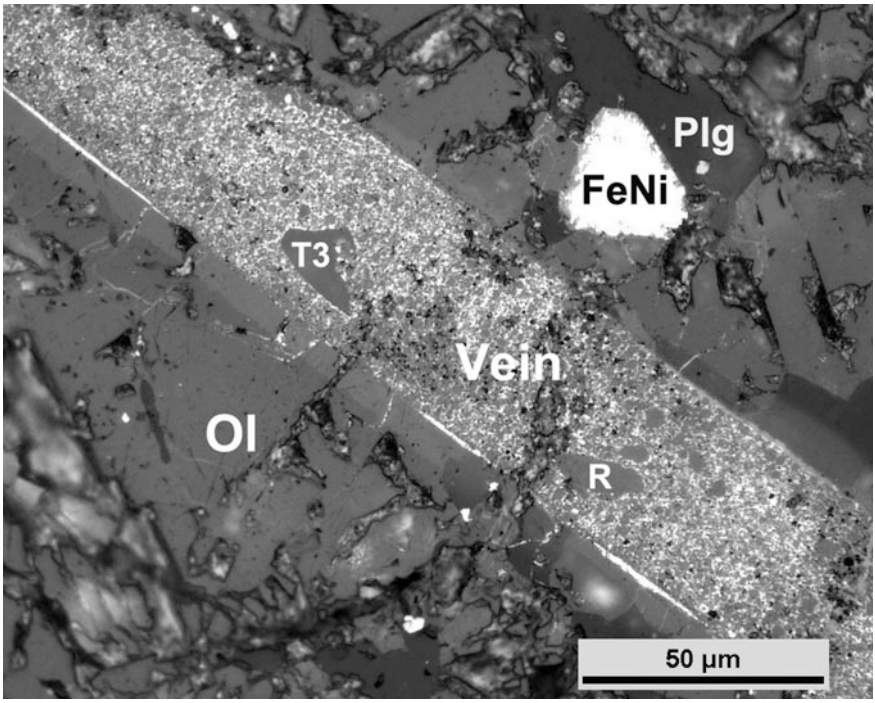

Fig. 5.26 Enlarged reflected light microphotograph of the *upper left rectangle area* in Fig. 5.4, showing the tuite grain *T*. R = ringwoodite, Ol = olivine, Plg = plagioclase, FeNi = metal (Xie et al. 2013)

weak peaks at 578, 640, and 1001 cm^{-1}. This spectrum is identical to the Raman spectra of Suizhou tuite, and the γ-$Ca_3(PO_4)_3$ phase synthesized directly from $Ca_3(PO_4)_2$ at 14 GPa and 1400 °C for 24 h (Fig. 5.21c). Hence, we conclude that the high-pressure phase of chlorapatite decomposition is tuite.

X-ray Diffraction Data of Synthetic Tuite from Chlorapatite Decomposition
We also measured the X-ray powder diffraction patterns for both synthetic tuite and its starting material chlorapatite (Fig. 5.29). The calculated cell parameters of the synthetic tuite are as follows: a = 5.2507 (13) Å, c = 18.6746 (60) Å, V = 445.89 (21) $Å^3$, and ρ = 3.465 (2) g/cm^3. From the above experimental data, it is evident that we have successfully synthesized tuite from chlorapatite through a decomposition reaction.

It should be pointed out that we did not detect any other phase except tuite in the synthesized sample by means of both Raman spectroscopy and X-ray diffraction. The microprobe element maps for the synthesized tuite sample show only Ca and P, and no measurable Cl. Nonetheless, very low level of Cl was detected in some interstices between tuite crystals (Fig. 5.30). The EDS analyses of elements Ca, P, O, and Cl also show that the contents of Cl for six synthesized tuite crystals with different sizes are extremely low (0.01–0.08 wt%) (Fig. 5.31 and Table 5.10).

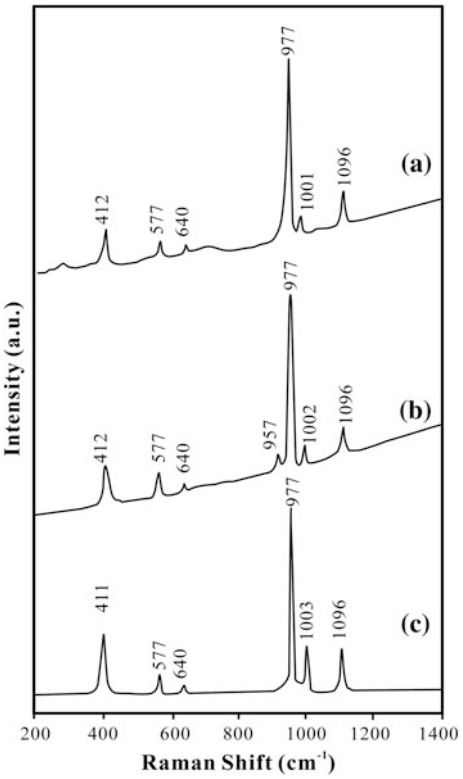

Fig. 5.27 Raman spectra of natural and synthetic tuites transformed from chlorapatite decomposition. *a*—Suizhou tuite grain T1, *b*—Suizhou tuite grain T2, *c*—tuite synthesized from chlorapatite (Xie et al. 2013)

Table 5.9 Microprobe analyses of three tuite grains in a Suizhou shock vein (wt%)

	Grain	T1	Grain	T2	Grain	T3
	(3)	s.d.	(3)	s.d.	(2)	s.d.
Na_2O	0.15	0.01	0.10	0.03	2.88	0.12
K_2O	0.01	0.01	–	–	–	–
MgO	0.85	0.12	0.24	0.07	3.43	0.25
CaO	53.01	0.08	54.35	0.41	46.71	0.58
MnO	–	–	0.01	0.01	–	–
Al_2O_3	–	–	–	–	–	
P_2O_5	45.24	0.07	44.65	0.54	47.90	0.43
Cl	0.15	0.02	1.65	0.14	–	–
	99.40		101.01			
–O = Cl	0.03		0.44			
Total	99.37		100.57		100.92	

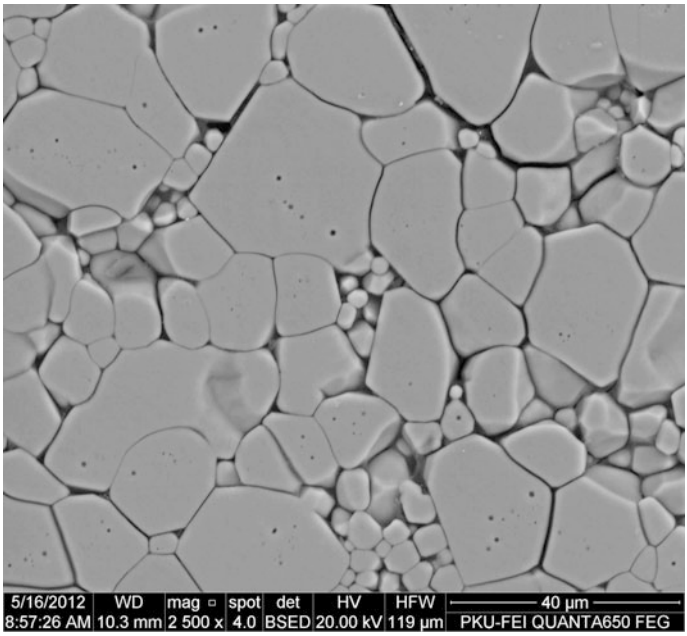

Fig. 5.28 BSE image showing aggregate of semi-euhedral tuite crystals synthesized from chlorapatite at 15 GPa and 1573 K for 24 h using a multianvil apparatus. Note the different sizes of tuite crystals (Xie et al. 2013)

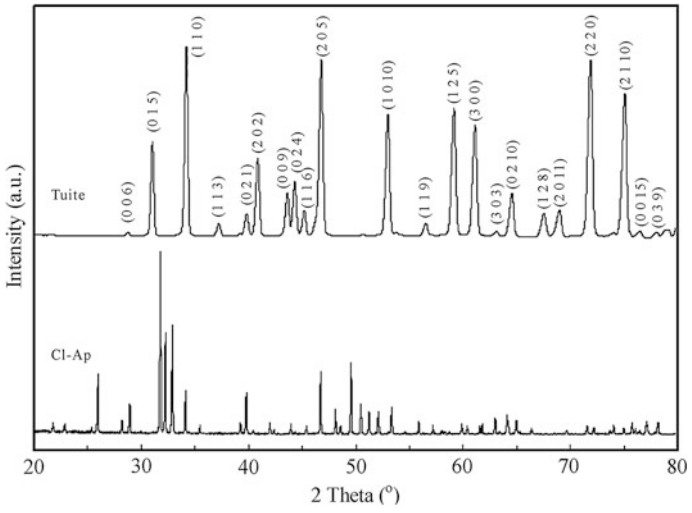

Fig. 5.29 X-ray powder diffraction patterns of synthesized tuite (*Tuite*) and starting material chlorapatite (*Cl-Ap*). Note the big difference between these two patterns (Xie et al. 2013)

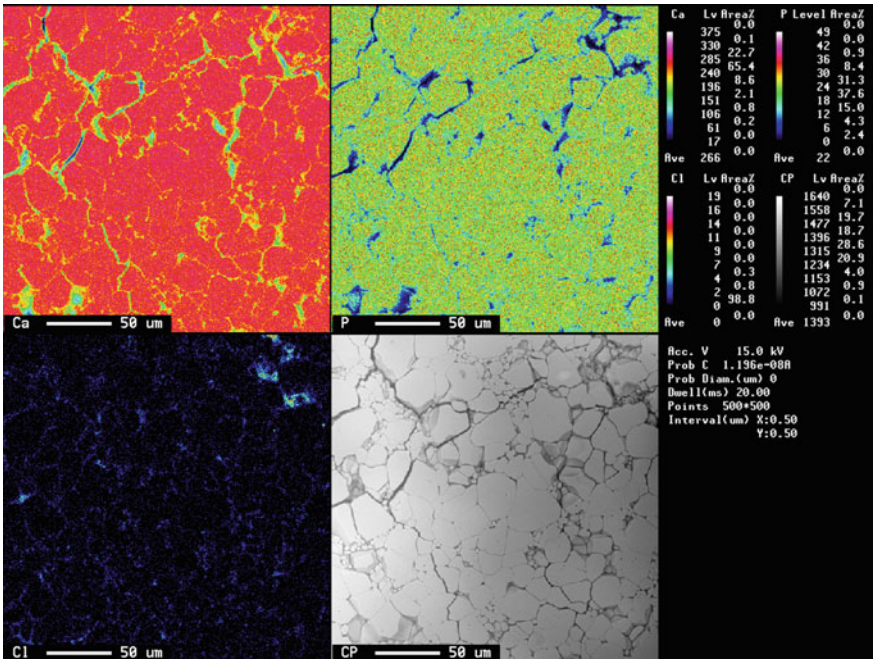

Fig. 5.30 Microprobe element maps of Ca, P, and Cl for synthesized tuite crystals. CP is the BSE image of synthesized tuite sample. Note that the chlorine is absent in tuite crystals (Xie et al. 2013)

Chlorapatite–Tuite Transformation Mechanism

Tuite was first identified in very thin shock veins of the Suizhou L6 chondrite as the high-pressure polymorph of whitlockite (Xie et al. 2002, 2003). Our recent study further demonstrates that tuite can also be formed as the high-pressure product of chlorapatite decomposition.

It is easy to understand that whitlockite changes to tuite just through an isochemical solid-state phase transition under high pressures and high temperatures, but the change of chlorapatite to tuite requires a decomposition reaction: $2\ Ca_5(PO_4)_3Cl \rightarrow 3\ \gamma\text{-}Ca_3(PO_4)_2 + CaCl_2$. Hence, the search for the $CaCl_2$ phase becomes crucial to understand the decomposition process for chlorapatite. However, as we mentioned above, our exhaustive examination with different experimental techniques did not uncover any $CaCl_2$ phase in either natural or synthetic sample. Interestingly, Murayama et al. (1986) synthesized tuite from hydroxylapatite [$Ca_3(PO_4)_2(OH)$] and fluorapatite [$Ca_3(PO_4)_2F$] at high temperatures (1100–2300 °C) and pressures (10–15 GPa). The only phase they identified from the runs above 12 GPa is tuite, despite their intensive search for diffraction peaks ascribable to the possible decomposition components, such as $Ca(OH)_2$, CaF_2, or CaO. Murayama et al. (1986) assumed that this is probably because the fractions of possible decomposition components are too small (<10 wt%) and too widely dispersed in the polycrystalline texture of tuite to be detected by X-ray

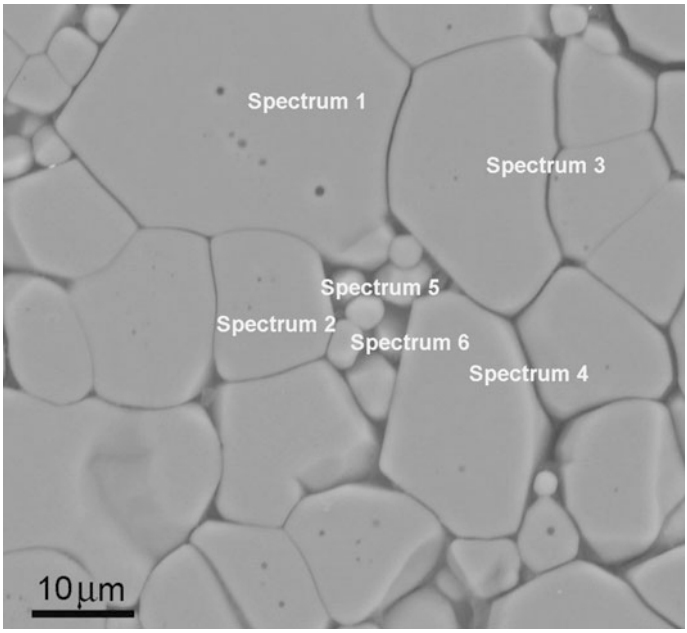

Fig. 5.31 BSE image of the enlarged central area of Fig. 5.27, showing the locations for energy-dispersive spectroscopic analyses

Table 5.10 EDS analyses of synthesized tuite crystals at six different locations (wt%)

Element	Sp*.1	Sp.2	Sp.3	Sp.4	Sp.5	Sp.6	Average
Ca	34.49	35.11	34.79	34.46	34.39	31.40	33.60
P	20.83	20.38	19.91	20.39	20.20	18.75	20.08
O	44.60	44.47	45.22	45.14	45.37	49.84	45.77
Cl	0.08	0.04	0.08	0.01	0.04	0.01	0.04
Total	100.00	100.00	100.00	100.00	100.00	100.00	

**Sp*. spectrum

diffraction. We agree with Muyarama's explanation since we also found the complete or substantial loss of Cl in our synthetic or natural samples.

P-T Conditions

On the basis of the experimental data for chlorapatite (this study) and those for both hydroxylapatite and fluorapatite (Murayama et al. 1986), it appears that tuite can form at pressures as low as 10 GPa, and it is probably stable up to 20 GPa or higher (Murayama et al. 1986). This pressure stability range for tuite formed through the chlorapatite decomposition should be compared with that (up to 22 GPa) estimated from the other high-pressure phases in the veins of the Suizhou meteorite (Xie et al. 2002).

Geochemical and Mineralogical Significance

The volatile element-bearing apatites are known to be stable at shallower horizons of the upper mantle (Beswick and Carmichael 1978). At higher pressures and temperatures in the deep upper mantle, where volatile components are lacking, apatites eventually decompose to tuite (Murayama et al. 1986; Xie et al. 2003). Since the Earth's mantle has a chondritic composition with ~0.26 wt% P_2O_5 (Mason 1966), the behavior of phosphate minerals at depths in the terrestrial mantle where neither apatite nor whitlockite exists stably is of great interest for understanding the behavior of rare earth elements (REE) and other large lithophile elements. Consequently, tuite, stable at deeper mantle pressures and temperatures, could act as a potential host for REE, Na, Sr, and Ba (Murayama et al. 1986; Sugiyama and Tokonami 1987; Xie et al. 2003).

Chen et al. (1995a, b) reported that chlorapatite in shock veins of the Sixiangkou meteorite was transformed to an unknown high-pressure polymorph called phase A. This phase has a similar composition as the unshocked chlorapatite, but its Cl content (3.72 wt%) is lower than that for unshocked chlorapatite (4.48 wt%). Its Raman spectrum is also noticeably different from that for the unshocked hexagonal or monoclinic apatite, because the intense peak at 962 cm^{-1} for chlorapatite is split into three peaks at 960, 974, and 998 cm^{-1} in phase A, and the 430 and 591 cm^{-1} peaks are shifted to 414 and 582 cm^{-1}, respectively, but the 1081 cm^{-1} peak is shifted to 1092 cm^{-1} (Chen et al. 1995a, b). By comparing the Raman spectrum of phase A with that of our natural or synthetic tuite formed from the chlorapatite decomposition, we noticed some similarities between the Raman spectra of two phases, namely the intense peak at 974 cm^{-1} and the weak peak at 998 cm^{-1}; in addition, the three peaks at 414, 582, and 1092 cm^{-1} for phase A are similar to those for tuite. However, the 960 and 668 cm^{-1} peaks for phase A appear to match those for chlorapatite. In particular, the 960 cm^{-1} peak is still considerably strong. Accordingly, we believe that the Raman spectrum of phase A is actually a mixture of tuite and chlorapatite and the coexistence of tuite and chlorapatite implies an incomplete decomposition transformation of chlorapatite in the shock veins of the Sixiangkou meteorite. The rather high Cl content in phase A (3.72 wt%) bears additional evidence for our inference. Nevertheless, the nature of phase A in the Sixiangkou meteorite is still not fully understood, and the further investigation on this phase is needed.

5.2.8 *Xieite, the $CaTi_2O_4$-Type Dense Polymorph of Chromite*

Chromite is an important member of the spinel group. It is known that spinel-type AB_2O_4 compounds occur in many geological settings of the Earth's crust and mantle, as well as in lunar rocks and meteorites. High-pressure AB_2O_4 compounds are of great importance for the understanding of the constituents of the deep Earth.

More than forty years ago, in search of denser polymorphs of the then newly discovered silicate spinel (ringwoodite) and modified spinel (wadsleyite) that are stable at the pressure and temperature conditions of the Earth's transition zone, Ringwood proposed orthorhombic $CaFe_2O_4$-type and $CaTi_2O_4$-type structures as the top candidates for "post-spinel" transitions in the Earth's mantle (Reid and Ringwood 1969, 1970). High-pressure experiments revealed that AB_2O_4 compounds at high pressure might adopt $CaFe_2O_4$-, $CaMn_2O_4$- and $CaTi_2O_4$-type structures, whereby their structures attain atomic arrangements such that these structures become denser than spinel (Reid and Ringwood 1970). Experimental investigations have also indicated that the spinel compounds Mn_2O_3 and Fe_2O_3, and $MgFe_2O_4$ transform to a $CaFe_2O_4$-type structure at pressure above 25 GPa, that the $CaAl_2O_4$ and $MgAl_2O_4$ transform to a $CaFe_2O_4$ structure at pressure above 26.5 GPa, and that the $MgAl_2O_4$ structure changes to a $CaTi_2O_4$ structure at pressure above 40 GPa (Reid and Ringwood 1969; Mao et al. 1974; Irifine et al. 1991; Funamori et al. 1998; Akaogi et al. 1999; Fei et al. 1999; Andrault and Bolfan-Casanova 2001). In addition, $CaFe_2O_4$-type $NaAlSiO_4$ was experimentally shown to be stable at lower mantle conditions (Liu 1978; Irifune et al. 1994; Yagi et al. 1994; Tutti et al. 2000). However, no dense post-spinel polymorphs have been discovered in nature and confirmed as new minerals.

Chromite is one of the opaque accessory minerals in the Suizhou meteorite. During our recent study of the shock-related mineralogical features of the Suizhou meteorite, we discovered two post-spinel polymorphs of chromite (the dense $FeCr_2O_4$ phases) in the shock melt veins and in the areas directly adjacent to veins (Chen et al. 2003a, b). They are $CaTi_2O_4$- and $CaFe_2O_4$-structured $FeCr_2O_4$. Both these phases are new minerals found in nature.

In February 2008, the Commission on New Minerals, Nomenclature and Classification of the IMA approved this new mineral and its name "xieite" for the $CaTi_2O_4$-structured phase (IMA 2007-056). The mineral name, xieite, is from Prof. Xiande Xie, the former president of the IMA from 1990 to 1994, in honor of his contribution to mineralogy and shock effects of minerals.

The finding of above-mentioned two new minerals is important for understanding the structural characteristics of natural AB_2O_4 compounds under high pressure and temperature. The brief introductions of these two post-spinel dense polymorphs are sequentially described in this paragraph.

Occurrence

The chromite grains in the Suizhou meteorite usually contain abundant cracks and fractures (Figs. 3.43 and 3.44). However, the grains of chromite composition inside the Suizhou shock veins show smooth, unfractured surface and much brighter color in comparison with chromite outside the veins and with other high-pressure minerals in veins. This high-pressure phase has then been identified as the $CaTi_2O_4$-structured $FeCr_2O_4$, a dense post-spinel polymorph of chromite. It occurs as compact polycrystalline aggregates of about 5–40 μm in grain size and commonly displays as pseudomorph of chromite crystals or its fragments.

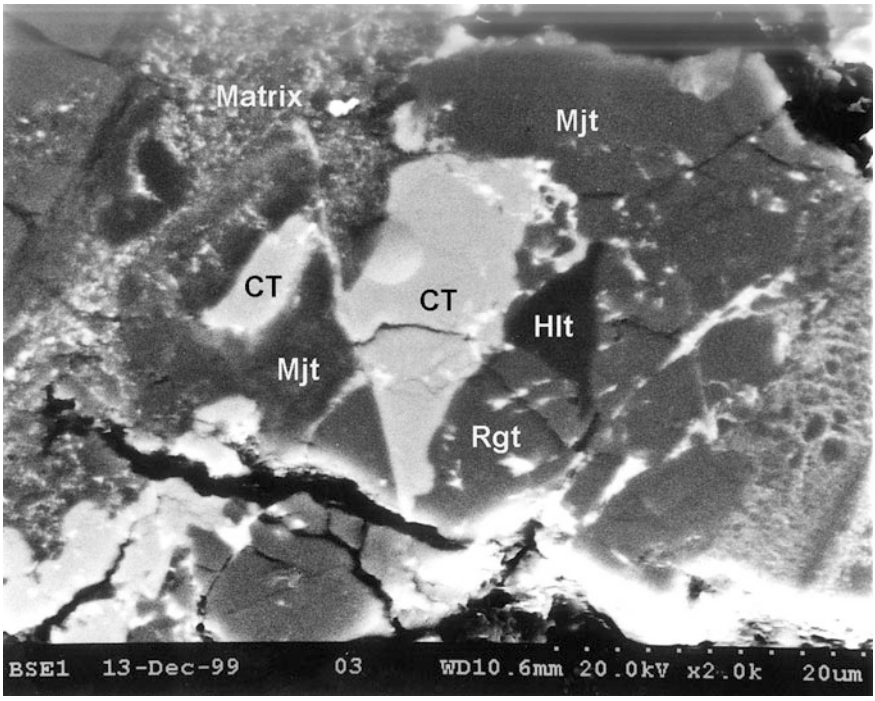

Fig. 5.32 BSE image showing two xieite (*CT*) grains surrounded by other high-pressure minerals. Rgt = ringwoodite, Mjt = majorite, Hlt = lingunite, Matrix = vein matrix

The grain sizes of xieite are relatively small (less than 20 μm). These small grains consist of dense phase only. Neither intergrowth of the dense phase and chromite, nor single grains of chromite have been observed inside the shock veins. Figure 5.32 is a BSE image displaying a semi-euhedral crystal of this dense phase that occurs in the close association with high-pressure minerals of the vein, such as ringwoodite, majorite, and lingunite. Figure 5.33 demonstrates a small single xieite grain of 10 μm × 4 μm in size embedded in the fine-grained vein matrix of the Suizhou meteorite. It is light gray in color and has smooth and unfractured surface.

Figures 3.34 and 5.35 show a xieite (CT) + chromite (Chr) intergrowth grain in a shock vein of the Suizhou meteorite. The xieite phase is directly contacting the vein wall, and the chromite phase is in the far side of the grain. It should be pointed out that there exists another high-pressure phase of chromite, the CF phase, in between the xieite and the chromite phases in this intergrowth grain.

Chemical Composition

The result of electron microprobe analysis of xieite is shown in Table 5.11. From this table, we can see that the chemical compositions of xieite are identical to those of chromite outside the veins (refer to Table 3.6). The main compositions of xieite are ~57 wt% Cr_2O_3 and 29 wt% FeO. The other minor components are Al_2O_3,

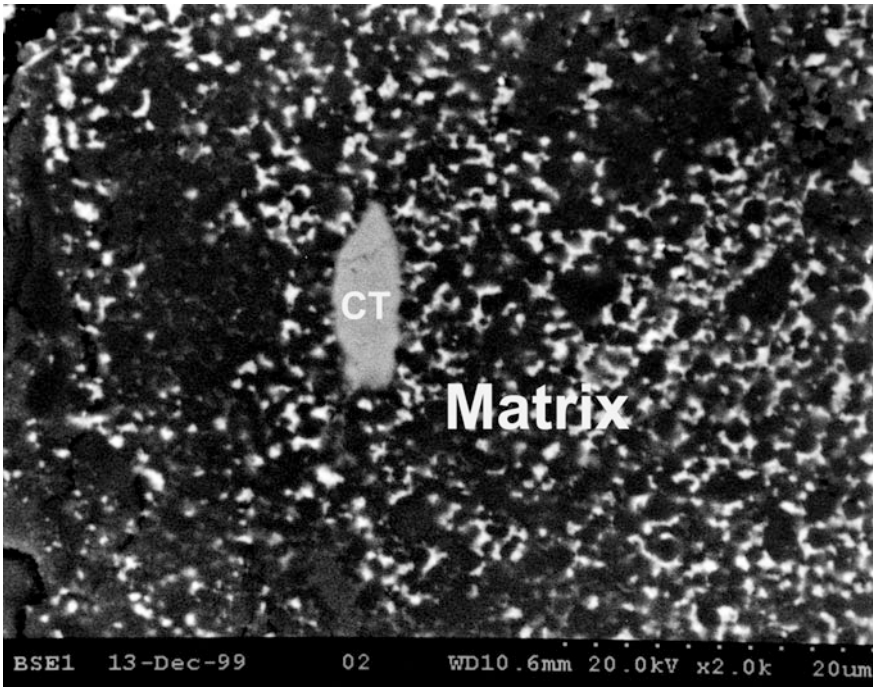

Fig. 5.33 BSE image showing a single polycrystalline xieite (*CT*) grain in the Suizhou vein matrix

MgO, TiO_2, MnO, and V_2O_3. The empirical formula of xieite is $(Fe_{0.87}Mg_{0.13}Mn_{0.01})_{1.01}$–$(Cr_{1.62}Al_{0.25}Ti_{0.08}V_{0.02})_{1.97}O_4$, based on 4 oxygen atoms per formula unit. The simplified formula for xieite is given as $FeCr_2O_4$.

The identity of chemical composition of the dense phase xieite and its host mineral chromite in their single grains indicates that this new phase formed directly from precursor chromite through solid-state phase transformation during a shock event. No additional elements were incorporated in the dense phase during its formation.

Physical and Optical Properties

Based on polishing relief, xieite is harder than chromite (a Mohs' hardness of 5.5). Calculated density is 5.63 g/cm^3 with empirical formula of xieite. Color of xieite under reflected light is gray. Bireflectance, pleochroism, anisotropy, and internal reflections could not be observed because of an occurrence of crystallite aggregate of xieite. The average reflectance values of xieite in air for the standard COM wavelengths are 19.9 % (470 nm), 19.7 % (546 nm), 18.6 % (589 nm), 17.6 % (65 nm), and 18.5 % (white light) (Chen et al. 2008).

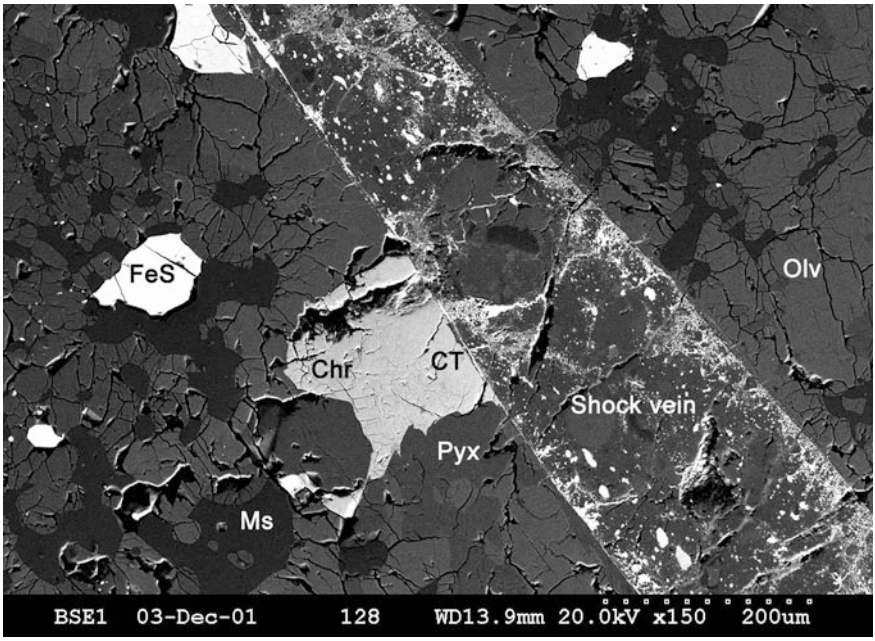

Fig. 5.34 BSE image showing a xieite (*CT*) + chromite (*Chr*) intergrowth grain contacting a shock vein in the Suizhou meteorite. Note that the CT phase is directly adjacent to the vein wall. Olv = olivine, Pyx = pyroxene, Ms = maskelynite, FeS = troilite

Raman Spectroscopy

There is a distinct difference in the feature of Raman spectra between xieite and chromite (Chen et al. 2008). The spectrum of xieite obtained by Raman microprobe shows a strong band at 605 cm^{-1} and a shoulder at 665 cm^{-1}, whereas the Raman spectrum of chromite displays distinct bands at 217, 280, 396, 595, and 680 cm^{-1} (Fig. 5.36). The Raman spectroscopic analyses demonstrate that the polycrystalline xieite grains within the shock veins consist of single phase of xieite, indicating a complete transformation from previous chromite to xieite (Figs. 5.30 and 5.31), whereas those chromite grains with lamellar texture in the chondritic portion adjacent to the shock vein show only partial transformation to xieite in the lamellar layers (Figs. 5.34 and 5.35). Chromite in chondritic portion far from the shock veins remains a spinel structure.

X-ray Diffraction Data

The crystal structure of xieite was measured in situ on polished sections of meteorite by using synchrotron X-ray diffraction analyses. Figure 5.37 shows two X-ray diffraction patterns recorded at different orientations of the sample, which show the polycrystalline nature of analyzed xieite grains. Table 5.12 lists the indexed peaks of X-ray diffraction pattern and Miller indices for xieite. The strongest lines in the X-ray powder diffraction pattern are [d(Å), I/I_o]: (2.675, 100), (2.389, 20), (2.089,

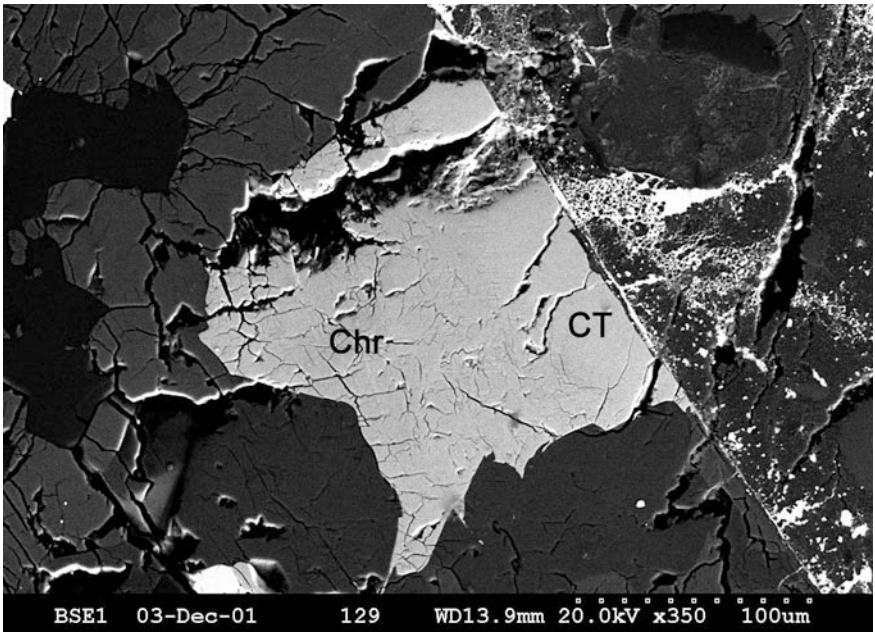

Fig. 5.35 Enlarged BSE image of the xieite (*CT*) + chromite (*Chr*) intergrowth grain contacting a shock vein. Note the smooth surface of xieite and the heavily fractured surface of chromite

Table 5.11 Compositions of xieite in/contacting the Suizhou shock veins (wt%)

Grain No.	1	2	3	4	5	Ave
MgO	2.63	2.74	2.60	2.59	2.53	2.62
FeO	29.61	29.51	29.74	29.67	29.98	29.70
MnO	0.82	0.83	0.73	0.79	0.88	0.81
CaO	n.d.	n.d.	n.d.	n.d.	n.d.	n.d.
TiO_2	2.61	2.33	2.68	2.59	2.73	2.59
Cr_2O_3	57.30	57.12	57.28	57.41	57.39	57.30
Al_2O_3	5.94	5.87	5.93	5.96	5.99	5.94
V_2O_3	0.97	0.91	0.96	1.02	0.99	0.97
Total	99.94	99.31	99.92	100.03	100.09	99.93

All data were measured by EPMA
1–4 single xieite grains in shock veins; *5* xieite in a three-zone grain contacting the vein; *n.d.* not detected

10), (1.953, 90), (1.566, 60), (1.439, 15), (1.425, 15), and (1.337, 40). Xieite is isostructural with synthesized $CaTi_2O_4$ with space group *Bbmm* and orthorhombic symmetry (Bertaut and Blum 1956; Bright et al. 1958). Cell parameters are as follows: a = 9.462 (6) Å, b = 9.562 (9) Å, c = 2.916 (1) Å (numbers in parentheses are standard deviations for the last significant digits), Z = 4, and V = 263.8 (4) $Å^3$.

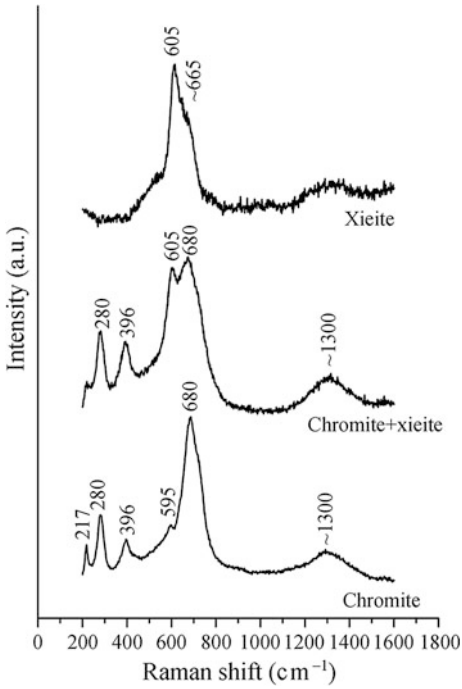

Fig. 5.36 Raman spectra of xieite (*upper*), its host chromite (*lower*), and a mixture consisting of both chromite and xieite (*middle*) (Chen et al. 2008)

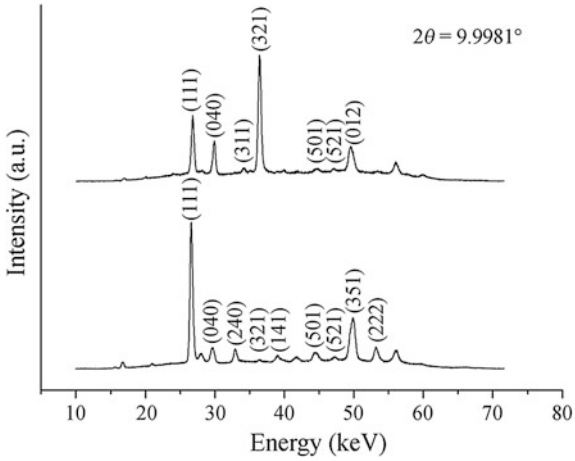

Fig. 5.37 X-ray diffraction patterns of polycrystalline aggregate of xieite obtained from two different orientations of the sample. The numbers listed at diffraction peaks are the Miller indices representative of the orientation of atomic planes in a crystal lattice (Chen et al. 2008)

Table 5.12 X-ray diffraction data of polycrystalline xieite[a]

h k l	d_{meas} (Å)	d_{cal} (Å)	I/I_0
1 1 1	2.6747	2.6754	100
0 4 0	2.3890	2.3905	20
2 4 0	2.1306	2.1336	5
4 2 0	2.1220	2.1203	5
3 1 1	2.0887	2.0895	10
3 2 1	1.9526	1.9542	90
1 4 1	1.8138	1.8144	8
5 0 1	1.5881	1.5875	10
5 1 1	1.5661	1.5661	60
5 2 1	1.5060	1.5066	5
0 1 2	1.4394	1.4414	15
3 5 1	1.4247	1.4263	15
2 2 2	1.3373	1.3377	40
4 1 2	1.2292	1.2309	2
6 0 2	1.0717	1.0706	6
2 6 2	1.0502	1.0490	5
6 3 2	1.0140	1.0149	8
6 4 2	0.9775	0.9771	7
1 2 3	0.9479	0.9477	2
3 2 3	0.9138	0.9119	3
3 3 3	0.8900	0.8918	4

[a]After Chen et al. (2008)

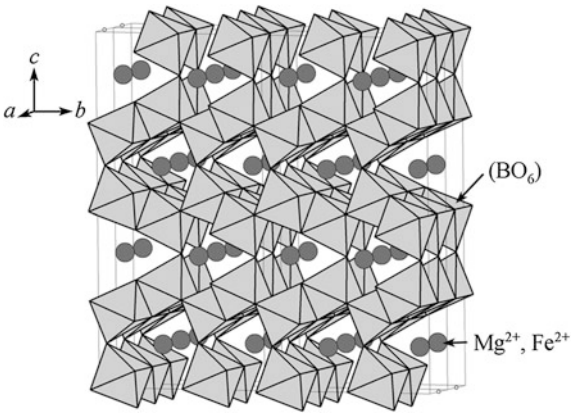

Fig. 5.38 Schematic view of xieite structure showing that Cr^{3+} and Al^{3+} occupy octahedral sites (BO_6), whereas Mg^{2+} and Fe^{2+} occupy dodecahedral sites (Chen et al. 2008)

Figure 5.38 is a schematic view of xieite structure showing edge- and corner-sharing octahedral and dodecahedral sites, where cations of Cr^{3+} and Al^{3+} occupy octahedral sites, whereas Mg^{2+} and Fe^{2+} occupy dodecahedral sites.

Chen et al. (2003b) also synthesized the pure $CaTi_2O_4$-type phase at high pressures from 20 to 25 GPa and a temperature of 2000 °C, using laser-heated

diamond anvil cells and a natural chromite crystal with a similar chemical composition as the chromite in the Suizhou meteorite as starting material. The quenched products recovered from the high *P-T* experiments were analyzed by synchrotron X-ray diffraction measurements and crystal structure determination. The X-ray diffraction pattern of the quenched $CaTi_2O_4$-type polymorph was indexed to give lattice parameters a = 9.467 (5) Å, b = 9.550 (7) Å, c = 2.905 (2) Å, V = 262.6 (4) $Å^3$, and Z = 4. The space group of this orthorhombic lattice is *Bbmm*. The d-spacings of the X-ray diffraction lines can be indexed in terms of the $CaTi_2O_4$ structure (Bright et al. 1958). The calculated density of the dense phase is 5.65 g/cm^3, which is 10.1 % denser than the original chromite (Chen et al. 2003b).

The above-obtained data suggest that both natural and synthetic xieite show almost identical cell parameters, thus giving confirmation of phase transformation of chromite in the Suizhou meteorite to the structure identical to $CaTi_2O_4$-structured phase synthesized experimentally.

Chromite–Xieite Transformation Mechanism

As we mentioned above, xieite occurs as compact polycrystalline aggregate grains and commonly displays as pseudomorph of chromite crystals or its fragments. Inside the shock veins, grains of chromite are completely transformed to massive xieite (Figs. 5.30 and 5.31). In the chondritic area adjacent to the shock veins, xieite may replace chromite completely for those grains closer to the vein, whereas those chromite grains relatively apart from the vein could only be replaced by lamellar xieite along fractures or special crystallography orientation (Figs. 5.32 and 5.33). Secondly, xieite has the same composition as chromite. Hence, we assume that the mineral xieite is formed through solid-state transformation of chromite, and its occurrence is intimately associated with the shock veins of meteorite.

***P-T* Conditions**

The occurrence of xieite is related to a shock vein in the Suizhou meteorite, where peak shock pressure and temperature experienced by this meteorite were located. The *P-T* conditions for the formation of xieite can be constrained according to the high-pressure mineral assemblage within the shock vein. The occurrence of ringwoodite, majorite, lingunite, tuite, magnesiowüstite, and majorite–pyrope garnet in the shock vein constrains the peak pressure and temperature to 20–23 GPa and 1800–2000 °C, respectively (Agee et al. 1995; Chen et al. 1996a; Gillet et al. 2000; Xie et al. 2002). There must be a sharp gradient of temperature from the shock veins to the surrounding less shocked material, as the dense phase is not observed beyond 40 μm from the edge of a shock vein. It indicates that the high-pressure phase transitions are not kinetically obstructed in hot regions, especially inside and close to the shock veins. In comparison with experimentally unquenchable $CaMn_2O_4$-structured Fe_3O_4 (Fei et al. 1999) and $CaFe_2O_4$ (or $CaTi_2O_4$)-structured $ZnCr_2O_4$ polymorph (Wang et al. 2002), this natural xieite phase is quenchable during decompression.

Our experimental synthesis study shows that chromite transforms into xieite at 20–25 GPa and 2000 °C. Other experimental investigations indicate that, with increasing pressure, the $MgAl_2O_4$ spinel dissociates first to Al_2O_3 plus MgO above 25 GPa, and then, both oxides recombine to a $CaFe_2O_4$-type phase above 34 GPa and finally to a $CaTi_2O_4$-structured phase above 40 GPa (Funamori et al. 1998). We did not find any evidence indicating that chromite was decomposed into Cr_2O_3 plus FeO or recombined to a $CaTi_2O_4$-structured phase. Direct phase transition from $FeCr_2O_4$ to $CaTi_2O_4$-structure phase at pressure of 20–23 GPa and temperature of 1800–2000 °C is, therefore, inferred. According to the above high-pressure experiments, we assume that the $CaTi_2O_4$-structured phase may survive over an extended pressure range, from 20 up to 40 GPa, i.e., from the lower part of upper mantle down to the upper part of lower mantle.

Crystallochemical and Geochemical Significance

The $CaTi_2O_4$ structure is intimately related to the $CaFe_2O_4$ and $CaMn_2O_4$ structures. The orthorhombic $CaTi_2O_4$-, $CaFe_2O_4$-, and $CaMn_2O_4$-type structures are composed of dodecahedral (AO_8) and octahedral sites (BO_6), in which the differences among these structures lie in slight modifications of the polyhedral linkage (Reid and Ringwood 1970; Andrault and Bolfan-Casanova 2001). The only natural occurrence of minerals of any these structural types is marokite ($CaMn_2O_4$) that has been found in two terrestrial rocks formed at low pressure (Graudefroy et al. 1963; Villiers and Herbstein 1968). A $CaTi_2O_4$ crystal with space group *Bbmm* was synthesized experimentally (Bertaut and Blum 1956; Bright et al. 1958). No natural occurrence of $CaTi_2O_4$- and $CaFe_2O_4$-structured minerals has been reported prior to our finding of the dense $CaTi_2O_4$-type (xieite) and $CaFe_2O_4$-type phases of chromite in the Suizhou meteorite. In the spinel group (AB_2O_4), the cationic substitutions between Al^{3+} and Cr^{3+} and between Mg^{2+} and Fe^{2+} are extensive. Chrome-spinel $(Mg,Fe)(Al,Cr)_2O_4$ is an important accessory mineral in the Earth's mantle, as, for example, seen in lherzolite from the upper mantle (Scarfe et al. 1979). If the compound $(Mg,Fe)(Al,Cr)_2O_4$ or its analogues exist in the transition zone and the lower mantle, they might take the structure of $CaTi_2O_4$- or $CaFe_2O_4$-type compounds. Experiments have indeed demonstrated the existence of $CaTi_2O_4$- and $CaFe_2O_4$-structured $MgAl_2O_4$ phases at *P-T* conditions of the lower mantle (Irifine et al. 1991; Funamori et al. 1998). The natural $CaTi_2O_4$-structured $FeCr_2O_4$ phase (xieite) in the Suizhou meteorite contains about 6 wt% of Al_2O_3 and 2.6 wt% of MgO, whereby the cations Al^{3+} and Cr^{3+} occupy octahedral sites (BO_6) and the Mg^{2+} and Fe^{2+} occupy the dodecahedral sites (AO_8). Therefore, the natural occurrence of the $CaTi_2O_4$-type phase in the Suizhou meteorite indicates that the $CaTi_2O_4$ structure could be an important host phase for Cr^{3+} and Al^{3+}, and other metal elements (Mg^{2+}, Fe^{2+}, Ni^{2+}, Mn^{2+}, Zn^{2+}, and Mn^{3+}) in the deep Earth.

5.2.9 *CF Phase, the $CaFe_2O_4$-Type Dense Polymorph of Chromite*

As it was described in the previous paragraph, in the late 1960s, Ringwood proposed two orthorhombic $CaFe_2O_4$-type and $CaTi_2O_4$-type structures as the top candidates for "post-spinel" transitions in the Earth's mantle (Reid and Ringwood 1969, 1970), and besides xieite, the $CaTi_2O_4$-structured $FeCr_2O_4$ phase, we also found another post-spinel polymorph of chromite in the Suizhou meteorite. This second polymorph of chromite has just a $CaFe_2O_4$-type structure (Chen et al. 2003b). It occurs in the close association with the $CaTi_2O_4$-structured $FeCr_2O_4$ phase in the regions directly contacting the shock veins.

Occurrence

Petrographical studies in the Suizhou meteorite demonstrate the existence of a gradient of shock-produced pressure and temperature from the shock veins to the neighboring host meteorite during the shock event. Some chromite grains in close association with the shock veins covered a shock-produced pressure gradient. As it was mentioned above, xieite, the $CaTi_2O_4$-type polymorph of chromite, was found from these chromite grains, in addition to those occurring inside the shock veins (Chen et al. 2003b). In the electron back-scattering images (BSE) these chromite grains show three zones of distinct densities corresponding to the temperature gradient, i.e., xieite, the $CaTi_2O_4$-type phase, is close to the shock vein, chromite zone relatively apart from the vein, and a lamella-rich zone between xieite and chromite zones.

Figure 5.39 is a BSE image showing an intergrowth grain of chromite in the direct contact with a Suizhou shock vein. This grain is in the form of three zones consisting of the inner xieite phase, the intermediate lamella-like phase, and the outer chromite phase (Chen et al. 2003a, b). On that image, we can see that the xieite phase and the lamella-like phase are electron brighter than the chromite phase. Such an occurrence implies that the formation of the xieite phase and the lamella-like slices was highly pressure-dependent. The width of the lamellae in the lamella-like phase is ranging from 0.5 to 1.5 μm. Two to three sets of regular lamella-like slices in the lamella-like phase grain clearly indicate that the produce of these slices may intimately associate with special crystallographic orientation and shock-produced deformation features of parent chromite phase. Such a lamella-like zone between the xieite zone and chromite zone was firstly interpreted as a mixture of xieite and chromite (Chen et al. 2003a), but then identified as a new post-spinel phase of chromite that has the $CaFe_2O_4$-type structure (Chen et al. 2003b). It, thus, appears that this is a new second dense phase of chromite that was also formed due to shock transformation from precursor chromite.

Chemical Composition

Electron microprobe analyses of three zones in the intergrowth grain shown in Fig. 5.35 give a uniform chemical composition of chromite: 2.62 wt% MgO, 29.70 wt% FeO, 0.81 wt% MnO, 2.59 wt% TiO_2, 57.30 wt% Cr_2O_3, 5.97 wt%

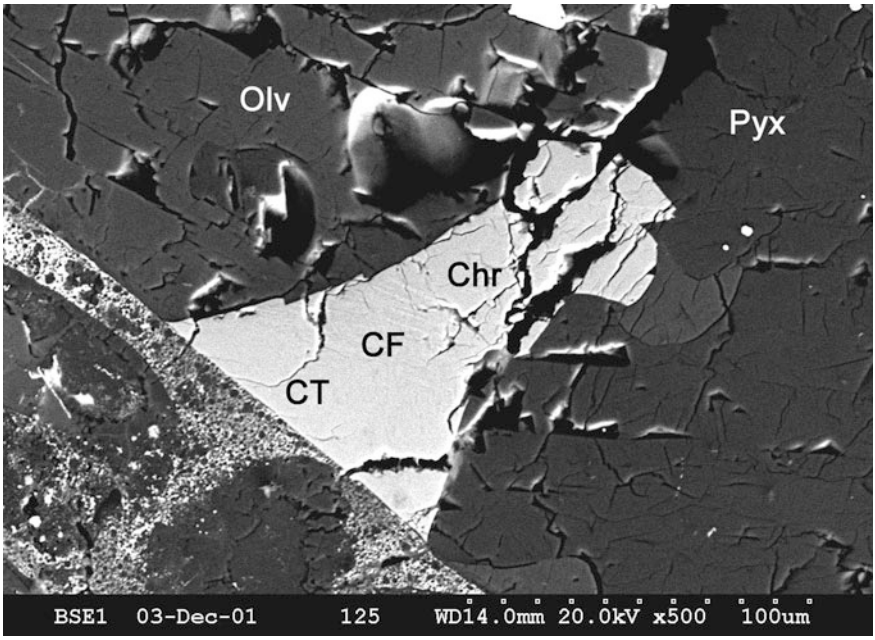

Fig. 5.39 BSE image showing a xieite (*CT*) + CF phase + chromite (*Chr*) intergrowth grain contacting a shock vein in the Suizhou meteorite. Note that the CF phase is in between the CT and chromite phases. Olv = olivine, Pyx = pyroxene (Chen et al. 2008)

Al_2O_3, 0.97 wt% V_2O_3, and 99.93 wt% in total. The chemical formula of the mineral chromite is $(Fe_{0.84}Mg_{0.14}Mn_{0.02})\left(Cr_{1.58}Al_{0.26}V_{0.03}Fe_{0.03}Ti^{4+}_{0.07}\right)_{1.97}O_4$. The identity of chemical composition of this new dense $FeCr_2O_4$ phase, xieite and chromite, indicates that this new phase also formed directly from precursor chromite through solid-state phase transformation during a shock event. No additional elements were incorporated in the dense phase during its formation.

X-ray Diffraction Data

Our high *P-T* experiment indicates that the quenched CF and CT phases of chromite are difficult to distinguish with commonly used petrographic probes, such as petrographic microscopy, scanning electron microscopy, electron microprobe, and micro-Raman spectroscopy, but are clearly distinguishable by their characteristic X-ray diffraction patterns.

The X-ray diffraction patterns of both the natural and synthesized $CaFe_2O_4$-type phase of chromite were obtained using the same synchrotron radiation technique as we did for the xieite phase. For the natural sample, we focused the X-ray microprobe on the lamella-like zone between the xieite and chromite zones in an intergrowth chromite grain (Fig. 5.39) and obtained the diffraction pattern which is consistent with the $CaFe_2O_4$-type phase with a few lines of its neighboring phases, xieite and chromite (Fig. 5.40).

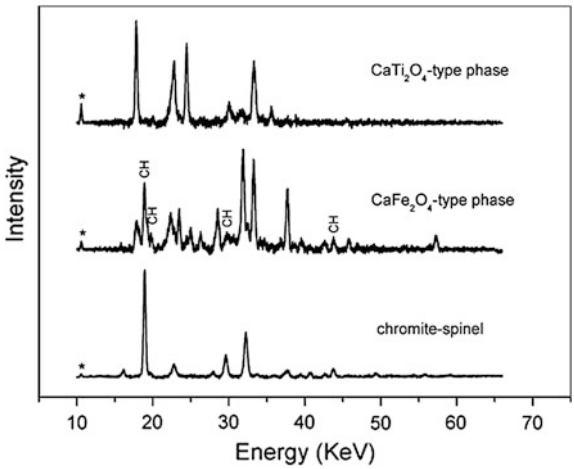

Fig. 5.40 X-ray diffraction patterns from chromite-spinel, CF, and CT phases. The peaks labeled with CH are from the residue of starting material chromite (Chen et al. 2003b). *Asterisk*, escape peaks

The X-ray patterns collected from different orientations of sample show a polycrystalline nature of the lamellae-like slices, with a preferential crystallographic orientation in the microcrystalline $CaFe_2O_4$-type phase (Fig. 5.41). We collected a total of 20 X-ray reflections from the natural $CaFe_2O_4$-type phase in addition to those from chromite (Table 5.13). They were indexed to an orthorhombic cell with

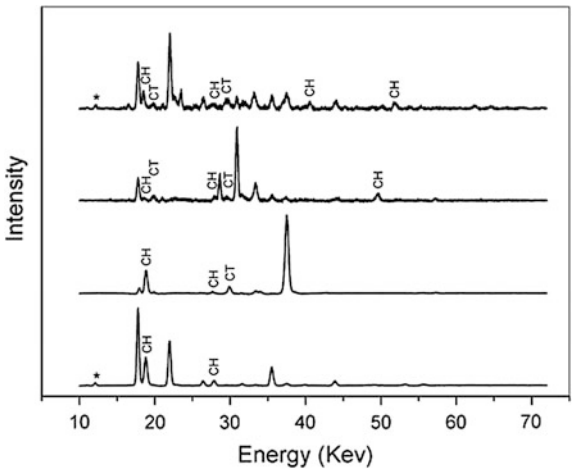

Fig. 5.41 X-ray diffraction patterns from natural CF phase. Each pattern was obtained at a different orientation of the sample. The peaks labeled with CH are from chromite and CT from CT phase. Other peaks that are unlabeled are from CF phase (Chen et al. 2003b). *Asterisk*, escape peaks

parameters a = 8.954 (7) Å, b = 2.986 (2) Å, c = 9.891 (7) Å, V = 264.5 (4) Å^3, and Z = 4 (Chen et al. 2003b). The space group of this orthorhombic lattice is *Pnma*. The calculated density of this natural dense phase is 5.62 g/cm^3, which is 9.4 % denser than the original chromite.

Chen et al. (2003b) synthesized a pure $CaFe_2O_4$-type phase with some residue of chromite above 12.5 GPa and 2000 °C. A total of 20 X-ray reflections from this phase were collected in addition to those from chromite (Table 5.13). The X-ray diffraction pattern of the quenched $CaFe_2O_4$-type polymorph was indexed to give lattice parameters a = 8.955 (7) Å, b = 2.985 (2) Å, c = 9.909 (7) Å, V = 264.9 (4) Å^3, and Z = 4. The space group of this orthorhombic lattice is *Pnma*. The calculated density of this natural dense phase is 5.61 g/cm^3.

It is evident that the crystal structure of our second natural dense phase of chromite is identical to that of the synthetic $CaFe_2O_4$-type phase obtained by high-pressure experiments. From the above data, we assume that the lamellae-like phase in the Suizhou meteorite is the first natural occurrence of $CaFe_2O_4$-type polymorph of chromite.

Table 5.13 Indexed peaks of the X-ray diffraction patterns and Miller indices collected from natural and synthetic CF phases (Chen et al. 2003b)

h k l	Natural		Synthetic	
	d_{obs} (Å)	d_{cal} (Å)	d_{obs} (Å)	d_{cal} (Å)
2 3 0	2.656 (2)$_s$	2.6549	2.657 (2)$_s$	2.6581
2 4 0	2.166 (2)$_s$	2.1647	2.169 (1)$_w$	2.1676
3 0 1	2.108 (3)$_w$	2.1111	2.108 (3)$_w$	2.1110
4 2 0	2.039 (1)$_s$	2.0394	2.035 (5)$_s$	2.0402
2 5 0	1.807 (2)$_w$	1.8095	1.808 (4)$_s$	1.8122
4 4 0	1.660 (3)$_s$	1.6596	1.663 (2)$_s$	1.6610
2 6 0			1.550 (7)$_w$	1.5498
5 0 1	1.536 (5)$_s$	1.5359		
0 0 2	1.498 (6)$_w$	1.4931	1.494 (2)$_s$	1 4928
5 2 1	1.468 (2)$_w$	1.4668	1.467 (1)$_w$	1.4670
1 6 1	1.425 (2)$_s$	1.4249	1.429 (2)$_s$	1 4267
2 6 1	1.372 (1)$_w$	1.3737	1.370 (5)$_w$	1.3753
3 0 2	1.336 (1)$_w$	1.3354	1.334 (1)$_w$	1.3352
3 2 2	1 285 (4)$_w$	1.2892	1.287 (2)$_w$	1.2892
1 4 2	1.267 (2)$_s$	1.2654	1.263 (2)$_s$	1.2658
4 2 2	1.206 (2)$_w$	1.2047	1.206 (2)$_w$	1.2048
5 2 2	1117 (1)$_w$	1.1172	1.115 (2)$_w$	1.1172
5 3 2	1.081 (2)$_w$	1.0832	1.084 (1)$_w$	1.0833
4 2 3	0.893 (1)$_w$	0.8945	0.891 (3)$_w$	0.8945
1 6 3	0.848 (1)$_w$	0.8483	0.849 (1)$_w$	0.8486
6 0 3	0.828 (2)$_w$	0.8281	0.829 (1)$_w$	0.8280

d_{obs} and d_{cal} are observed and calculated d-values, respectively; $_s$, strong diffraction peak; and $_w$, weak diffraction peak

Chromite–CF Phase Transformation Mechanism

The CF phase occurs only in the form of lamella-like zone between the CT and chromite-spinel zones in shocked chromite grains. No individual grains of CF phase were observed so far in the Suizhou meteorite. Furthermore, the CF phase has the same composition as its precursor chromite. So, the occurrence and mineral composition of this CF-structured polymorph of chromite in the Suizhou meteorite support a solid-state mechanism for the transformation of chromite to CF phase. There is no evidence for an intermediate decomposition process, such as the post-spinel transitions of $MgAl_2O_4$ (Funamori et al. 1998). The results indicate that the solid-state phase transformation is, in general, a dominating mechanism for the formation of high-pressure minerals in naturally shocked meteorites (Chen et al. 1996a).

***P-T* Conditions**

The occurrence of the $CaTi_2O_4$- and $CaFe_2O_4$-structured phases of chromite is related to a shock vein in the Suizhou meteorite, where peak shock pressure and temperature experienced by this meteorite were located. The *P-T* conditions for the formation of both $CaTi_2O_4$- and $CaFe_2O_4$-structured phases can be constrained according to the high-pressure mineral assemblage within the shock vein. The occurrence of ringwoodite, majorite, $NaAlSi_3O_8$ hollandite, tuite, and majorite–pyrope garnet in the shock vein constrains the peak pressure and temperature to 20–23 GPa and 1800–2000 °C, respectively (Agee et al. 1995; Chen et al. 1996a; Gillet et al. 2000; Xie et al. 2002).

The presence of a sharp gradient of temperature from the shock veins to the surrounding less shocked material, the $CaTi_2O_4$- and $CaFe_2O_4$-structured phases, as two dense phases of chromite should be experienced high-pressure and high-temperature regime close or a bit lower than the *P-T* conditions in the veins themselves. The pressure of 18–23 GPa and temperature of 1800–2000 °C are estimated for the shocked intergrowth grains of chromite, for which a solid-state transformation from chromite to CF phase takes place at about 18–23 GPa and ≤1800 °C.

Crystallochemical and Geochemical Significance

It is well known that the chromite $(Mg,Fe)(Al,Cr)_2O_4$ is an important accessory mineral in the Earth's mantle. If the compound $(Mg,Fe)(Al,Cr)_2O_4$ or its analogues exist in the transition zone and the lower mantle, they might take the structure of $CaTi_2O_4$- or $CaFe_2O_4$-type compounds. Experiments have indeed demonstrated the existence of $CaTi_2O_4$- and $CaFe_2O_4$-structured $MgAl_2O_4$ phases at *P-T* conditions of the lower mantle (Irifine et al. 1991; Funamori et al. 1998). The natural $CaFe_2O_4$-structured $FeCr_2O_4$ phase in the Suizhou meteorite contains about 6 wt% of Al_2O_3 and 2.6 wt% of MgO, whereby the cations Al^{3+} and Cr^{3+} occupy octahedral sites (BO_6) and the Mg^{2+} and Fe^{2+} occupy the dodecahedral sites (AO_8). Therefore, the natural occurrence of the $CaFe_2O_4$-structured $FeCr_2O_4$ phase in the Suizhou

meteorite indicates that besides the $CaTi_2O_4$ structure, the $CaFe_2O_4$ structure could also be an important host phase for Cr^{3+}, Al^{3+}, and other metal elements (Mg^{2+}, Fe^{2+}, Ni^{2+}, Mn^{2+}, Zn^{2+} and Mn^{3+}) in the deep Earth (Chen et al. 2003b).

5.2.10 *Multi-phase Grains of Silicate and Oxide Minerals*

It is revealed that some unusual occurrences of shock-produced high-pressure phases were observed in the Suizhou shock veins. They are two-phase or three-phase grains. These grains or fragments consist of high-pressure polymorphs of two or three silicate minerals, namely ringwoodite, majorite, and lingunite (Figs. 5.42, 5.43, and 5.44). The boundaries between different high-pressure polymorphs of silicate minerals are sharp and even, or slightly curved, and sometimes irregular. Besides, Xie et al. (2011b) reported rather distinct two-phase grains consisting of xieite and a high-pressure polymorph of one of the above-mentioned three silicate minerals (Fig. 5.45). These distinct two-phase grains are small, 20–25 μm in length, and show rounded or drop-like outlines.

It is interesting that the boundaries between high-pressure polymorphs of silicate or oxide minerals are quite sharp (Figs. 5.44 and 5.45), implying that partial melting

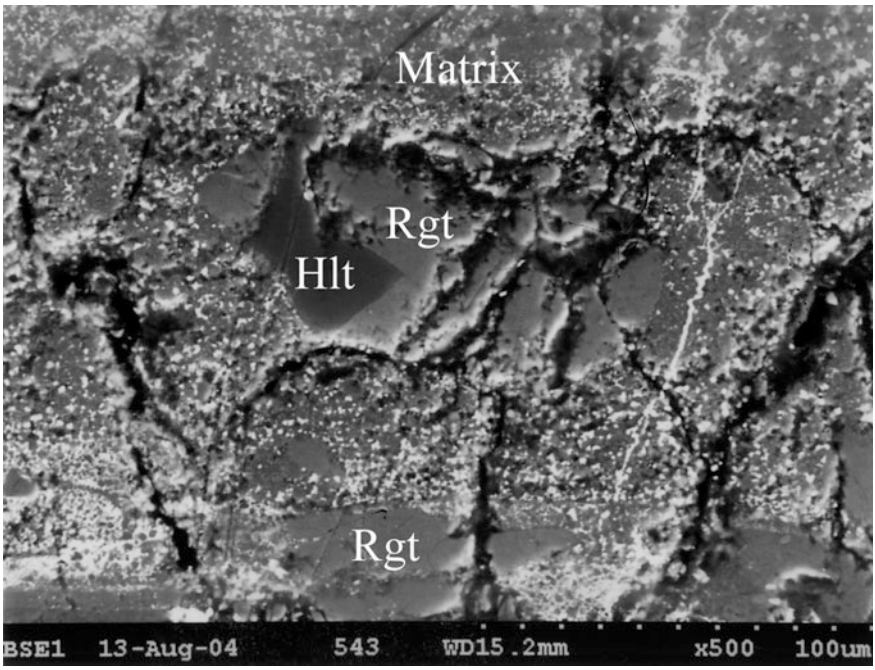

Fig. 5.42 BSE image showing a two-high-pressure-phase grain of ringwoodite (*Rgt*) and lingunite (*Hlt*) in the Suizhou vein matrix. Note the clear boundaries between these two phases

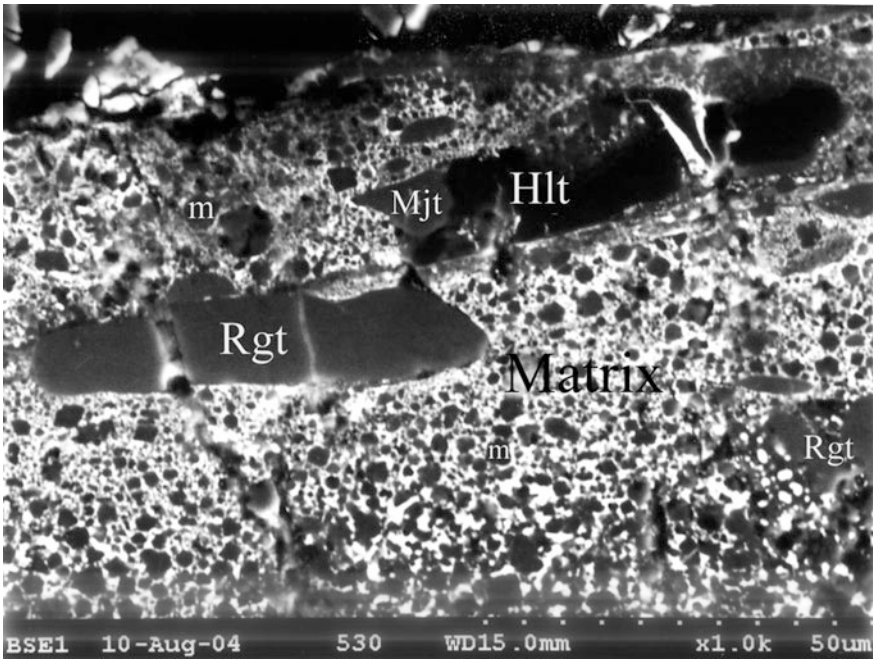

Fig. 5.43 BSE image showing a two-high-pressure-phase grain of majorite (*Mjt*) and lingunite (*Hlt*) in the Suizhou vein matrix (*Matrix*). Rgt = ringwoodite, m = majorite–pyrope garnet

does not take place at the boundary areas. All these two-phase and three-phase grains show smooth surface, and no zoning and no fractures or cracks were observed. All mineral phases in these multi-phase grains were identified by both Raman microprobe spectroscopy (Fig. 5.46) and chemical analysis. The Raman spectrum of xieite in a two-phase grain gives Raman bands at 536, 607 and 666 cm^{-1} (Fig. 5.46a) which is identical to that of xieite in its single grain (Fig. 5.36). The Raman spectra of the three silicate high-pressure minerals in two-phase grains (Fig. 5.46b–d) are also similar to those in their single grains (Figs. 5.5a, 5.14a and 5.16_1). In this section, we shall lay our stress on the two-phase grains of xieite and a silicate mineral.

5.2.10.1 Ringwoodite + Lingunite Grain

The two-high-pressure-phase grains of ringwoodite + lingunite were observed in shock veins of the Suizhou meteorite. Figures 5.42 and 5.47 are BSE images showing two such grains in the vein matrix. These two grains are of elongated elliptic shape with 80 and 110 μm in length and 40 and 50 μm in width, respectively. In these two grains, ringwoodite is the major high-pressure phase and lingunite takes up secondary position. However, ringwoodite in this grain was fractured (Fig. 5.42) or broken (Fig. 5.47), but lingunite shows intact feature.

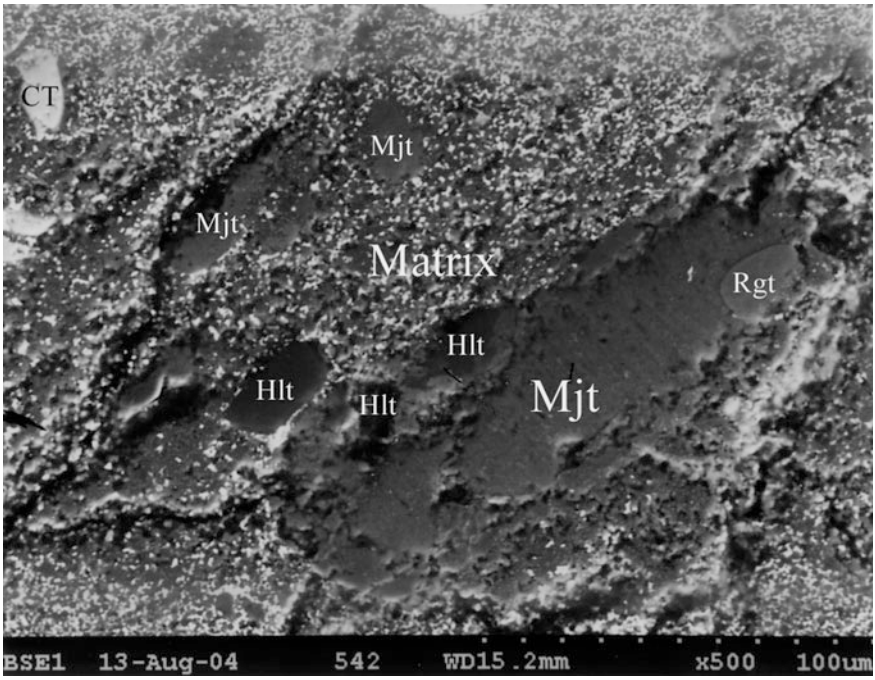

Fig. 5.44 BSE image showing a large three-phase grain of ringwoodite (*Rgt*), majorite (*Mjt*), and lingunite (*Hlt*) in the Suizhou shock vein matrix (*Matrix*). CT = xieite

Under SEM in back-scattered mode, the boundaries between the gray-colored ringwoodite and the black-colored lingunite are quite sharp, which may reflect the original occurrence of their precursor minerals olivine and plagioclase in these two meteorite fragments. No trace of partial melting in boundary areas was observed in both grains.

5.2.10.2 Lingunite + Majorite Grains

The two-high-pressure-phase grains of lingunite + majorite were also observed in shock veins of the Suizhou meteorite. Figure 5.43 is a BSE image showing such a two-high-pressure-phase grain of lingunite and majorite in the vein matrix. This two-phase grain has elongated shape with 60 μm in length and 20 μm in width. In this grain, lingunite is the main high-pressure phase and majorite takes secondary position. The surfaces of both lingunite and majorite are smooth, and no fractures or cracks were observed in these two high-pressure minerals.

Under SEM in back-scattered mode, the boundaries between the black-colored lingunite and the dark gray-colored lingunite are also quite sharp, which may reflect the original occurrence of their precursor minerals such as plagioclase and low-Ca

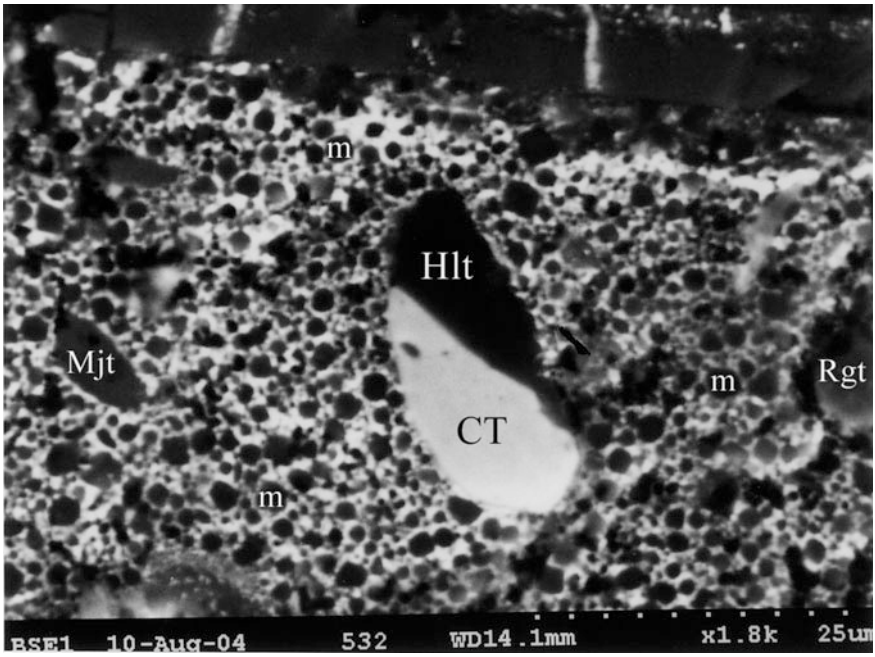

Fig. 5.45 BSE image showing a drop-like two-high-pressure-phase grain of xieite (*CT*) and lingunite (*Hlt*) in the Suizhou vein matrix. Rgt = ringwoodite, Mjt = majorite, m = majorite–pyrope garnet (Xie et al. 2011a)

pyroxene in that meteorite fragment. No trace of partial melting in boundary area between these two phases was detected.

5.2.10.3 Ringwoodite + Majorite + Lingunite Grains

The three-high-pressure-phase grains of ringwoodite + majorite + lingunite were also observed in shock veins of the Suizhou meteorite. Figure 5.44 is a BSE image showing a three-high-pressure-phase grain of ringwoodite, majorite, and lingunite in the shock vein matrix. This three-phase grain also has elongated oval shape with 150 μm in length and 80 μm in width. In this large grain, majorite is the main high-pressure phase. There are only one small ringwoodite and two small lingunite fragments embedded in majorite phase. The surfaces of both ringwoodite and lingunite fragments are smooth, and no fractures or cracks were observed in these two minerals.

Under SEM in back-scattered mode, the boundary between the gray-colored ringwoodite and the dark gray-colored majorite and the boundaries between the black-colored lingunite and the dark gray-colored majorite are also quite sharp, which may reflect the original occurrence of their precursor minerals such as olivine, low-Ca pyroxene, and plagioclase in that meteorite fragment. No trace of partial melting in boundary area between these three-high-pressure phases was observed.

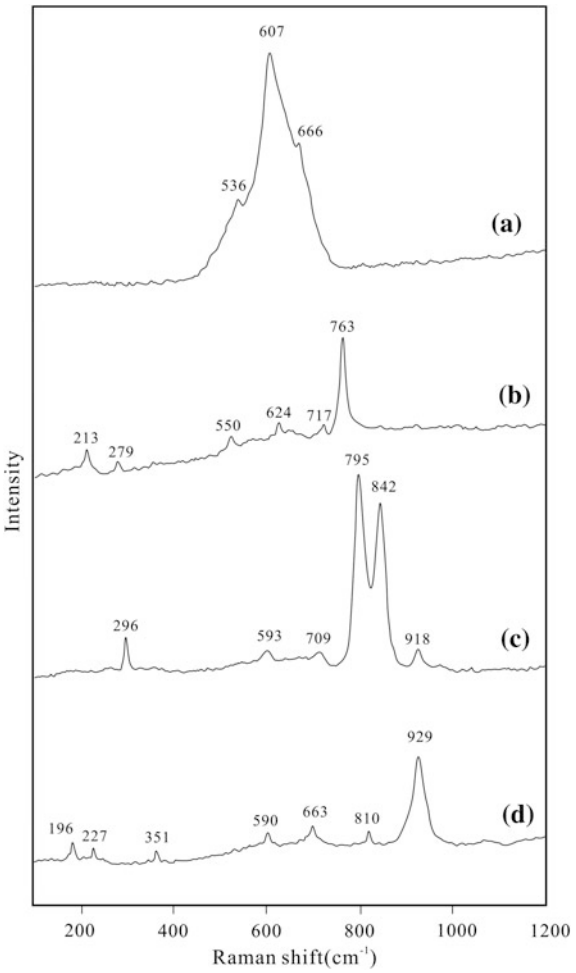

Fig. 5.46 Raman spectra of minerals in two-phase grains. **a** Xieite, **b** lingunite, **c** ringwoodite, and **d** majorite (Xie et al. 2011a)

5.2.10.4 Ringwoodite + Majorite + Perovskite Glass Grains

The three-phase grains of ringwoodite + majorite + perovskite glass were also observed in shock veins of the Suizhou meteorite (Chen et al. 2004c). Figure 5.48 is a BSE image showing an ovoid-shaped three-phase grain of ringwoodite, majorite, and perovskite glass in the vein matrix. This three-phase grain is of 100 μm in length and 40 μm in width. This grain is little bit different with other three-high-pressure-phase grains because it, originally, was a two-phase fragment consisted of pyroxene and olivine. At the shock-produced high pressure and high temperature, olivine transformed to ringwoodite, but pyroxene transformed to its two high-pressure polymorphs, namely perovskite in the interior area due to a relatively low

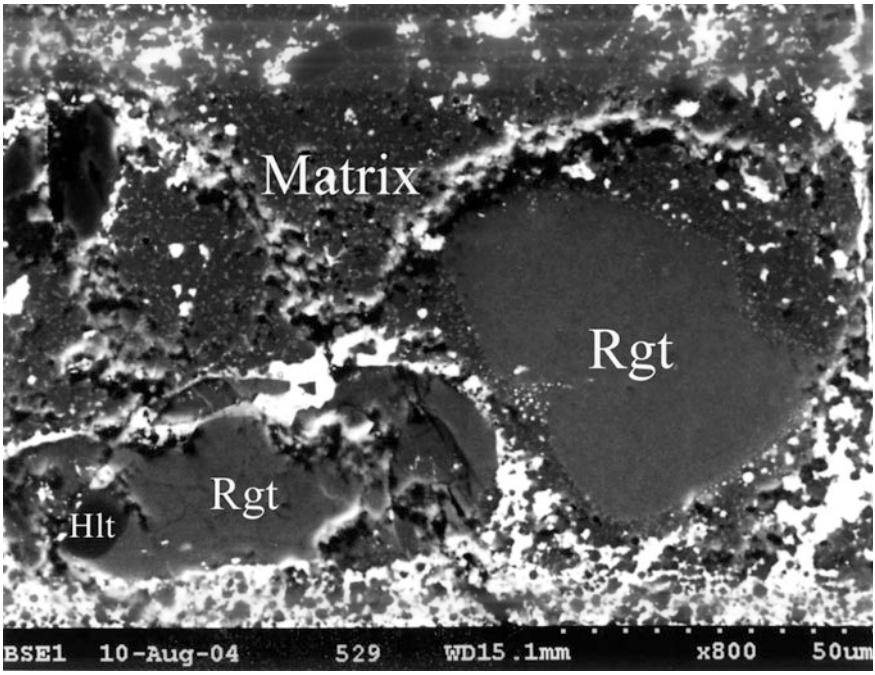

Fig. 5.47 BSE image showing a two-phase grain of ringwoodite (*Rgt*) and lingunite (*Hlt*) in the Suizhou shock vein matrix (*Matrix*)

temperature and majorite at the rim region due to a higher temperature. After pressure release, perovskite vitrified at post-shock temperature (Chen et al. 2004c).

In this large grain, the surfaces of both perovskite glass and ringwoodite are smooth and even, and no fractures or cracks were observed in perovskite glass interior, and only one fine fracture was seen in ringwoodite. However, quite a lot irregular cracks developed in majorite rim because of the volume increase induced by the vitrification of perovskite.

Under SEM, the boundary between perovskite glass interior and majorite rim is rough and uneven. Microprobe analyses show that the low-Ca pyroxene in the Suizhou chondritic host, the majorite, and the perovskite glass phase in the ovoid grains are identical in composition (Chen et al. 2004c). This indicates that no element exchange between these three phases took place during shock metamorphism.

5.2.10.5 Xieite + Lingunite Grains

An unusual occurrence of shock-produced high-pressure phases in the Suizhou melt veins is the two-phase grains consisting of xieite and a high-pressure polymorph of

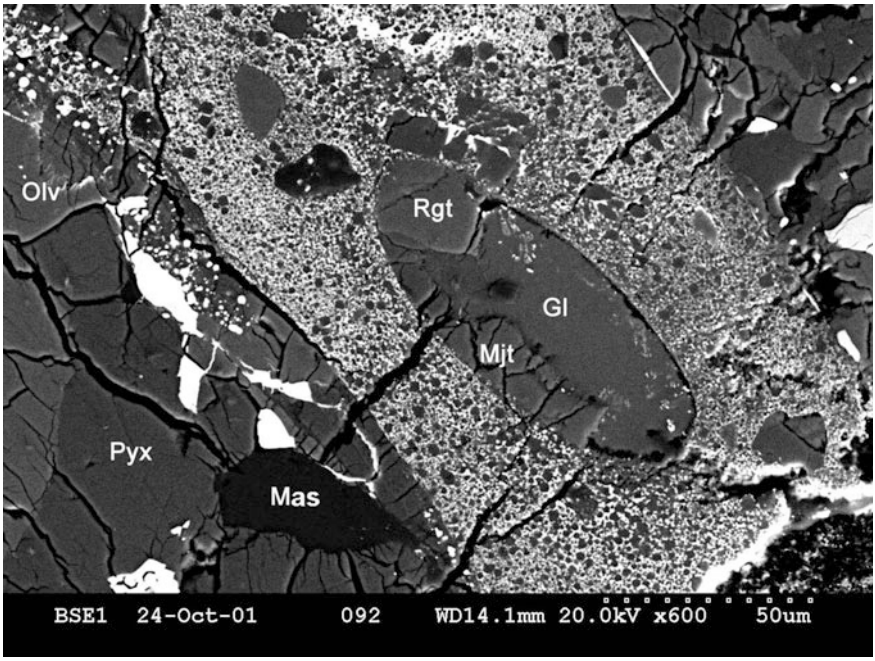

Fig. 5.48 BSE image showing an ovoid-shaped three-phase grain of ringwoodite (*Rgt*), majorite (*Mjt*), and perovskite glass (*Gl*) in a Suizhou shock vein. Olv = Olivine, Pyx = pyroxene, Mas = maskelynite

one of the three main rock-forming silicate minerals, namely lingunite, ringwoodite, and majorite (Xie et al. 2011b). However, the rather common two-phase grains are consisted of xieite + lingunite. Figure 5.45 is a BSE image showing such a two-phase grain in the Suizhou vein matrix. It is interesting that this grain has a drop-like shape and its size is relatively small (30 μm × 13 μm). The volumes of both xieite and lingunite in this grain are almost equal, and the boundary between these two phases is sharp, but little bit curved. It implies that no obvious partial melting in boundary area took place. Figure 5.49 shows another type of xieite and lingunite two-phase grain of larger size (80 μm × 25 μm), where xieite is the main body, and lingunite take up only very small portion of this grain. The boundary between two phases is also sharp but curved, implying that both xieite and lingunite might experience partial melting in the boundary area.

Compositions of xieite and lingunite in the two-phase grain were measured by EDS technique, and the results are shown in Table 5.14. For comparison, the compositions of their precursors such as chromite and plagioclase outside the Suizhou shock vein were also measured and shown in this table. It is revealed that the xieite contains higher content of Al_2O_3 (6.19 vs. 5.45 wt%) and lower content of Cr_2O_3 (56.48 vs. 57.98 wt%) than its precursor chromite. On the other hand, the lingunite contains higher contents of Cr_2O_3 (0.32 vs. 0.03 wt%) and FeO (1.97 vs.

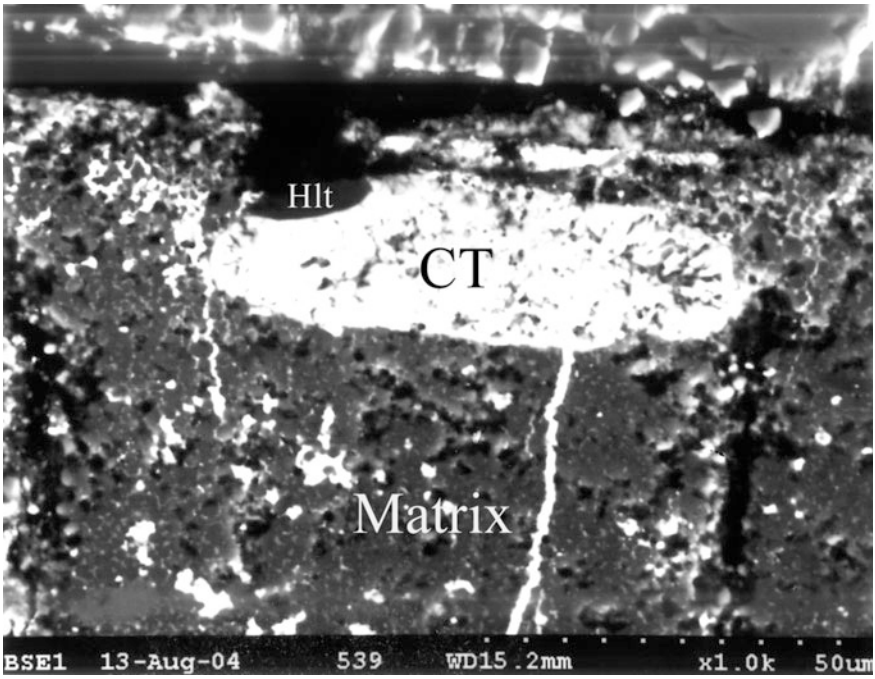

Fig. 5.49 BSE image showing a two-phase grain of xieite (*CT*) + lingunite (*Hlt*) in the Suizhou shock vein matrix (*Matrix*). Note the curved boundary between xieite and lingunite phases

0.41 wt%) and lower contents of Al_2O_3 (19.98 vs. 21.73 wt%) than its precursor plagioclase (Xie et al. 2011b). This implies that the element diffusion appeared between the two phases in which some of the chromium and iron migrated from xieite to lingunite and some of the aluminum migrated from lingunite to xieite.

5.2.10.6 Xieite + Ringwoodite Grains

The two-high-pressure-phase grains of xieite + ringwoodite were also observed in shock veins of the Suizhou meteorite (Xie et al. 2011b). Figure 5.50 is a BSE image showing such a two-phase grain in the vein matrix. Its grain size is 30 μm long and 15 μm wide. This grain originally has an ovoid form, but its lower and left parts were ground off during thin section preparation. The volumes of both xieite and lingunite phases in this grain are almost equal, and the boundary between these two phases is sharp, but slightly curved. This implies that no obvious partial melting in boundary area took place.

Compositions of xieite and ringwoodite in the two-phase grain were also measured by EDS technique, and the results are shown in Table 5.15. For comparison, the compositions of their precursors such as chromite and olivine outside the

Table 5.14 Composition of xieite and lingunite in two-phase grain and their precursors (wt%)

	Chromite in chondrite	Xieite in two-phase grain	Lingunite in two-phase grain	Plagioclase in chondrite
SiO_2			65.8	65.57
Al_2O_3	5.5	6.2↑	20.0↓	21.73
MgO	2.3	2.4		0.00
FeO	30.4	30.8	2.0↑	0.41
CaO			2.3	2.12
MnO	–	0.7	–	0.02
TiO_2	2.9	2.4		0.04
Cr_2O_3	58.0	56.5↓	0.3↑	0.03
V_2O_3	0.9	1.0		
Na_2O			8.4	8.87
K_2O			1.2	1.31
Total	100.0	100.0	100.0	100.38

Plagioclase in Suizhou chondrite was analyzed by EPMA. All other data were measured by EDS technique

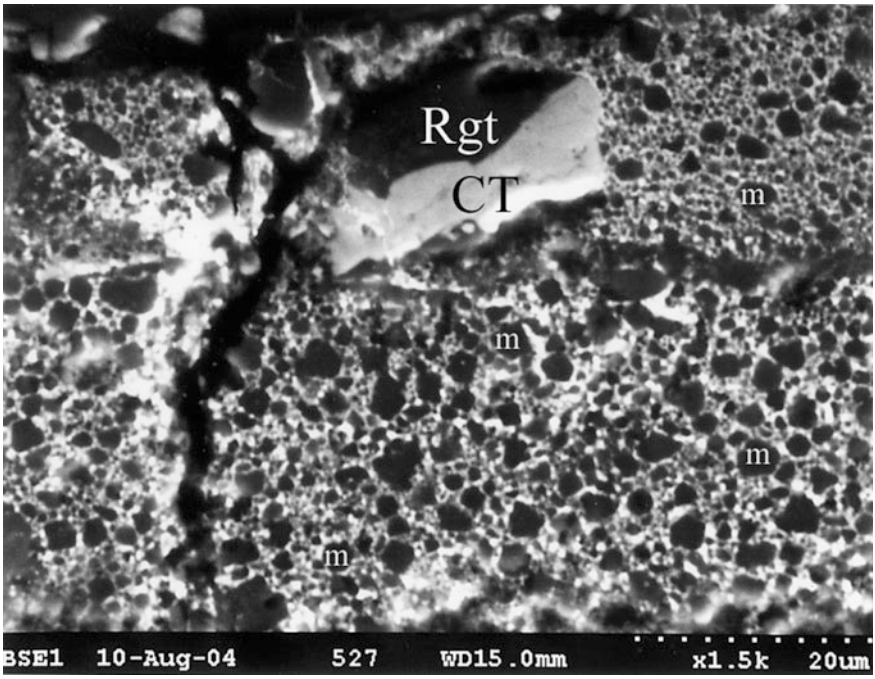

Fig. 5.50 BSE image showing a two-phase grain of xieite (*CT*) + ringwoodite (*Rgt*) in the Suizhou vein matrix (*Matrix*). Note the curved boundary between xieite and ringwoodite phases. M = majorite–pyrope garnet (Xie et al. 2011a)

Table 5.15 Composition of xieite + ringwoodite in two-phase grain and their precursors (wt%)

	Chromite in chondrite	Xieite in two-phase grain	Ringwoodite in two-phase grain	Olivine in chondrite
SiO_2			39.9	38.3
Al_2O_3	5.5	5.9		
MgO	2.3	2.2	39.5	39.4
FeO	30.4	32.0↑	20.0↓	22.3
MnO	–	0.7		
TiO_2	2.9	2.5		
Cr_2O_3	58.0	55.6↓	0.6↑	0.0
V_2O_5	0.9	1.1		
Total	100.0	100.0	100.0	100.0

All data were measured by EDS technique

Suizhou shock vein were also measured and shown in this table. It is revealed that the general phenomena of element diffusion in xieite + ringwoodite grains are similar to that in xieite + lingunite grains, but the Al_2O_3 constituent is replaced by FeO, since olivine does not contain Al_2O_3. Comparing to the precursor mineral chromite, the xieite contains higher content of FeO (31.96 vs. 30.39 wt%) and lower content of Cr_2O_3 (55.57 vs. 57.98 wt%). On the other hand, in comparison with the precursor mineral olivine, the content of FeO in ringwoodite decreased from 22.35 to 19.95 wt% and the content of Cr_2O_3 increased from 0.03 to 0.58 wt% (Xie et al. 2011b). This implies that the element diffusion also took place between these two phases in which some of the chromium migrated from xieite to ringwoodite and some of the iron migrated from ringwoodite to xieite.

5.2.10.7 Xieite + Majorite Grains

The two-high-pressure-phase grains of xieite + majorite can also be observed in shock veins of the Suizhou meteorite. Figure 5.51 is a BSE image showing such a two-phase grain in the vein matrix (Xie et al. 2011b). Its grain size is only 20 μm long and 18 μm wide. Xieite phase in this grain has an ovoid form, but majorite phase shows irregular form. The boundary between these two phases is sharp enough and curved. This implies that no obvious partial melting in boundary area took place.

Compositions of xieite and majorite in the two-phase grain were measured by EDS technique, and the results are shown in Table 5.16. For comparison, the compositions of their precursors such as chromite and low-Ca pyroxene outside the Suizhou shock vein were also measured and shown in this table. From this table, we can see that the situation of element diffusion in xieite + majorite grains is remarkably different from that for the above-described two cases. On the whole, the composition of xieite in this two-phase grain is similar to that of its precursor chromite, only with slight increase in Al_2O_3 (5.69 vs. 5.45 wt%) and very little

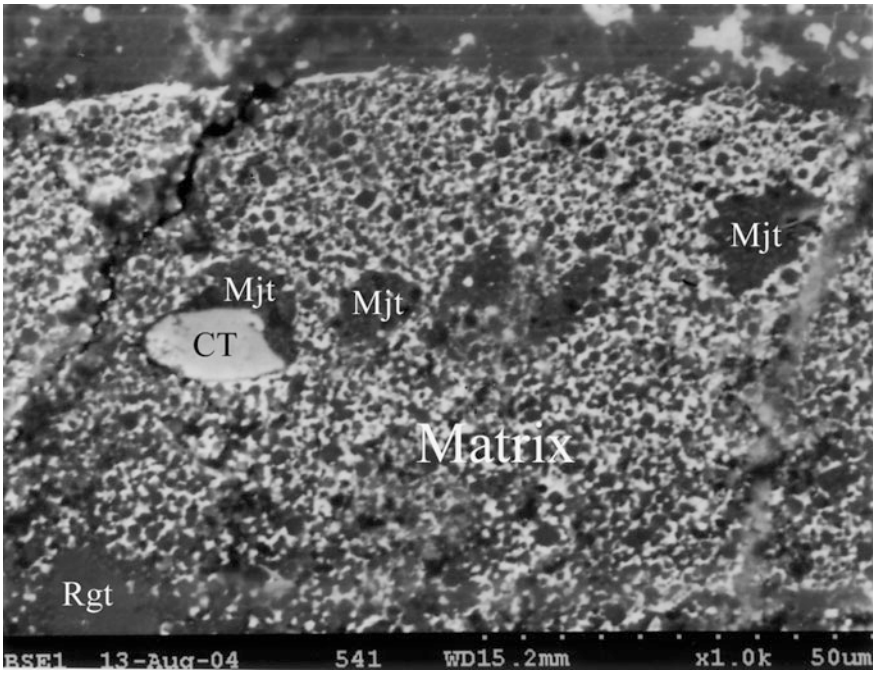

Fig. 5.51 BSE image showing a two-phase grain of xieite (*CT*) + majorite (*Mjt*) in the Suizhou vein matrix (*Matrix*). Note the curved boundary between xieite and majorite phases. Rgt = ringwoodite (Xie et al. 2011a)

Table 5.16 Composition of xieite + majorite in two-phase grain and their precursors (wt%)

	Chromite in chondrite	Xieite in two-phase grain	Majorite in two-phase grain	Pyroxene in chondrite
SiO_2			50.7↓	55.8
Al_2O_3	5.5	5.7	4.3↑	0.2
MgO	2.3	2.0↓	27.6↓	29.3
FeO	30.4	31.3↑	14.8↑	13.9
CaO			1.7 ↑	0.7
MnO	–	0.7		
TiO_2	2.9	2.7		
Cr_2O_3	58.0	57.6↓	0.9↑	0.1
V_2O_3	0.9	1.0		
Total	100.0	100.0	100.0	100.0

All data were measured by EDS technique

decrease in Cr_2O_3 (57.54 vs. 57.98 wt%), but the content of FeO increased from 30.39 to 31.32 wt%, and the content of MgO decreased from 2.32 to 2.00 wt%. On the other hand, the chemical composition of majorite in this two-phase grain is significantly different from that of its precursor low-Ca pyroxene. The main difference is shown in that the majorite shows remarkable decrease of SiO_2 (50.71 vs. 55.78 wt%) and MgO (27.61 vs. 29.31 wt%); remarkable increase of Al_2O_3 (4.29 vs. 0.16 wt%); and small increase of FeO (14.76 vs. 13.95 wt%), CaO (1.73 vs. 0.70 wt%), and Cr_2O_3 (0.91 vs. 0.10 wt%) (Xie et al. 2011b). This indicates that the element exchange between xieite and majorite in this kind of two-phase grain is relatively limited. Only very small amount of aluminum and iron migrated from majorite to xieite, and very little amount of chromium migrated from xieite to majorite. However, the remarkable difference in composition between majorite and its precursor pyroxene demonstrates that some majorite components, such as Al_2O_3 and CaO, must be captured from the surrounding shock-induced silicate melt. Hence, there exist two types of element exchange for xieite + majorite grains: exchange between two phases inside the grain and exchange between majorite inside the grain and Al- and Ca-bearing silicate melt outside the grain.

5.3 Fine-Grained High-Pressure Minerals in Shock Veins

It is known that the main constituent of shock veins in Suizhou is fine-grained matrix that makes up 80–90 % of the veins by volume. Our SEM, EPMA, and Raman spectroscopic investigations showed that the matrix material consists mainly of isometric granular garnet of majorite–pyrope composition, irregular FeNi metal, and FeS grains in eutectic intergrowths which filled the interstices of garnet grains (Fig. 5.52). Their grain sizes are ranging from 0.2 to 2 μm (Xie et al. 2001a).

In order to identify the extremely small-sized vein matrix minerals and to reveal their crystallinity, 5 areas on a polished thin section were selected for synchrotron radiation X-ray diffraction in situ analysis (Xie et al. 2005b). The X-ray beam is 15 μm × 15 μm in size that covers an area of 225 μm^2 on the polished thin section. This would give us good X-ray powder diffraction patterns of matrix minerals since the volume of each of the X-ray beamed sample will be of 6750 μm^3 (225 μm^2 × 30 μm, the later is the thickness of probed thin section), and such a volume would contain at least 6750 fine grains of matrix minerals if we take 1 μm in diameter as the mean grain size for all matrix minerals. In fact, we did obtain beautiful patterns, which clearly show sharp diffraction peaks of all constituent minerals in vein matrix, and the resolution of diffraction lines was high enough that almost no overlapping of diffraction peaks was observed (Fig. 5.53). Following results were obtained from the X-ray diffraction analyses:

(i) The vein matrix is really consisted of three minerals, namely majorite garnet (the high-pressure polymorph of pyroxene), kamacite (FeNi metal), and troilite (FeS) (Fig. 5.53). The characteristic diffraction lines of these minerals are as

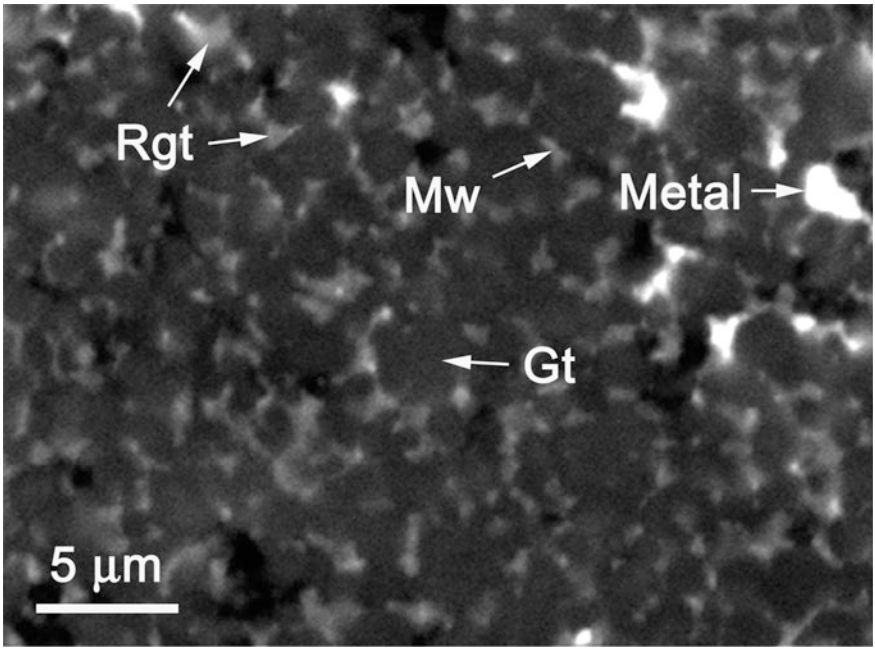

Fig. 5.52 BSE image showing the fine-grained high-pressure assemblage consisting of majorite–pyropess garnet (*Gt*), magnesiowüstite (*Mw*), and ringwoodite (*Rgt*). Metal = FeNi metal

follows: majorite garnet: d = 2.571, 2.88, 2.451, 1.538, 2.349, 2.255, and 1.596 Å; FeNi metal: d = 2.026, 1.170, and 1.453 Å; and troilite: d = 2.091, 2.667, 2.99, 1.934, and 1.728 Å.

(ii) The vein matrix is rather homogeneous in mineral composition, e.g., all three constituent minerals can be detected by every analysis. However, each of the minerals may not be so evenly distributed in vein matrix. Figure 5.53a shows that the probed area is consisted of majorite–pyrope garnet, kamacite, and troilite, but the diffraction peaks of eutectic intergrowths of kamacite and troilite are stronger than those of majorite–pyrope garnet. Figure 5.53b demonstrates that the probed area is also consisted of majorite–pyrope garnet, kamacite, and troilite, but garnet and kamacite show similar intensities.

(iii) All the X-ray powder diffraction patterns we obtained show sharp or rather sharp diffraction peaks with good resolution for all three constituent minerals, and no amorphous phases in any of the probed areas were found, indicating good crystallinity of the minerals. This implies that all the shock-induced molten materials in veins had long enough time (a few seconds) to crystallize into different minerals with good crystallinity under pressure (Chen et al. 1996a), and the cooling rate of the veins was big enough to survive all crystalline phases after pressure release.

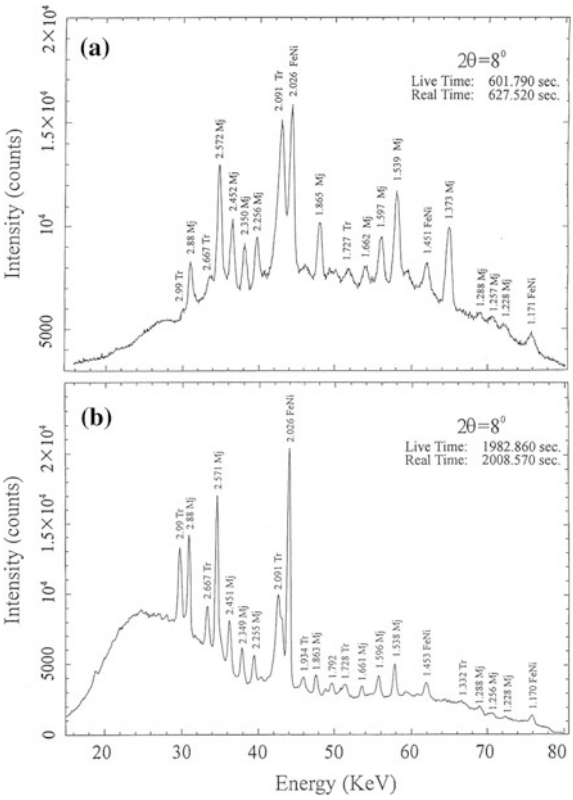

Fig. 5.53 Synchrotron radiation X-ray diffraction patterns of fine-grained vein matrix in the Suizhou meteorite. Patterns **a** and **b** obtained at two different probed areas on a polished section. Mj = majorite–pyrope garnet in solid solution, FeNi = FeNi metal, Tr = troilite (Xie et al. 2005a)

5.3.1 Majorite–Pyrope Garnet

One of the shock-induced effects on the Suizhou meteorite is the melting of silicate minerals, such as olivine, pyroxene, and plagioclase, in veins. The shock-produced silicate melt is a liquid phase of SiO_2, (Mg,Fe)O, Al_2O_3, Na_2O, and CaO. The main mineral phase crystallized from this melt under pressure is majorite–pyrope garnet.

Occurrence

Majorite–pyrope garnet occurs as tiny idiomorphic crystals ranging from 0.3 to 2.5 μm in diameter in the vein matrix of Suizhou (Fig. 4.6). Under SEM in back-scattered mode, garnet is black in color and has smooth surface. No fractures were observed in garnet crystals. Generally, majorite–pyrope garnet crystals are surrounded by magnesiowüstite and microcrystalline ringwoodite, but sometimes by FeNi metal + FeS intergrowth grains.

Chemical Composition

The electron microprobe analyses show that in contrast to the coarse-grained polycrystalline low-Ca majorite, these idiomorphic matrix garnets are richer in

Table 5.17 Chemical composition of majorite–pyrope$_{SS}$ in the Suizhou shock veins (wt%)

	SZ-MjPr-1	SZ-MjPr-2	SZ-MjPr-3	Mjt-Pyr$_{SS}$ average	Majorite average	Pyroxene average
SiO_2	50.279	50.209	51.094	50.527↓	55.797	55.775
TiO_2	0.135	0.075	0.149	0.120	0.191	0.162
Al_2O_3	3.605	3.672	3.260	**3.512**↑	0.123	0.158
Cr_2O_3	0.372	0.447	0.169	**0.329**↑	0.121	0.110
MgO	27.866	28.004	28.518	28.129	28.891	29.239
CaO	1.976	1.835	1.943	**2.918**↑	0.710	0.715
MnO	0.371	0.353	0.368	0.364	0.499	0.496
FeO	13.777	13.739	13.309	13.608↓	14.365	13.952
NiO	0.197	0.232	0.301	**0.243**↑	0.076	0.007
Na_2O	0.927	0.842	0.840	**0.870**↑	0.119	0.043
K_2O	0.033	0.048	0.057	**0.046**↑	0.023	0.009
Total	99.534	99.455	100.188	100.666	100.915	100.666
Fs	6.25	6.39	6.02	6.21	20.85	20.12
En	89.20	89.40	89.77	89.45	77.78	78.41
Wo	4.55	4.21	4.31	4.34	1.37	1.38

All values were determined by EPMA in wt%
Fs—Ferrosite, En—Enstatite, Wo—Wollastonite

Al_2O_3, CaO, Na_2O, and K_2O and contain appreciable amount of Cr_2O_3 and NiO (Table 5.17). The rather high content of Al_2O_3 (up to 3.51 wt%) indicates that the garnet is constituted not only of majorite composition, but also of pyrope composition. Hence, we call this liquidus garnet phase as majorite–pyrope solid solution. Since the main silicate minerals such as olivine and low-Ca pyroxene in the Suizhou unmelted chondritic rock contain little Al, Na, and Cr, the majorite–pyrope solid solution could not have formed by direct transformation from these phases, but rather crystallized from a shock-induced melt that was enriched in Al_2O_3, CaO, Na_2O, K_2O, and Cr_2O_3. Such phenomenon was firstly observed in the Sixiangkou shock veins, where the majorite–pyrope solid solution scavenged all of the Na, a majority of the Al and Ca, a part of the Cr in the shock-induced Sixiangkou melt (Chen et al. 1996a).

Raman Spectroscopy

The fine-grained garnet of majorite–pyrope composition shows Raman spectrum with peaks at 928, 664, 536, and 350 cm^{-1} (Fig. 5.7b) which is quite different with the Raman peaks of pyroxene outside the veins (Fig. 3.7c). Although the Raman pattern of fine-grained majorite–pyrope garnet is similar to that of the coarse-grained majorite, the intensity of the Raman peak at 664 cm^{-1} is higher than that of the coarse-grained majorite (Fig. 5.7a). This kind of Raman spectra is characteristic for liquidus majorite garnet.

Synchrotron Radiation X-ray Diffraction Data

The majorite–pyrope grains in the Suizhou shock veins are relatively small (0.3–2.5 μm in diameter) and they are in close association with fine-grained FeNi metal and troilite, so it is difficult to obtain single-phase sample of this mineral for X-ray diffraction analysis. However, we succeeded in getting its X-ray diffraction pattern using the in situ synchrotron radiation microprobe technique.

As it was introduced in Chap. 2, we did obtain beautiful patterns from the vein matrix assemblages by using synchrotron radiation X-ray diffraction technique. These patterns clearly show sharp diffraction peaks of majorite–pyrope garnet, FeNi metal, and troilite, and the resolution of diffraction lines was high enough that almost no overlapping of diffraction lines of these minerals was observed (Fig. 5.53). All together 16 diffraction reflections were obtained for our majorite–pyrope garnet (Table 5.18). This pattern is similar to that of standard majorite of JCPDS No. 25-0843 (Table 5.18, right column), and our data can be considered as the characteristic X-ray diffraction pattern for the liquidus majorite–pyrope garnet. It is also worth to mention that the diffraction peaks we obtained for majorite–pyrope garnet are sharp enough, and no amorphous phases in any of the probed areas were observed.

TEM Observations

TEM observations conducted on an ion-thinned Suizhou fine-grained vein matrix sample revealed that majorite–pyrope garnet is the most abundant constituent

Table 5.18 Synchrotron radiation X-ray diffraction data of majorite–pyrope garnets in the Suizhou vein matrix (Xie et al. 2011a)

Maj-Prp garnet #1 in vein matrix		Maj-Prp garnet #2 in vein matrix		Majorite garnet JCPDS No. 25-0843	
d (Å)	*I*	*d* (Å)	*I*	*d* (Å)	*I*
2.880	70	2.880	70	2.881	70
2.572	100	2.571	100	2.575	100
2.453	50	2.451	40	2.454	45
2.350	35	2.349	35	2.352	30
2.256	35	2.255	30	2.262	35
2.104	10	2.105	10	2.103	18
2.038	20	2.037	30	2.038	25
1.865	50	1.863	25	1.868	25
1.821	10	1.820	10	1.820	10
1.662	20	1.661	20	1.663	20
1.597	40	1.596	30	1.597	40
1.539	70	1.538	50	1.540	60
1.438	10	1.438	10	1.439	17
1.288	10	1.288	15	1.288	15
1.257	15	1.256	10	1.258	20
1.228	15	1.228	10	1.228	14

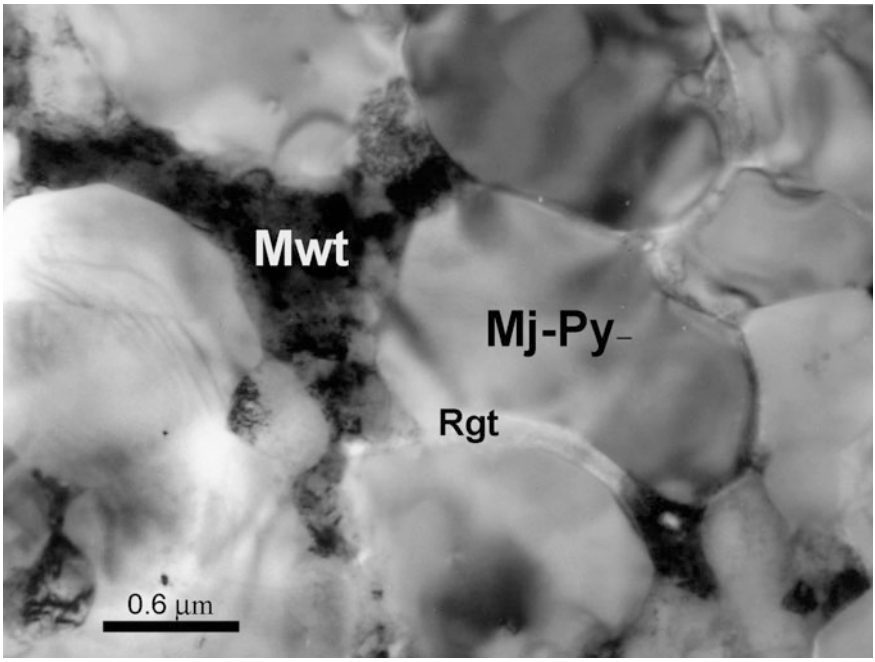

Fig. 5.54 TEM bright field image showing the idiomorphic crystals of majorite–pyrope garnet (*Grt*) and irregular microcrystalline magnesiowüstite (*Mwt*) and ringwoodite (*Rwd*) in interstices between garnet crystals

high-pressure mineral crystallized from silicate melt in shock veins. It occurs in the form of equant idiomorphic crystals (Fig. 5.54). The grain size of such garnet is ranging from 0.3 to 3 μm. The largest garnet crystals can reach to 5 μm in diameter. It is revealed that all garnet crystals show rather smooth surface but slight waving optical features can be observed in some garnet crystals.

Figure 5.55 is the selected area electron diffraction pattern of the Suizhou majorite–pyrope garnet showing the rather regular diffraction spots in cubic symmetry, with space group *Ia3d*, and cell parameter 1.147 nm (Zhang et al. 2006). The appearance of sharp rounded diffraction spots implies that majorite–pyrope garnets in the Suizhou shock veins were crystallized from silicate melt under a rather steady confining high pressure.

Formation Mechanism

In the study of the shock melt veins of the Sixiangkou L6 chondrite, Chen et al. revealed that because the low-Ca pyroxene and olivine in unshocked region of the Sixiangkou meteorite contain little Al, Na, and Cr, the majorite–pyrope solid solution could not have formed by direct transformation from these phases or their high-pressure equivalents, but rather crystallized from a melt that was enriched in Na_2O, CaO, and Cr_2O_3 (Chen et al. 1996a). Chen et al. (1996a) also pointed out

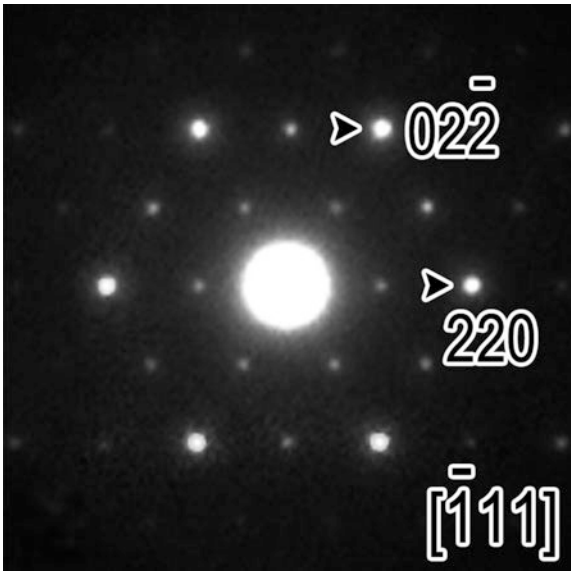

Fig. 5.55 Selected area electron diffraction pattern of the Suizhou majorite–pyrope garnet (After Zhang et al. 2006)

that the shock event on the Sixiangkou L6 chondrite formed a silicate melt of Sixiangkou bulk composition and that both majorite–pyrope garnets and magnesiowüstite are crystallized from this melt under very high pressure and temperature. Since majorite–pyrope garnet in shock veins of the Suizhou meteorite is also enriched in Na_2O, CaO, and Cr_2O_3, it is evident to maintain that our Suizhou matrix majorite–pyrope garnet should be a liquidus phase that crystallized from the shock-induced silicate melt under high pressure and high temperature in the form of majorite–pyrope solid solution.

P-T Conditions

The garnet- and metal + sulfide-rich matrix assemblage in the Suizhou shock veins are relatively homogeneous and constitute about 80–90 % of the veins by volume. Therefore, we assume that this matrix assemblage is originated from the chondritic material by melting of silicates plus FeNi, FeS, and chromite during a shock-produced high-pressure and high-temperature event.

On the basis of phase relations in the Mg_2SiO_4–Fe_2SiO_4 and $MgSiO_3$ systems (Ito et al. 1984; Hogrefe et al. 1994) and high-pressure melting experiments on peridotite (Zhang and Herzberg 1994) and the Allende carbonaceous chondrite (Agee et al. 1995), the majorite–pyrope garnet + magnesiowüstite assemblage is crystallized from 2050 to 2300 °C and 20–24 GPa (Chen et al. 1996a). The lack of perovskite in the fine-grained assemblage of the veins indicates that the pressure during crystallization did not exceed about 24 GPa. In the study of the Sixiangkou shock veins, Chen et al. (1996a) proposed a new model of shock events in meteorites in that the shock-induced high-pressure and high-temperature regime may retain for up to several seconds. The shock melt veins in Suizhou are extremely

narrow, but the presence of abundant two high-pressure mineral assemblages in veins, the good crystallinity, the lack of amorphous phases, and the idiomorphic forms of the fine-grained majorite–pyrope garnets in the vein matrix suggests a relatively low nucleation rate. Hence, we maintain that the duration of pressure and temperature regime in the Suizhou veins must last, at least, for several seconds.

5.3.2 Magnesiowüstite

At ambient conditions, both FeO (wüstite) and MgO (periclase) adopt the cubic closely packed structure of rock salt. This structure can be envisioned as a stacking of closely packed monolayers along the [111] direction. However, at high pressures, FeO undergoes several phase transitions, whereas MgO does not. The phase believed to occur in the lower mantle is called magnesiowüstite by many investigators, but it actually should be called ferropericlase because all models of the lower mantle assume only 10–20 Fe (Prewitt and Downs 1998). However, magnesiowüstite seems to be the dominate terminology for intermediate compositions and many investigators continue that usage in their publications (Prewitt and Downs 1998). Here, we introduce general characteristics of this mineral found in the Suizhou vein matrix.

Occurrence

Grains of magnesiowüstite in the Suizhou shock veins are very small. It can not be seen by an optical microscope. It is also difficult to be observed under SEM in back-scattered mode. However, the occurrence of magnesiowüstite can clearly be observed by a transmission electron microscope. Under TEM, magnesiowüstite occurs as tiny grains (up to 4 μm long) of irregular form filling the interstitial channels between idiomorphic majorite–pyrope garnet crystals.

Chemical Composition

Compositions of magnesiowüstite in the Suizhou shock veins were measured by EDS technique, and the obtained results are as follows (wt%): MgO—35.45, FeO—62.16, TiO_2—0.20, Cr_2O_3—0.92, SiO_2—0.37, totals—99.10. Its empirical formula is $Wü_{53}$-Per_{47}, where Wü is wüstite and Per is periclase.

Interestingly, the composition of magnesiowüstite in the Suizhou shock veins is quite similar to that of magnesiowüstite in the Sixiangkou shock veins. Both of them contain ~35 wt% of MgO, ~62 wt% of FeO, and ~1 wt% of Cr_2O_3 (Chen et al. 1996a). It was clear that Cr_2O_3 in both Sixiangkou and Suizhou melt was partitioned to magnesiowüstite.

TEM Observations and Electron Diffraction Data

TEM observations revealed that the irregular grains of magnesiowüstite fill the interstices between garnet crystals in the Suizhou vein matrix (Fig. 5.56). It is revealed that the magnesiowüstite grains show polycrystalline nature. Their SAED patterns show sharp diffraction spots of magnesiowüstite (insets of Fig. 4.7a, d), and

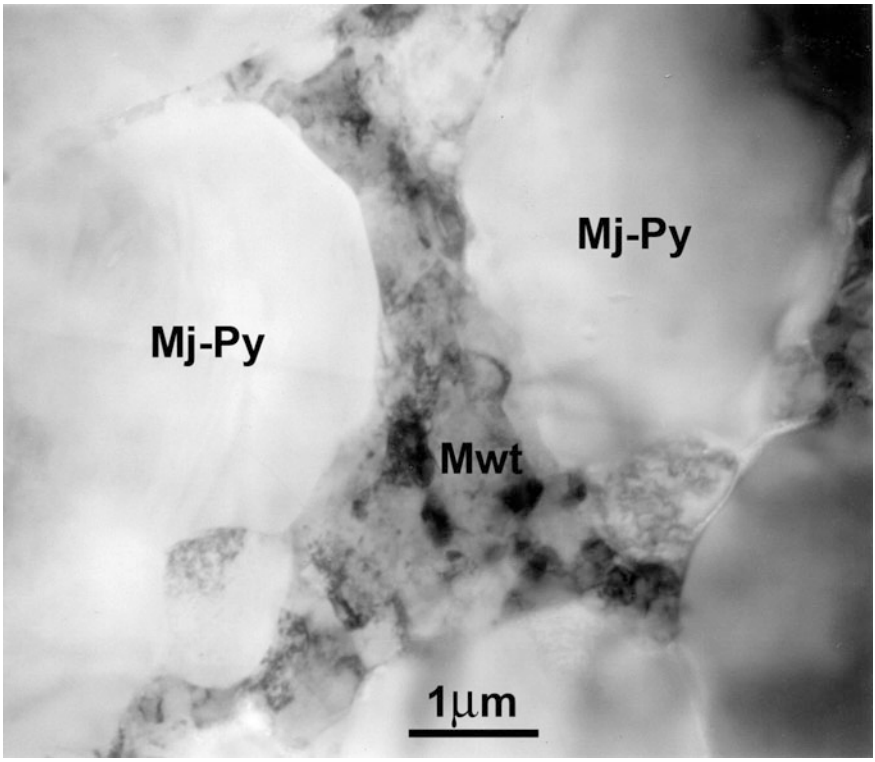

Fig. 5.56 TEM bright field image showing irregular microcrystalline magnesiowüstite (*Mwt*) filling the interstitial channels between idiomorphic majorite–pyrope garnet (*Mj-Py*) crystals

the calculated strong diffraction lines are as follows: 2.120 (100), 1.492 (60), and 2.439 (40) Å, which can be compared with those of periclase (MgO) in JCPDS No. 4-289 (Table 5.19). The slight increase of *d*-values is due to the presence of FeO in its composition.

Formation Mechanism

Chen et al. (1996a) reported that both majorite–pyrope garnets and magnesiowüstite are crystallized from a silicate melt formed by a shock event on the Sixiangkou L6 chondrite. They revealed that Sixiangkou garnet is enriched in Na_2O, CaO, and Cr_2O_3, and magnesiowüstite is enriched in Cr_2O_3. Similar phenomena were observed in the Suizhou L6 chondrite, e.g., the shock event on the Suizhou L6 chondrite formed a silicate melt of Suizhou bulk composition. Since magnesiowüstite in shock veins of the Suizhou meteorite is also enriched in Cr_2O_3, it is evident that our Suizhou magnesiowüstite should be a liquidus phase that crystallized from the shock-induced silicate melt under high pressure. The location of magnesiowüstite in the interstitial channels between idiomorphic majorite–pyrope garnet crystals indicates that garnet began to crystallize prior to magnesiowüstite.

Table 5.19 Selected area electron diffraction data of fine-grained magnesiowüstite in the Suizhou vein matrix (Xie et al. 2011a)

Fine-grained Mg-wüstite #1 in vein matrix		Fine-grained Mg-wüstite #2 in vein matrix		Periclase (MgO) JCPDS No. 4-289	
d (Å)	*I*	*d* (Å)	*I*	*d* (Å)	*I*
2.439	40	2.437	70	2.431	20
2.120	100	2.116	100	2.106	100
1.492	50	1.499	60	1.489	60
1.273	20	1.275	30	1.270	25
1.216	15	1.218	15	1.216	15
1.065	20	1.065	20	1.055	15
0.968	15	0.963	20	0.966	10
0.946	10	0.945	20	0.942	15
0.887	10	0.886	15	0.860	15
0.8201	10	0.821	10	0.811	3

_P-T_ Conditions

As we mentioned before, majorite–pyrope garnet + magnesiowüstite assemblage is crystallized from silicate melt at 2050–2300 °C and 20–24 GPa (Chen et al. 1996a). The lack of perovskite in the fine-grained assemblage of the Suizhou veins indicates that the pressure during crystallization did not exceed about 24 GPa.

5.3.3 Fine-Grained Ringwoodite Aggregates

As we described earlier in Sect. 5.2.1, ringwoodite, the high-pressure polymorph of olivine, is the main constituent mineral of the coarse-grained assemblage in the Suizhou shock vein. However, we also identified ringwoodite in the fine-grained assemblage in the same Suizhou shock veins. In this section, we shall report the difference in occurrences between these two ringwoodites.

Occurrence

Fine-grained ringwoodite aggregates in the Suizhou vein matrix occur in the form of narrow bands filling the interstitial channels between majorite–pyrope garnet crystals or between garnet and magnesiowüstite grains (Fig. 5.52). They are too small to be observed under the optical microscope or the scanning electron microscope. We identified the fine-grained ringwoodite in the Suizhou vein matrix by using transmission electron microscopic and SAED techniques.

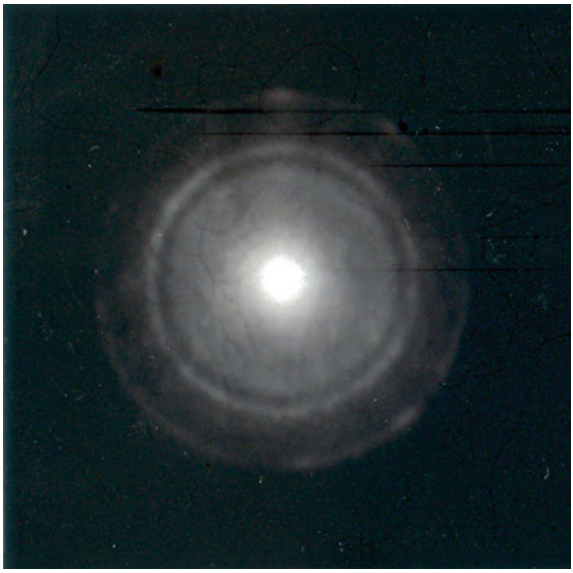

Fig. 5.57 Selected area electron diffraction pattern of the fine-grained ringwoodite in the Suizhou vein matrix

TEM Observations and Selected Area Electron Diffraction Data

Under TEM, three types of microcrystalline ringwoodite bands were revealed, namely fine granular (Fig. 4.7d), blocky (Fig. 4.7e), and fiber-like (Fig. 4.7f).

The SAED patterns show rather sharp concentric diffraction rings for the fiber-like type ringwoodite aggregate (Fig. 4.7f, inset image) and concentric diffraction rings with intermittent diffraction spots for the fine-granular ringwoodite (Fig. 5.57).

The calculated X-ray diffraction data for the fine-grained ringwoodite are shown in Table 5.20. The strongest 4 diffraction lines are at 2.446 (100), 2.028 (70), 1.434 (60), and 2.872 (30) Å. They are almost identical to the main reflections of ringwoodite in JCPDS No. 21-1258. This indicates that the crystallinity of the fine-grained ringwoodite aggregates is still good enough, and no glassy material was detected in this phase (Xie et al. 2011a).

Formation Mechanism

According to the interstitial occurrence between majorite–pyrope garnet crystals or between garnet and magnesiowüstite grains, it is believed that the Suizhou fine-grained ringwoodite in shock veins should also be a liquidus phase that crystallized from the same Suizhou melt under high pressure after solidification of majorite–pyrope garnet and magnesiowüstite.

***P-T* Conditions**

The results of high-pressure melting experiments on the Allende carbonaceous chondrite (Agee et al. 1995) and peridotite (Zhang and Herzberg 1994) indicate that the majorite–pyrope garnet and magnesiowüstite assemblage are crystallized from 20 to 24 GPa and 2050–2300 °C. The presence of fine-grained ringwoodite rather

Table 5.20 Selected area electron diffraction data of fine-grained ringwoodite in the Suizhou vein matrix (Xie et al. 2011a)

Fine-grained ringwoodite #1 in vein matrix		Fine-grained ringwoodite #2 in vein matrix		Ringwoodite JCPDS No. 21-1258	
d (Å)	*I*	*d* (Å)	*I*	*d* (Å)	*I*
2.872	30	2.879	20	2.872	20
2.446	100	2.445	100	2.447	100
2.028	70	2.027	70	2.028	40
–	–	1.661	5	1.656	<5
1.555	20	1.561	20	1.560	20
1.434	60	1.436	60	1.434	60
1.240	20	1.237	10	1.237	<5
1.170	15	1.176	10	1.172	10
1.021	15	1.015	15	1.014	5
0.901	10	0.901	10	0.907	<5
–	–	0.852	10	0.850	<5
0.827	10	0.828	10	0.828	10

than wadsleyite in the Suizhou vein matrix constrains the pressure to be greater than about 20 GPa. Hence, crystallization of fine-grained ringwoodite would take place at about 20 GPa. This pressure is a bit lower than that for crystallization of the majorite–pyrope garnet and magnesiowüstite assemblage.

5.4 FeNi Metal and Troilite in Shock Melt Veins

Metallic phases in ordinary chondrites are susceptible to the shock metamorphism, both in the solid state and as a result of melting. Shock melting of metal and troilite is observed in ordinary chondrites that have been shocked to shock stage S4 and higher. Melting must have occurred at temperatures >900 °C (Wood 1967; Taylor and Heymann 1971; Smith and Goldstein 1977), and the textural characteristics of the melted metal and sulfide change as the maximum shock temperature increases. In L chondrites of shock stage S4, metal melt droplets are very rare in comparison with troilite droplets and are also much smaller (<2 μm). Fine-grained mixtures of troilite and metal occur at shock stages S4 and above. This texture was thought by Wood (1967) to be the result of eutectic melting. In chondrites of shock stage S6, metal and sulfide melt droplets occur adjacent to most opaque grains and the droplets can reach 50 μm in size. Extensive melting results in the formation of ovoid metal grains (1–200 μm), agglomerated within troilite grains (Taylor and Heymann 1971).

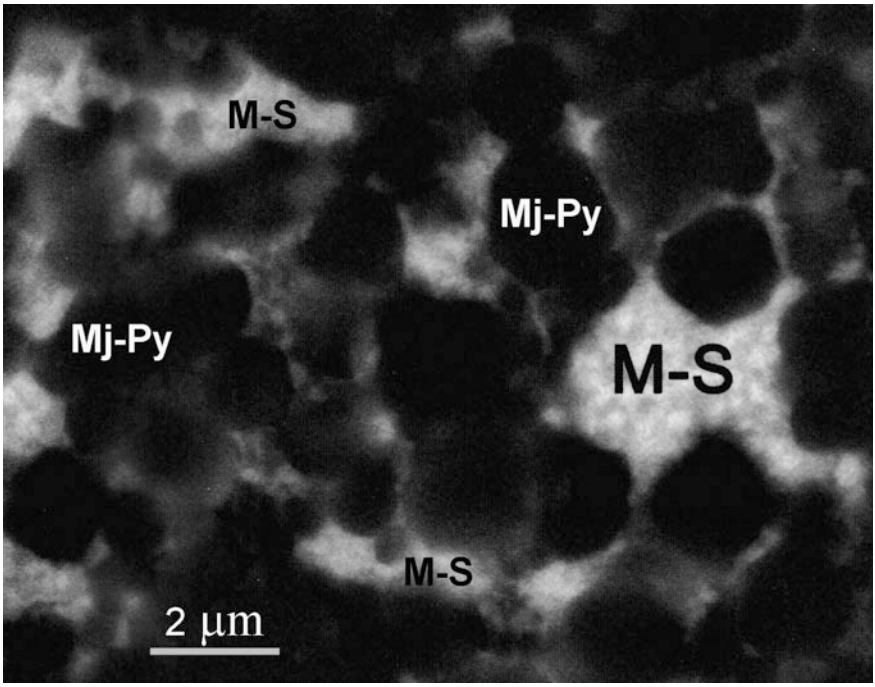

Fig. 5.58 BSE image showing the FeNi metal and troilite eutectic intergrowths (M-S) in the Suizhou shock vein. Note the rounded FeNi metal "islands" (*white*) in the troilite (*gray*) groundmass. Mj-Py = majorite–pyrope garnet in solid solution

Occurrence

In the shock veins of the Suizhou L6 meteorite, FeNi metal and troilite occur mainly in the form of eutectic intergrowths which consist of rounded FeNi metal "islands" in the troilite groundmass (Fig. 5.58). Since the shock melt veins in the Suizhou meteorite are very narrow, the eutectic intergrowths of metal and sulfide in the form of rounded or ellipsoid spherules, or irregular grains, are very small with the diameter less than 2–3 μm. In other cases, molten troilite was injected into shock-induced fractures in silicate or other opaque minerals in the form of opaque melt veins cutting through different minerals in shock melt veins (Fig. 4.2) or forms network of opaque melt veinlets in the Suizhou shock veins.

Chemical Composition

Chemical compositions of FeNi metal and troilite in some metal–sulfide intergrowths are given by Shen and Zhuang (1990) using electron microprobe analysis. For FeNi metal, it gives following results (in wt%): Fe—90.09–91.11, Ni—7.93–7.99, Co—0.44–0.54, Cu—0.00–0.02, Ga—0.06–0.44, Ge—0.29–0.33, S—1.00–1.08 %, and total—99.97–101.45 %. For troilite, the results are (in wt%) as follows: Fe—65.58–78.87, Ni—3.06–14.94, Co—0.00–0.89, Cu—0.00–0.32, Ga—0.00–0.58, Ge—0.06–0.45, S—15.04–30.42, and total—97.82–100.59 %. The average

Table 5.21 Chemical composition of FeNi metal + FeS intergrowths in veins (wt%)

Components	Grain 1	Grain 2	Grain 3	Average
Fe	90.26	90.98	92.82	91.35
Ni	6.14	3.41	3.34	4.30
S	3.60	5.61	3.84	4.35
Total	100.00	100.00	100.00	100.00

All values were determined by EDS

composition for troilite is as follows: Fe—72.21, Ni—7.05, Co—0.30, Cu—0.15, Ga—0.09, Ge—0.24, S—15.50, and total—99.54. From above listed data, we can see that FeNi metal in intergrowths contains small amount of S, and troilite contains some amount of Ni.

In the Suizhou shock veins, some FeNi metal + FeS intergrowth grains are too small to distinguish the two constituent FeNi and FeS phases. Table 5.21 shows the chemical composition of three such FeNi metal + FeS intergrowth grains in a Suizhou shock vein. From this table, we can see that these grains consist of Fe, Ni, and S, reflecting the common composition of these two phases.

As it was pointed out in the Chap. 3 that some small rounded FeNi metal grains of 0.1–5 μm in diameter are also observed in the cracks or intersecting joints of shock-induced planar fractures in olivine and pyroxene (Fig. 3.28). The EPMA results show that this type of metal grains has a much lower Fe content (84.58–85.47 wt%) and higher Ni content (14.53–15.42 wt%) than the large unmelted metal grains in the unmelted chondritic rock. This indicates that the small rounded metal grains are taenite and they formed by precipitation of metal during shock-induced high-temperature melting or even evaporation that might have caused chemical fractionation of Fe and Ni in these metal grains.

Synchrotron Radiation X-ray Diffraction Data

FeNi metal and troilite in some metal–sulfide intergrowths that we observed in the Suizhou shock veins are extremely small. The largest intergrowths are only 2 μm × 3 μm in sizes. They are surrounded all round and underneath by other vein matrix minerals, namely majorite–pyrope garnet, magnesiuwüstite, and ringwoodite (Fig. 5.52). Therefore, the synchrotron radiation X-ray diffraction in situ analysis was used to obtain X-ray diffraction data for FeNi metal and troilite in intergrowths, and the following data were obtained (Fig. 5.53): for FeNi metal: 2.026 (100), 1.453 (20), and 1.171 (10); for troilite: 2.091 (100), 2.99 (60), 2.667 (50), 1.934 (20), 1.782 (20), and 1.332 (10). The above X-ray diffraction data obtained for the FeNi metal and troilite in the Suizhou shock veins are in good consistence with those for the corresponding standard minerals (JCPDS No. 37-0474 for kamacite, and JCPDS No. 37-0477 for troilite).

It should be mentioned that the diffraction peaks we obtained for both FeNi metal and troilite are sharp enough, and no amorphous phases in any of the probed areas were found. This implies that the crystallinity of these two metallic minerals in the Suizhou shock veins is also good enough no matter how fine their grains are.

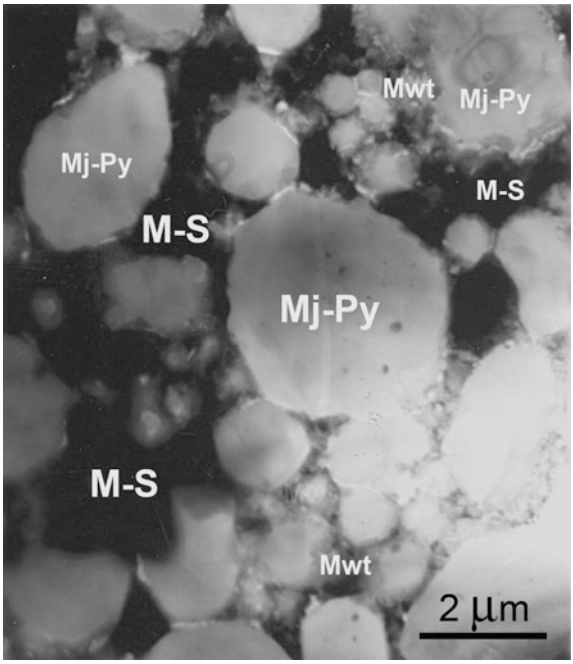

Fig. 5.59 TEM micrograph showing the occurrence of FeNi metal and FeS intergrowths (M-S). Mj-Py = majorite–pyrope solid solution, Mwt = magnesiowüstite

TEM Observations

Since the grains of FeNi metal + FeS intergrowths are not transparent under TEM, it is hard to explore the microstructure of these grains. The only information that we could obtained is the dark grain configurations (Fig. 5.59). From this figure, as well as the SEM BSE image (Fig. 5.58), we can see that the FeNi metal + FeS intergrowth grains are very small, and they really occur in the interstitial channels between the idiomorphic crystals of majorite–pyrope garnet.

Formation Mechanism and *P-T* Conditions

In the Suizhou shock veins, FeNi metal and FeS occur in the form of fine-grained intergrowths. This texture was thought to be the result of eutectic melting (Wood 1967). Since the shock melt veins in the Suizhou meteorite are extremely thin, the size of metal and sulfide melt droplets is also very small, usually only a few μm in size.

According to the experiments, eutectic melting of FeNi metal and FeS occurs at temperatures lower than 900 °C at normal pressure (Wood 1967; Smith and Goldstein 1977). This indicates that the FeNi metal and FeS intergrowths, being the last crystallization product in the Suizhou shock veins, solidified after pressure release when the vein temperature decreases lower than 900 °C.

5.5 Summary

(1) Almost all minerals, including silicate, phosphate, and oxide minerals in the Suizhou shock veins, have transformed to their high-pressure polymorphs. The only one mineral that we could not find its high-pressure polymorph is ilmenite.
(2) Ten high-pressure minerals were identified in the shock melt veins of the Suizhou meteorite in two assemblages: One is the coarse-grained assemblage which is consisted of ringwoodite, majorite, akimotoite, vitrified perovskite, lingunite, tuite, xieite, and the CF phase; and another is the fine-grained assemblage which is consisted of matrix minerals majorite–pyrope garnet in solid solution, magnesiowüstite, and microcrystalline ringwoodite.
(3) These two high-pressure mineral assemblages constitute up to 90 % of materials in veins by volume. The other 10 % constituents of veins are fine-grained metal–troilite eutectic intergrowths and blebs which fill the interstices of majorite–pyrope garnet or in the form of metal–sulfide veinlets.
(4) Besides the monomineralic fragments of high-pressure phases in the Suizhou shock veins, some polymineralic fragments of different high-pressure phases are also observed, namely the unique zonal xiete + CF phase + chromite fragments and perovskite + akimotoite + low-Ca pyroxene fragments in adjacent to the vein walls and the three-phase fragments of majorite + vitrified perovskite + ringwoodite, as well as many other two-phase fragments of xieite + one of the high-pressure silicate minerals in the shock veins.

References

Agee CB, Li J, Shannon MC et al (1995) Pressure-temperature phase diagram for Allende meteorite. J Geophys Res 100:17725–17740

Akaogi M (2000) Clues from a shocked meteorite. Science 287:1602–1603

Akaogi M, Hamada Y, Suzuki T et al (1999) High pressure transitions in the system $MgAl_2O_4$–$CaAl_2O_4$: a new hexagonal aluminous phase with implication for the lower mantle. Phys Earth Planet Int 115:67–77

Anderson DL, Bass JD (1986) Transition region of the Earth's upper mantle. Nature 320:321–328

Andrault D, Bolfan-Casanova N (2001) High-pressure phase transformation in the $MgFe_2O_4$ and Fe_2O_3–$MgSiO_3$ system. Phys Chem Mineral 28:211–217

Bell MS, Thomas-Keprta K, Wentworth SJ et al (1999) Pyroxene glass in ALH 84001. Lunar Planet Sci 30:CD-ROM, Abstract #1951

Bertaut EF, Blum P (1956) Determination delta structure de Ti_2CaO_4 par la méthode self-consistante d'approache directe. Acta Crystal 9:121–126

Beswick AE, Carmichael ISE (1978) Constraints on mantle source compositions imposed by phosphorous and the rare-earth elements. Contrib Mineral Petrol 67:317–330

Binns RA (1970) $(Mg,Fe)_2SiO_4$ spinel in a meteorite. Phys Earth Planet Inter 3:156–160

Binns RA, Davis RJ, Read SJB (1969) Ringwoodite, a natural $(Mg,Fe)_2SiO_4$ spinel in the Tenham meteorite. Nature 221:943–944

Bowden KE (2002) Effects of loading path on the shock metamorphism of porous quartz: an experimental study. Ph.D. thesis, University College, London, p 228
Bright NFH, Rowland JF, Wurm JG (1958) The compound $CaO \cdot Ti_2O_3$. Can J Chem 36:492–495
Buchwald VF (1984) Phosphate minerals in meteorites and lunar rocks. In: Nriagu JO, Moore PB (eds) Phosphate minerals. Springer, Berlin, pp 199–214
Chen M, Xie XD (1993) The shock effects of olivine in the Yanzhuang chondrite. Acta Mineral Sin 13(2):109–114
Chen M, Xie XD (2015) Shock-produced akimotoite in the Suizhou L6 chondrite. Sci China: Earth Sci 58:876–880
Chen M, Wopenka B, Xie XD et al (1995a) A new high-pressure polymorph of chlorapatite in the shocked chondrite Sixiangkou(L6). Lunar Planet Sci 26:237–238
Chen M, Xie XD, El Goresy A (1995b) Nonequilibrium solidification and micro-structures of metal phases in the shock-induced melt of the Yanzhuang (H6) chondrite. Meteoritics 30:28–32
Chen M, Sharp TG, E1 Goresy A et al (1996a) The majorite–pyrope + magnesiowüstite assemblage: constrains on the history of shock veins in chondrites. Science 271:1570–1573
Chen M, Wopenka B, El Goresy A (1996b) High-pressure assemblage in shock melt vein in Peace River (L6) chondrite: compositions and pressure-temperature history. Meteoritics 31(Suppl.): A27
Chen M, Xie XD, El Goresy A et al (1998) Cooling rates in the shock veins of chondrites: constraints on the $(Mg,Fe)_2SiO_4$ polymorph transformations. Sci China, Series D 41:522–552
Chen M, Shu JF, Xie XD et al (2003a) Natural $CaTi_2O_4$-structured $FeCr_2O_4$ polymorph in the Suizhou meteorite and its significance in mantle mineralogy. Geochim Cosmochim Acta 67 (20):3937–3942
Chen M, Shu J, Mao HK et al (2003b) Natural occurrence and synthesis of two new postspinel polymorphs of chromite. Proc Natl Acad Sci USA 100(25):14651–14654
Chen M, El Goresy A, Frost D et al (2004a) Melting experiments of a chondritic meteorite between 16 and 25 GPa: implications for Na/K fractionation in a primitive chondritic Earth's mantle. Eur J Miner 16:201–211
Chen M, Xie XD, El Goresy A (2004b) A shock-produced $(Mg,Fe)SiO_3$ glass in the Suizhou meteorite. Meteor Planet Sci 39:1797–1808
Chen M, El Goresy A, Gillet P (2004c) Ringwoodite lamellae in olivine: clue to olivine-ringwoodite phase transition mechanisms in shocked meteorites and in subducting slabs. Proc Natl Acad Sci USA 101:15033–15037
Chen M, Shu JF, Mao HK (2008) Xieite, a new mineral of high-pressure $FeCr_2O_4$ polymorph. Chin Sci Bull 53:3341–3345
Coleman LC (1977) Ringwoodite and majorite in the Catherwood meteorite. Can Mineral 15:97–101
Dowty E (1977) Phosphate in Angra Dos Reis: structure and composition of the $Ca_3(PO_4)_2$ minerals. Earth Planet Sci Lett 35:347–351
Engvik AK, Golla-Schindler U, Berndt J et al (2009) Intragranular replacement of chlorapatite by hydroxy-fluor-apatite. Lithos 112:236–246
Fei Y, Wang Y, Finger LW (1996) Maximum solubility of FeO in $(Mg,Fe)SiO_3$-perovskite as a function of temperature at 26 GPa: implication for FeO content in the lower mantle. J Geophys Res 101:11525–11530
Fei Y, Frost DJ, Mao HK et al (1999) In situ structure determination of the high-pressure phase of Fe_3O_4. Am Mineral 84:203–206
Ferroir T, Beck P, Van de Moortèle B et al (2008) Akimotoite in the Tenham meteorite: crystal chemistry and high-pressure transformation mechanisms. Earth Planet Sci Lett 275:26–31
Frondel C (1941) Whitlockite, a new calcium phosphate. Am Mineral 26:145
Funamori N, Jeanoz R, Nguyen JH et al (1998) High-pressure transformations in $MgAl_2O_4$. J Geophys Res 103:20813–20818
Gasparik P (1992) Melting experiments on the enstatite-pyrope joint at 80–152 kbar. J Geophys Res 97:15181–15188

Gillet P, Chen M, Dubrovinsky L et al (2000) Natural $NaAlSi_3O_8$ –hollandite in the Sixiangkou meteorite. Science 287:1633–1637

Goltrant O, Cordier P, Doukhan JC (1991) Planar deformation features in shocked quartz: a transmission electron microscopy investigation. Earth Planet Sci Lett 106:103–155

Gopal R, Calvo C, Ito J, Sabine WK (1974) Crystal structure of synthetic Mg-whitlockite, $Ca_{18}Mg_2H_2(PO_4)_4$. Can J Chem 52:1152–1155

Graudefroy C, Jouravsky C, Permingeat F (1963) La marokite, $CaMn_2O_4$, une nouvelle espèce minerale. Bull Soc Franç Mineral Crystallogr 86:359–367

Griffin WL, Åmli R, Heier KS (1972) Whitlockite and apatite from lunar rock 14310 and from ÖdegÅrden, Norway. Earth Planet Sci Lett 15:53–68

Hogrefe A, Rubie DC, Sharp TG et al (1994) Metastability of enstatite in deep subducting lithosphere. Nature 372:351–353

Irifine T, Fujino K, Ohtani E (1991) A new high-pressure form of $MgAl_2O_4$. Nature 349:409–411

Irifune T, Ringwood AE, Hibberson WO (1994) Subduction of continental crust and terrigeneous and pelagic sediments: an experimental study. Earth Planet Sci Lett 126:351–368

Ito E, Takahashi E, Matsui Y (1984) The mineralogy and chemistry of the lower mantle: an implication of the ultrahigh-pressure phase relation in the system of MgO-FeO-SiO_2. Earth Planet. Sci. Lett 67:238–248

Jolliff BL, Freeman JJ, Wopenka B (1996) Structural comparison of lunar, terrestrial, and synthetic whitlockite using laser Raman microprobe spectroscopy. Lunar Planet Sci 27:613–614

Kato T, Kumasuwa M (1985) Melting experiment on natural lherzolite at 20 GPa: formation of phase B coexisting with garnet. Geophys Res Lett 13:181–184

Kawai N, Tachimori M, Ito E (1974) A high-pressure hexagonal form of $MgSiO_3$. Proc Jpn Acad 50:378–380

Kerschofer L, Sharp TG, Rubie DC (1996) Intracrystalline transformation of olivine to wadsleyite and ringwoodite under subduction zone conditions. Science 274:79–81

Kerschofer L, Dupas C, Liu M et al (1998) Polymorphic transformation between olivine, wadsleyite and ringwoodite: mechanism of intracrystalline nucleation and the role of elastic strain. Mineral Mag 62:617–638

Kerschofer L, Rubie DC, Sharp TG et al (2000) Kinetics of intracrystalline olivine-ringwoodite transformation. Phys Earth Planet Inter 121:59–76

Kimura M, Suzuki A, Kondo T et al (2000) The first discovery of high-pressure polymorphs, jadeite, hollandite, wadsleyite and majorite, from an H-chondrite, Y-75100. Antarct Meteor 25:41–42

Langenhorst F, Poirier JP (2000) 'Ecologitic' minerals in a shocked basaltic meteorite. Earth Planet Sci Lett 176:259–265

Langenhorst F, Joreau P, Doukhan JC (1995) Thermal and shock metamorphism of the Tenham chondrite: a TEM examination. Geochim Cosmochim Acta 59:1835–1845

Liu LG (1974) Silicate perovskite from phase transformations of pyrope-garnet at high pressure and temperature. Geophys Res Lett 1:277–280

Liu LG (1976) The high-pressure phases of $MgSiO_3$. Earth Planet Sci Lett 31:200–208

Liu LG (1978) High-pressure phase transformations of albite, jadeite and nepheline. Earth Planet Sci Lett 37:438–444

Liu LG, El Goresy A (2007) High-pressure phase transitions of the feldspars and further characterization of lingunite. Int Geol Rev 49:854–860

Malavergne V, Guyot F, Benzerara K et al (2001) Description of new shock-induced phases in the Shergotty, Zagami, Nakhla and Chassigny meteorites. Meteor Planet Sci 36:1297–1305

Mao HK, Takahashi T, Bassett WA et al (1974) Isothermal composition of magnetite to 320 kbar and pressure-induced phase transformation. J Geophys Res 79:1165–1170

Mao HK, Shen G, Hemley RJ (1997) Multivariant dependence of Fe–Mg partitioning in the lower mantle. Science 278:2098–2100

Mason B (1966) Composition of the earth. Nature 21:616–618

Mason B, Nelen J, White JS Jr (1968) Olivine-garnet transformation in a meteorite. Science 160:66–67

McCammon CA (1998) Crystal chemistry of ferric iron in $Fe_{0.05}Mg_{0.95}SiO_3$ perovskite as determined by Mossbauer spectroscopy in the temperature range 80–293 K. Phys Chem Miner 25:292–300

McMillan P (1984a) Structural studies of silicate glasses and melts; application and limitations of Raman spectroscopy. Am Mineral 69:622–644

McMillan P (1984b) A Raman spectroscopic study of glasses in the system CaO-MgO-SiO_2. Am Mineral 69:645–659

McMillan P, Akaogi M (1987) Raman spectra of β-Mg_2SiO_4 (modified spinel) and γ-Mg_2SiO_4 (spinel). Am Mineral 72:361–364

Miyagima N, El Goresy A, Dupas-Bruzek C, Seifert F, Rubie BC, Chen M, Xie XD (2007) Ferric iron in Al-bearing akimotoite coexisting with iron-nickel metal in a shock-melt vein. Am Mineral 92:1545–1549

Mosenfelder JL, Marton FC, Ross CR et al (2001) Experimental constraints on the depth of olivine metastability in subducting lithosphere. Phys Earth Planet Inter 127:165–180

Murayama JK, Kato M, Nakai S (1986) A dense polymorph of $Ca_3(PO_4)_2$: a high pressure phase of apatite decomposition. Phys Earth Planet Inter 44:293–303

Nash WP (1984) Phosphate minerals in terrestrial igneous and metamorphic rocks. In: Nriagu JO, Moore PB (eds) Phosphate minerals. Springer, Berlin, pp 215–241

Presnall DC, Gasparik T (1990) Melting of enstatite ($MgSiO_3$) from 10 to 16.5 GPa and the forsterite (Mg_2SiO_4)—majorite ($MgSiO_3$) eutectic at 16.5 GPa: implications for the origin of the mantle. J Geophys Res 90:15771–15777

Prewitt CT (1975) Meteoritic and lunar whitlockites. Lunar Planet Sci 6:647–648

Prewitt CT, Downs RT (1998) High-pressure crystal chemistry. Rev Miner 37:287–317

Price GD, Putnis A, Agrell SO (1979) Electron petrography of shock-produced veins in the Tenham chondrite. Contrib Miner Petrol 71:211–218

Putnis A, Price GD (1975) High-pressure (Mg, Fe) Si_2O_4 phases in the Tenham chondritic meteorite. Nature 280:217–218

Reid AF, Ringwood AE (1969) Newly observed high pressure transformation in Mn_3O_4, $CaAl_2O_4$, and $ZrSiO_4$. Earth Planet Sci Lett 6:205–208

Reid AF, Ringwood AE (1970) The crystal chemistry of dense M_3O_4 polymorph: High pressure Ca_2GeO_4 of K_2NiF_4 structure type. J Solid State Chem 1:557–565

Ringwood AE (1962) Mineralogical constitution of the deep mantle. J Geophys Res 67:4005–4010

Ringwood AE, Major A (1966) Synthesis of Mg_2SiO_4–Fe_2SiO_4 solid solutions. Earth Planet Sci Lett 1:241–245

Ringwood AE, Reid AF, Wadsley AD (1967) High-pressure $KAlSi_3O_8$, an aluminosilicate with sixfold coordination. Acta Cryst 23:1093–1095

Roux P, Louër D, Bonel G (1978) Sur nouvelle forme crystalline du phosphate tricalcique. C.R. Acad Sci Paris Ser C 286:549–551

Rubin AE (1997) Mineralogy of meteorite groups. Meteor Planet Sci 32:231–247

Saxena SK, Dubrovinsky LS, Lazor P et al (1996) Stability of perovskite ($MgSiO_3$) in the Earth's mantle. Science 274:1357–1359

Scarfe CM, Mysen BO, Rai CS (1979) Invariant melting behavior of mantle material: partial melting of two lherzolite nodules. Carnegie Inst Wash Yearb 78:498–501

Serghiou G, Zerr A, Boehler R (1998) (Mg,Fe)SiO_3-perovskite stability under lower mantle conditions. Science 280:2093–2095

Sharp TG, DeCarli PS (2006) Shock effects in meteorites. In: Binzel RP (ed) Meteorites and the early solar system II. The University of Arizona Press, Tucson, pp 653–677

Sharp TG, Chen M, El Goresy A (1997a) Mineralogy and microstructures of shock-induced melt veins in the Tenham (L6) chondrite. Lunar Planet Sci 28:1283–1284

Sharp TG, Lingemann CM, Dupas C et al (1997b) Natural occurrence of $MgSiO_3$-ilmenite and evidence for $MgSiO_3$–perovskite in a shocked L chondrite. Science 277:255–352

Shen SY, Zhuang XL (1990) A study of the opaque minerals and structural characteristics of the Suizhou meteorite. In: A synthetical study of Suizhou meteorite. Publishing House of the China University of Geosciences, Wuhan, 40–52 (in Chinese)

Smith BA, Goldstein JI (1977) The metallic microstructures and thermal histories of severely reheated chondrites. Geochim Cosmochim Acta 41:1061–1072

Smith JV, Mason B (1970) Pyroxene-garnet transformation in Coorara meteorite. Science 168:822–823

Sugiyama S, Tokonami M (1987) Structure and crystal chemistry of a dense polymorph of tricalcium phosphate $Ca_3(PO_4)_2$: a host to accommodate large lithophile elements in the earth's mantle. Phys Chem Miner 15:125–130

Taylor GJ, Heymann D (1971) Postshock thermal histories of reheated chondrites. J Geophys Res 76:1879–1893

Tomioka N, Fujino K (1997) Natural (Mg,Fe)SiO_3-ilmenite and -perovskite in the Tenham meteorite. Science 277:1084–1086

Tomioka N, Fujino K (1999) Akimotoite, (Mg, Fe) SiO_3, a new silicate mineral of the ilmenite group in the Tenham chondrite. Am Mineral 84:267–271

Tomioka N, Kimura M (2003) The breakdown of diopside to Ca-rich majorite and glass in a shocked H chondrite. Earth Planet Sci Lett 208:271–278

Tomioka N, Mori H, Fujino K (2000) Shock-induced transition of $NaAlSi_3O_8$ feldspar into a hollandite structure in a L6 chondrite. Geophys Res Lett 27:3997–4000

Tutti F, Dubrovinsky LS, Saxena SK (2000) High pressure phase transformation of jadeite and stability of $NaAlSiO_4$ with calcium-ferrite type structure in the lower mantle conditions. Geophys Res Lett 27:2025–2028

Villiers PR, Herbstein FH (1968) Second occurrence of marokite. Am Mineral 53:495–496

Wang DD (1993) An introduction to Chinese meteorites. Science Press, Beijing, 101–106 (in Chinese)

Wang WY, Takahashi E (2000) Subsolidus and melting experiments of K-doped peridotite KLB-1 to 27 GPa: its geophysical and geochemical implications. J Geophys Res 105:2855–2868

Wang Z, Lazor P, Saxena SK et al (2002) High-pressure Raman spectroscopic study of spinel ($ZnCr_2O_4$). J Solid State Chem 165:165–170

Wood JA (1967) Chondrites: their metallic minerals, thermal histories, and parent planets. Icarus 6:1–49

Xie XD, Chao ECT (1987) Studies on the lattice distortion and substructures of shock lamellae in naturally shocked quartz. Chin J Geochem 6:19–32

Xie XD, Chen M (2009) Shock melting and fractional crystallization of meteorite minerals under dynamic high-pressures and their geochemical significance. Earth Sci Front 16:134–145 (in Chinese with English Abstract)

Xie XD, Chen M, Wang DQ (2001a) Shock-related mineralogical features and P-T history of the Suizhou L6 chondrite. Eur J Miner 13(6):1177–1190

Xie XD, Chen M, Wang DQ et al (2001b) $NaAlSi_3O_8$-hollandite and other high-pressure minerals in the shock melt veins of the Suizhou L6 chondrite. Chin Sci Bull 46(13):1121–1126

Xie XD, Minitti ME, Chen M et al (2002) Natural high-pressure polymorph of merrillite in the shock vein of the Suizhou meteorite. Geochim Cosmochim Acta 66:2439–2444

Xie XD, Minitti ME, Chen M et al (2003) Tuite, γ-$Ca_3(PO_4)_2$, a new phosphate mineral from the Suizhou L6 chondrite. Eur J Mineral 15:1001–1005

Xie XD, Shu JF, Chen M (2005a) Synchrotron radiation X-ray diffraction in situ study of fine-grained minerals in shock veins of Suizhou meteorite. Sci China, Ser D 48:815–821

Xie XD, Chen M, Wang DQ (2005b) Two types of silicate melts in naturally shocked meteorites. Papers and abstracts of the 5th annual meeting of IPACES, Guangzhou, pp 12–14

Xie ZD, Sharp TG (2004) High-pressure phases in shock-induced melt veins of the Umbarger L6 chondrite: Constraints of pressure. Meteor Planet Sci 39:2043–2054

Xie ZD, Sharp TG, DeCarli PS (2006) High-pressure phases in a shock-induced melt vein of the Tenham L6 chondrite: constraints on shock pressure and duration. Geochim Cosmochim Acta 70:504–515

Xie XD, Chen M, Wang CW (2011a) Occurrence and mineral chemistry of chromite and xieite in the Suizhou L6 chondrite. Sci China Earth Sci 54:1–13

Xie XD, Sun ZY, Chen M (2011b) The distinct morphological and petrological features of shock melt veins in the Suizhou L6 chondrite. Meteor Planet Sci 46:459–469

Xie XD, Zhai SM, Chen M, Yang HX (2013) Tuite, γ-$Ca_3(PO_4)_2$, formed by chlorapatite decomposition in a shock vein of the Suizhou L6 chondrite. Meteor Planet Sci 48:1515–1523

Xue X, Zhai S, Kanzaki M (2009) Si-Al distribution in high-pressure $CaAl_4Si_2O_{11}$: A ^{29}Si and ^{27}Al NMR study. Am Mineral 94:1739–1742

Yagi Y, Suzki T, Akaogi M (1994) High pressure transitions in the system $KAlSi_3O_8$–$NaAlSi_3O_8$. Phys Chem Mineral 21:12–17

Yamada H, Matsui Y, Ito E (1984) Crystal-chemical characterization of $KAlSi_3O_8$ with the hollandite structure. Mineral J (Jpn) 12:29–34

Zhang J, Herzberg C (1994) Melting experiments on anhydrous peridotite KLB-1 from 5.0 to 22.5 GPa. J Geophys Res 99:17729–17742

Zhang J, Ko J, HazenR M et al (1993) High-pressure crystal chemistry of $KAlSi_3O_8$ hollandite. Am Mineral 78:493–499

Zhang K, Wang JB, Wang RH (2006) Electron microscopic studies of the mineral phases in the Suizhou meteorite. J Chin Electr Microsc Soc 25(Suppl.):354–355 (in Chinese)